Doctoral Thesis

Evaluation of Human Impacts on Groundwater Resources in Mountainous Catchments, Western Japan

SHARON BIH KIMBI

Graduate School of Integrated Arts and Sciences

Hiroshima University

September 2022

Abstract

The long-term cumulative effect of increasing urbanization, population and climate change on watershed hydrology has altered the spatial availability of groundwater resources in many regions. In recent years, demographic trends have led to concerns on how population growth will affect water resources. In many Asian and Western countries, population densities are declining despite global population growth with a significant increase in the proportion of the elderly. With an increasing number of citizens over 65 and many cities experiencing depopulation, Japan has experienced this demographic change faster than most Western and Asian countries. Despite these social changes, it still faces serious environmental problems related to groundwater quality and quantity. Population growth and increasing economic condition have led to the continuous expansion and transformation of many Japanese's mountainous rural catchments with associated groundwater resource problems. Despite the significant impact of urbanization (population growth) on groundwater resources, most studies have focused on qualitative, regional impact, with little attention focused on the combine effects of social and environmental issues on groundwater resources in mountainous rural catchments. Therefore, it is necessary to understand how environmental and social aspects affects groundwater resources. This study provides an insight into groundwater resources degradation resulting from an aging and depopulation society as well as urbanization and climate change effects.

The effects of population aging and depopulation on groundwater nitrate contamination in an island with intensive citrus cultivation, was examined by comparing two neighbouring villages and watersheds with little different in their social aspects. The northern one (Kubi) has a little higher farmer average age of 76 years, and the decreasing rate of farmland for 10 years from 2005 to 2015 of 46%, as compared with the eastern (Ocho) of 73 years and 37%,

respectively. The population in Ocho was 830, and twice of that in Kubi. Higher mean concentrations of NO_3^-−N were recorded in Kubi village (6.55 mg/L) than in the Ocho area (4.75 mg/L). NO_3^-−N contamination mainly was estimated to originate from chemical fertilizer in Kubi and Organic fertilizer in Ocho, using stable nitrogen isotopes and a Bayesian isotope mixing model. These source distributions were closely associated with a greater extent land use and social aspects such as aging and depopulation. A substantial quantity of chemical fertilizer applied by the more aged farmers in more depopulated Kubi was suggested to lead to inefficient nitrogen uptake by plants, which results in higher leaching that pollutes its groundwater more than those of Ocho.

Likewise, the hydrochemistry and dual isotope approach was used to evaluate groundwater contamination status in Saijo watershed. Results showed that, calcium (Ca^{2+}) and bicarbonate (HCO_3^-) were the most abundant cation and anion respectively and the major water type in the study area was of Ca–Mg–HCO3 type. Inferring from the contamination sources in the watershed using $\delta^{15}N\text{-}NO_3^-$ and $\delta^{18}O\text{-}NO_3^-$ measurements indicated that two major contamination sources with values characteristic for nitrate derived from nitrification of soil organic nitrogen (+0.2 ‰ to +7.3 ‰ for $\delta^{15}N$) and nitrate derived from animal wastes or human sewage, e.g., via septic systems (+8.9 ‰ to + 12.3 ‰ for $\delta^{15}N$) in two distinct zones. Despite agricultural activities in the study area, we found no evidence of nitrate originating from synthetic fertilizers in the groundwater.

Furthermore, the spatial variation in groundwater recharge under the effects of urbanization and climate change, was investigated using SWAT over a period of three decades. Results suggest, the water balance in the last 30yrs is greatly influenced by land-use change with urbanization. The most significant change was observed in the decrease in the mean annual groundwater recharge by approximately 25% (i.e., from 184.5 mm in the 1980s to 120.2 mm in the 2000s). Rice paddy areas are observed to be the major recharge zones in the

catchment, with the highest recharge compared to forest and residential areas. Higher rainfall interception by forest canopy were responsible for the lower recharge values observed at forested sites. Furthermore, the predicted scenario highlighted that groundwater recharge will be significantly affected by future climate change which is projected to decrease groundwater recharge by 29% in the next 30years**.** Land and water resource management can be improved if the findings from the study are used by decision-makers, planners, and managers the region. planners, and managers the region.

Contents

List of figures

List of Tables

Chapter 5

Acknowledgements

This PhD thesis would not have been achieved without the support and help of many institutions and individuals that I met while conducting research for the PhD project. And for this reason, I wish to acknowledge their contributions

First and foremost, I thank the Almighty God for giving me good health, courage, endurance, and determination to successfully go through this academic process despite the numerous challenges encountered during my studies.

I am highly indebted and thoroughly grateful to the Ministry of Education, Culture, Sports, Science and Technology (MEXT), Japan for funding the last three years of my PhD research project.

It is with great appreciation that I acknowledge my supervisor, Professor Shin-ichi Onodera, whose academic mentoring, constructive criticism and immense support have enabled me to successfully complete this project, which is of great interest to me and society as a whole. Furthermore, thank you for hosting me in your team and helping me to achieve a level of research that I could not have imagined. You have triggered and nurtured my intellectual maturity. Being your student was an honour, Sensei.

I would like to thank Prof. Toshihisa Asano, Associate Professor Hisashi Ozawa, Associate Professor Tadashi Yokoyama, and Prof. Itaru Nagasaka for their guidance and supervisory roles during my PhD research project.

Special acknowledgement goes to Prof. Ichirow Kaihostu who provided the major input and data set for my modelling programme as well as provided constructive criticisms and suggestions throughout my research. I also owe special thanks to Associate Prof. Mitsuyo Saito and Assistant Prof. Takuya Ishida from Hiroshima University who invested their time, appeal

knowledge and energy both during the fieldwork, analysis processing, and editing of manuscripts drafted for this PhD work.

My sincerest thanks go out to Dr. Yuta Shimizu from NAFRO, Japan, as well as Dr Kunyang Wang from the Biogeochemical Laboratory at Hiroshima University for guiding, encouraging and supervising my PhD thesis modelling work. As a result of the numerous workshops and one-on-one discussions I had with them, I gained a deeper understanding of the factors governing groundwater occurrence and movement. Thanks to their constructive criticism and valuable advice, I developed my research skills in modelling.

My profound gratitude to the Mamena Association, Osakishimojima, for providing accommodation, data provision and their continued support when I was conducting fieldwork.

I owe special thanks to Dr. Fantong Wilson Yetoh for maintaining an open line of communication despite his busy schedule, stimulating discussions, constructive criticism, and suggestions throughout this PhD research project. In addition, I would like to give special recognition to Dr Fantong Emilia, who provided moral support and advice throughout the whole process.

I am also highly indebted and thoroughly grateful to my beloved family for supporting me throughout my research. Their prayers, words of encouragement, and moral support goes beyond words can express. Many thanks also go to colleagues and friends at Hiroshima University for their stimulating discussions, constructive criticisms and suggestions during our PhD Research Seminars and their support in any respect during the PhD research project. Many thanks also to Yusuke Tomozawa, Shingo Nozaki, and Tamura Masayuki for their kind assistance during fieldwork and laboratory analysis.

Throughout this project, I am deeply indebted to Dr. Anna Fadliah Rusydi of the Indonesian Institute of Sciences, Indonesia, and Dr. Naohiro Imamura of the Forestry and

Forest Products Research Institute, Japan, for their kind assistance and collaboration; for always motivating me and becoming an inspiration and role model of a hard-working person to emulate. Dr Anna Fadliah Rusydi, thank you for teaching me how to operate the SWAAT analysis tool, which is a fundamental part of my results. I also appreciate your unwavering support, comforting words, and motherly advice, which always encourages me when I feel downcast. I look forward to having many more opportunities to learn from you in the future.

Lastly, this acknowledgement would not be complete if I failed to thank all those who directly or indirectly contributed to this thesis and whose names have been forgotten.

Chapter 1

Introduction

1.1 Background of Study

According to Rockstrom et al. (2009), planetary boundaries represent the limits at which environmental changes take place and Earth's regulatory capacity maintains conditions for human survival and development. As a result of the uncontrolled development of anthropogenic activities after the industrial revolution in the eighteenth century, human's activities have reached threshold which is gradually harming the earths systems. This could have dramatic and irreversible effects on the environment with severe impact on water resources which have become increasingly more vulnerable (Al-Sudani, 2019).

Globally, about 54% of the population resides in cities, and that number is projected to increase from 60% to 92% by the year 2050 (Ritchie and Roster, 2018). In recent years, half of the top 20 cities in terms of average annual population growth rate (percent) are developing cities in East, Southeast, and South Asia (http://www.citymayors.com). There has been a significant change in the structure and size of the population as a result of changing demographic factors (Reynaud and Miccoli, 2018). These demographic factors have raised concerns with respect to the effect of population growth on water resources quantity and quality. Despite rapid global population growth, population densities are declining in some regions and the proportion of aged people in most developed countries rising (Figure 1.1). In most countries, the number of elderly people (greater than 60) has increased dramatically in recent years, and this trend is expected to accelerate in the coming decades with a faster aging pace in the developed countries of Asian and Pacific region accompanied by significant social

transformations (United Nations, 2015). In spite of this global trends, Japan has experienced this demographic transition faster than most Western and Asian countries, with an increasing number of citizens over the age of 65 (Hayashi et al., 2021).

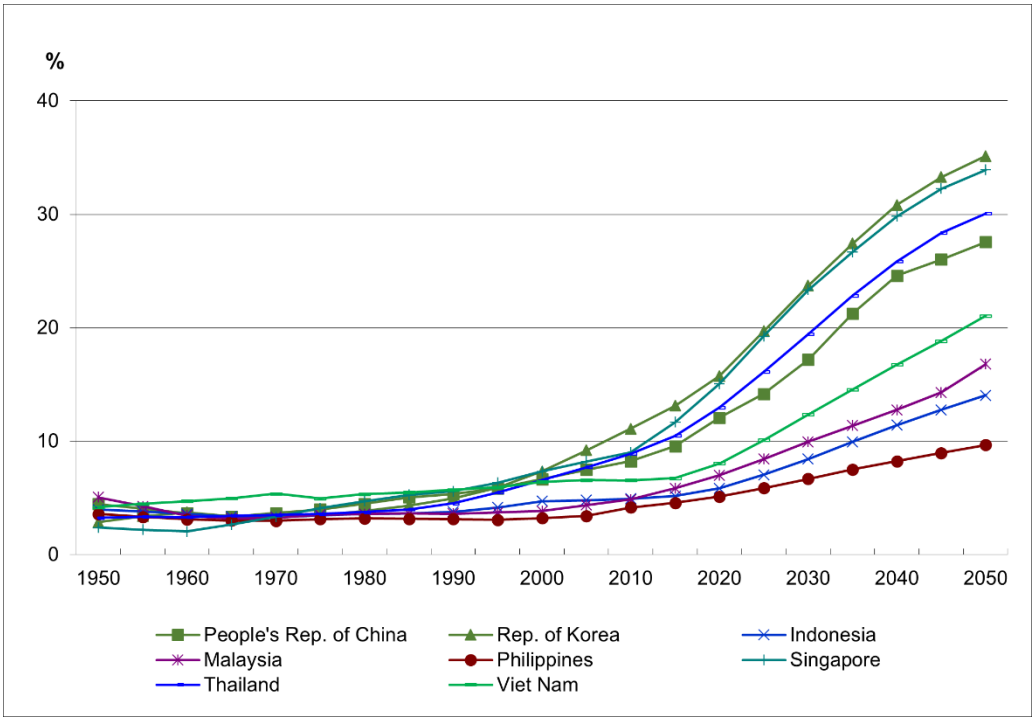

Figure 1.1: Ratio of population aged ≥ 65 to total population, 1950–2050 (Source:United Nations, Department of Economic and Social Affairs, Population Division, 2015).

However, despite these changes in its demographics, it still faces serious environmental problems related to groundwater quantity and quality as documented by (Tase, 1992; Onodera et al., 2011; Haque et al., 2013). Also, between the 1950s and 1970s, Japanese megacities such as Tokyo, Osaka, and Nagoya experienced severe groundwater drawdowns and significant groundwater-related problems (Onodera and Saito, 2005). Due to severe air and water pollution caused by rapid economic growth in Japan in the 1950s and 1960, significant pollution control policies and technological measures were enacted since the 1970s to curb this problem (Barrett and Therivel, 1991). Hence understanding the effects of changing population demographics on

the groundwater environment and its related environmental and social implication are of guiding importance for future water resources management especially with increasing urbanization and population aging.

Rational management of water resource quality and quantity necessitates a basic understanding of the natural processes that affect water resources as well as human impacts on these processes (Hem, 1989; Deutsch, 1997; Appelo and Postma, 2005; IAEA, 2006). The scientific and technological advances of the 20st century led to a rapid global increase in urbanization and industrialization (Hayashi et al., 2009) with an increasing pressure on the freshwater resources. In response to urbanization, land-use practices in many regions have changed with the reduction of natural land area and increase in impervious cover, affecting water balance, particularly in the catchment, and leading to a decline in groundwater availability (Lerner, 2002; Weng and Yang, 2004). In addition, as cities face more water-related environmental problems, this could cause water shortages and groundwater overuse, as well as an overall impact on the quantity and quality of freshwater resources (Onodera, 2011; Steffen et al., 2015; Doveri et al., 2015; Liu et al., 2020). Land use is a key determinant of water balance, which in turn affects water resource availability (Calder, 1993; Wang et al., 2021; Ridwansyah et al., 2020) and has been recognised as a key issue threatening watershed management (Yigzaw and Hossain, 2016). Considering the changes in the hydrological cycle due to urbanization, it is important to study the impact of urbanization on local water resources (Wakode et al., 2014).

The sustainability of water supply is not only affected by anthropogenic changes, but also by climate change (Leta et al. 2016; Zareian et al., 2016). Extreme events such as droughts and floods are becoming more frequent and intense as a result of global warming (PEACE, 2007). The combined changes in rainfall patterns and temperature increases have significant implications for the availability of water sources (Gibson et al., 2005). It is therefore important

to assess the impacts of climate change and anthropogenic activities on changes in the water balance to plan and manage water resources for future sustainable use (Wang et al., 2018). Numerous studies have demonstrated the impact of land use and climate change on water balance and hydrological processes at the global and watershed scales (Leta et al., 2016; Kundu et al., 2017; Bajracharya et al., 2018; Ridwansyah et al., 2020). These impacts can be evaluated based on hydrological models contained in references such as (Meenu et al., 2013; Ou et al., 2017; Kundu et al., 2017; Saefulloh et al., 2018). These models when calibrated can be used to assess the temporal and spatial effects of land-use change and climate change as well as predict possible future impact through scenario analysis.

Amongst these models, the Soil Assessment Tool (Arnold et al., 2012; Grassman et al., 2007), is a comprehensive, semi-distributed, continuous-time, processed-based model which has been widely used to correlate the relationship between surface water and groundwater as well as predict the effects of potential changes in hydrologic components at the catchment scale (Ridwansyah et al., 2012). However as hydrologic components tend to show spatial-temporal variability owing to different climatic conditions, land use, and hydrogeological settings, previous studies have integrated semi-distributed catchment scale model (SWAT with fully distributed MODFLOW groundwater models such as SWAT−MODFLOW (Chung et al., 2007; Kim et al., 2008; Dowlatabadi and Zomorodian, 2016). Hence, the use of a watershed model to understand how land use change with urbanization and climate change affects the hydrological cycle is critical with major implications for future sustainable water use and land use planning (Baker and Miller, 2013). The ever-growing demand for freshwater, coupled with the rate at which much of the earth's fresh waters are being adversely affected by human activities, portends a developing crisis if appropriate management procedures are not implemented (IAHS, 1997). Hence, there is a need to identify approaches that would minimize human impacts on the urban groundwater environments with results applied to areas currently

experiences ground water related problems associated to either, urbanization, climate change, depopulation, and population aging.

1.2 Problem Statement

Population growth and increasing economic condition have led to the continuous expansion and transformation of rural catchments with subsequent related groundwater problems. Despite the numerous studies on the impacts of anthropogenic activities on groundwater resources in Japan both qualitative and quantitatively, little attention has been paid on the combine effects of social and environmental issues on groundwater resources in mountainous rural catchments. Most of these catchments are either rapidly been transformed into urban catchments or experiencing rapid depopulation such as in Osakishimojima island. Aging populations is a major issue for Asian countries, and Japan stands as a model for dealing with environmental issues under these changes. Despite the decrease in contaminant loads originating from human activities as population declines rural catchments, these catchments may equally phase an increase in contaminant loads in the groundwater sources originating from non-point sources (e.g., agricultural fields and sewage systems) which becomes neglected and poorly managed. Thus, a need to evaluate the effects of social challenges on groundwater resource availability.

On the other hand, compared to continental catchments, most of Japan's water catchments are located in mountainous areas, which are known to have higher groundwater potential flows, supporting substantial groundwater resources. In spite of these benefits to the groundwater resource environment, environmental problems arising from urbanization processes, land use changes and climatic changes can result in a significant decrease in groundwater resources, such as in Saijo and Kurose. As a result, we seek to confirm not only the environmental impacts (urbanization and climate change) on the groundwater resource

environment but also the social impacts (depopulation and population aging) so that we can propose sustainable water resource management schemes under such changing social and environmental trends.

Additionally, this study will provide the public with a glimpse into the environmental and social challenges posed by aging and depopulating societies, since many cities in Japan and third-world countries are either experiencing or are rapidly approaching similar demographic challenges.

1.3 Objective

The general objective of this study is to provide a comprehensive evaluation of human impacts on groundwater resources in mountainous catchments, western Japan. Furthermore, the specific objectives are focused on three sub-objectives which provide an insight into changes brought about by anthropogenic activities on groundwater resource quality and quantity using environmental isotopes and watershed hydrological model.

1. Investigate the social impacts (depopulation and population aging) on groundwater nitrate-nitrogen contamination and potential sources in an intensive citrus cultivation island.
2. Estimate the spatial variation in groundwater recharge under the influence of urbanization and climate change in the last three decades.
3. Evaluate the groundwater chemistry and contamination status in Saijo basin.

1.4 Structure of Thesis

This thesis is divided in seven chapters (Figure 1.2). Chapter 1 describes general introduction, background, and objectives. Chapter 2 provides knowledge related to selected study sites, samples collection, and study literature pertaining to specific objectives. Furthermore, summary of data analysis and interpretation are described within three chapters: Chapter 3, Chapter 4 and Chapter 5. Chapter 6 stresses on the total discussion of the human impact on water resources associated to the three previous chapters. Finally, the conclusion is delivered in Chapter 7.

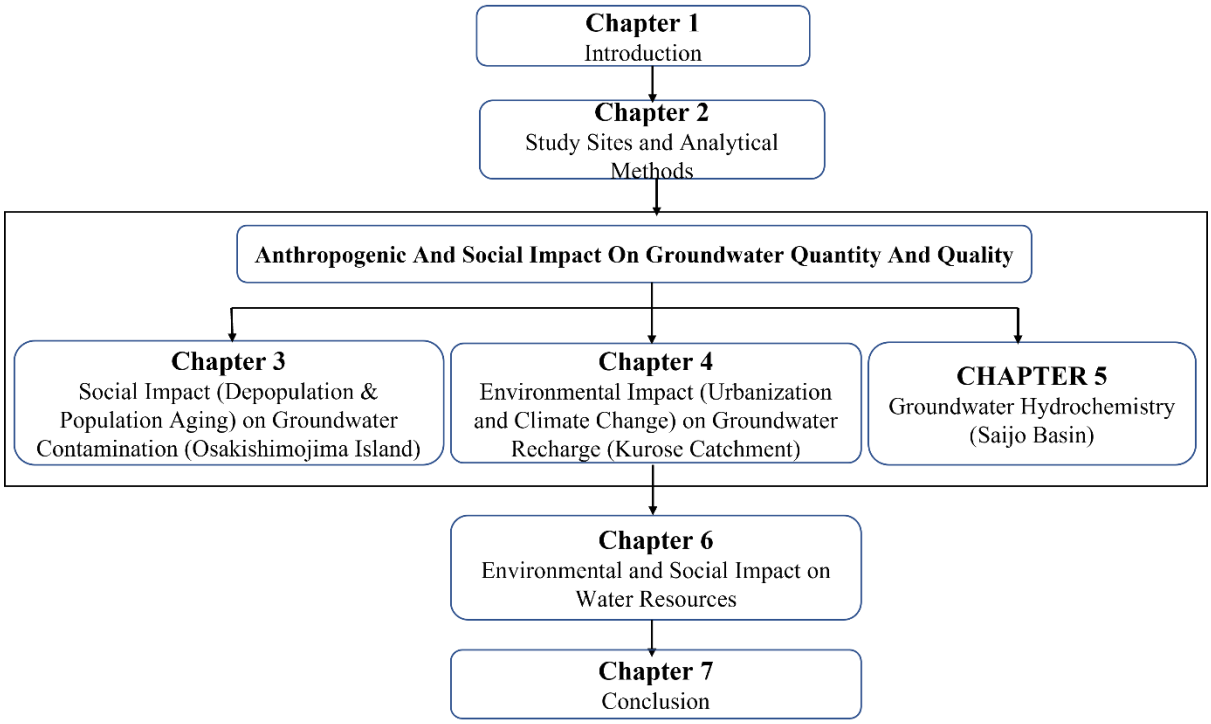

Figure 1.2: Structure of thesis.

Chapter 3 (Paper 1) entitled "Nitrate Contamination in Groundwater: Evaluating the Effects of Demographic Aging and Depopulation in an Island with Intensive Citrus Cultivation" deals with groundwater nitrate contamination and their potential sources in two neighbouring villages and watersheds with little differences in their social aspect (population aging and

depopulation) using hydrochemistry data, dual isotope approach as a source tracer and a Bayesian mixing model to determine the source contribution ratios.

Chapter 4 (Paper 1) entitled "Simulation of daily streamflow with SWAT illuminates the impact of land-use change with urbanization and climate change on groundwater recharge over the last three decades". Based on the SWAT model approach, this chapter examines the spatial variation in groundwater recharge under the effects of urbanization and climate change, based on water balance components over a period of three decades (1980s-2000s), in western Japan. Because SWAT can output both direct and relative urbanization impact, these results will provide a better understanding of groundwater resource availability and implication for future management at the regional scale especially as the study area is currently undergoing rapid transformation from rural to urban environment.

Chapter 5 (Paper 3) entitled "Groundwater contamination status in saijo basin: insights from hydrochemistry and dual isotope" addresses groundwater quality using hydrochemical data. Also, the potential sources of groundwater contamination are addressed using environmental tracer approach. This chapter examines more closely the relationship between groundwater and surface water dissolved inorganic nitrogen (DIN)sources.

Chapter 6: represents a general discussion on the anthropogenic impacts on groundwater resources from the model approach. Further, Social impacts on ground water nitrate-nitrogen is discussed and compare using three sites as case study.

Chapter 7 presents the general conclusions and summary of the major results of the study outlined in chapters 3 to 5

1.5 References

Al-Sudani, H.I.Z. Groundwater system of Dibdibba sandstone aquifer in south of Iraq. *Appl. Water. Sci.* **2019***,* 9, 72.

Appelo, C.A.J., Postma, D. Geochemistry, groundwater, and Pollution. 2nd ed., Balkema, Amsterdam, **2005**, 636.

Arnold J.G., Moriasi D.N., Gassman, P.W., Abbaspour, K.C., White, M.J., Srinivasan, R., Santhi, C., Harmel, R.D., Van Griensven A., Van Liew, M.W., Kannan, N., Jha, M.K. SWAT model use calibration, and validation. *Trans. ASABE*. **2012**, 55, 1491–1508.

Bajracharya, A.R., Bajracharya, S.R., Shrestha, A.B., Maharjan, S.B. Climate change impact assessment on the hydrological regime of the Kaligandaki Basin, Nepal. *Sci. Total. Environ*. **2018**, 625, 837–848.

Baker, T.J., Miller, S.N. Using the Soil and Water Assessment Tool (SWAT) to assess land use impact on water resources in an East African watershed. *J. Hydrol*. **2013**, 486, 100-111.

Barrett, B.F.D., Therivel, R. Environmental Policy and Impact Assessment in Japan. 1st ed., Routledge, New York, **1991**, 288. https://doi.org/10.4324/9780429199165.

Calder, I.R. Hydrologic effects of land-use change. In: Maidment, D.R. 1st ed., Handbook of Hydrology. McGraw-Hill, New York, **1993**, 13.1–13.50.

Chung, I.-M., Kim, N.-W., Lee, J., Sophocleous, M. Assessing distributed groundwater recharge rate using integrated surface water-groundwater modelling: Application to Mihocheon watershed, South Korea. *Hydrogeol. J*. **2010**, 18, 1253–1264.

Deutsch, W.J. Groundwater geochemistry: fundamentals and application to contamination. CRC, Boca Raton, **1997**, 221.

Doveri, M., Menichini, M., Scozzari, A. Protection of groundwater resources: worldwide regulations and scientific approaches. In Threats to the Quality of Groundwater Resources. Springer, Berlin, Heidelberg, **2015**, 13-30.

Dowlatabadi, S., Zomorodian, S.M.A. Conjunctive simulation of surface water and groundwater using SWAT and MODFLOW in Firoozabad watershed. KSCE *J. Civ. Eng*. **2016**, 20, 485–496.

Drever, J.I. The geochemistry of natural waters. 2nd edn., Prentice Hall Inc, Englewood Cliffs, **1988**, 402.

Gassman, P.W., Reyes, M., Green, C.H., Arnold, J.G. The soil and water assessment tool: Historical development, applications, and future directions. *Trans. ASABE*. **2007**, 50, 1211–1250.

Gibson, C.A., Meyer, J.L., Poff, N.L., Hay, L.E, Georgakakos, A. Flow regime alterations under changing climate in two river basins: implications for freshwater ecosystems. *River Res Applic*. **2005**, 21, 849– 864.

Haque, S.J., Onodera, S., Shimizu, Y. An overview of the effects of urbanization on the quantity and quality of groundwater in South Asian megacities. *Limnol*ogy. **2013**, 14, 135–145.

Hayashi, K., Shibata, H., Oita, A., Nishina, K., Ito, A., Katagiri, K., Shindo, J., Winiwarter, W. Nitrogen budgets in Japan from 2000 to 2015: Decreasing trend of nitrogen loss to the environment and the challenge to further reduce nitrogen waste. *Env. Pol*. **2021**, 286, 117559.

Hayashi, T., Tokunaga, T., Aichi, M. S., Jun, T. M. Effects of human activities and urbanization on groundwater environments: An example from the aquifer system of Tokyo and the surrounding area. *Sci. Total. Environ*. **2009**, 407, 3165-3172.

Hem, J. Study and Interpretation of the Chemical Characteristics of Natural Water. U.S Geological Survey Water-Supply Paper.**1989**, 2254.

IAHS (International Association of Hydrological Science). Hydrogeochemistry. Proceedings of an international symposium. In: Peters N.E. and Coudrain-Ribsten A. 1st ed., IAHS Press, Rabat, Morocco.**1997**.

IAEA (International Atomic Energy Agency). Use of chlorofluorocarbons in hydrology: A guidebook.**2006**. http://www-pub.iaea.org/MTCD/publication/PDF/Pub1238_web.pdf.

Kim, N.W., Chung, M., Won, Y.S., Arnold, J.G. Development and application of the integrated SWAT–MODFLOW model. *J. Hydrol*. **2008**, 356.

Kundu, S., Khare, D., Mondal, A. (2017). Individual and combined impacts of future climate and land use changes on the water balance. *Ecol. Eng*. **2017**, 105, 42–57.

Lerner, D.N. Identifying and quantifying urban recharge: a review. *Hydrogeol. J.* **2002**,10, 143–152.

Leta, O.T, El-Kadi, A.I., Dulai, H., Ghazal, K.A. (2016). Assessment of climate change impacts on water balance components of Heeia watershed in Hawaii. *J. Hydrol. Reg. Stud*. **2016**, 8, 182–197.

Liu, X., Huang, Y., Xu, X. High-spatiotemporal-resolution mapping of global urban change from 1985 to 2015. *Nat Sustain*. **2020**, 3, 564–570.

Meenu, R., Rehana, S., Mujumdar, P. Assessment of hydrologic impacts of climate change in Tunga-Bhadra River basin, India with HEC-HMS and SDSM. *Hydrol. Process*. **2013**, 27, 1572–1589.

Onodera, S., Saito, M. (2005). Approaches to estimation of contaminant load variation at Mega-cities. Proceedings of RIHN International Symposium on Human Impacts on Urban Subsurface Environments. **2005**, 32–5.

Onodera, S. Subsurface pollution in Asian megacities. In Groundwater and Subsurface Environments: Human Impacts in Asian Coastal Cities; Springer: Berlin/Heidelberg, Germany. **2011**,159–18.

Onodera, S.-I. Groundwater and Subsurface Environments. Human Impacts in Asian Coastal Cities. Springer Tokyo. **2011**, 159–184.

Ou, X, Gharabaghi, B., McBean, E., Doherty, C. Investigation of the tank model for urban storm water management. *J. Water. Manag. Model*. **2017**, 233-240.

PEACE. Indonesia and climate change: current status and policies. **2007**, pp 1–2.

Reynaud, C., Miccoli, S. Depopulation and the Aging Population: The Relationship in Italian Municipalities. *Sustainability*. **2018**, 10.

Ridwansyah, I., Yulianti, M., Apip, Onodera, S.i., Shimizu, Y., Wibowo, H., Fakhrudin, M. The impact of land use and climate change on surface runoff and groundwater in Cimanuk watershed, Indonesia. *Limnol*ogy. **2020**, 21, 487–498.

Ritchie, H., Roser, M. Urbanization. Our world in data. **2018**.

Rockström, J., Steffen, W., Noone, K. Persson, Å., Chapin III., S.F., Lambin, E.F., Lenton,T.M., Scheffer, M., Fole, C., Schellnhuber, H.J., et al. A safe operating space for humanity. *Nature*. **2009**, 461, 472–475.

Saefulloh, D.F., Hadihardaja, I.K., Harlan, D. Modeling of triangular unit hydrographs using an artificial neural network in a tropical river basin. *Int. J. Geo*. **2018**, 15, 69–76.

Tase, N. Groundwater contamination in Japan. Environ. Geol. Water Sci. **1992**, 20, 15–20.

United Nations, Department of Economic and Social Affairs, Population Division. World Population Prospects: The 2015 Revision, DVD Edition. **2015**.

Wakode, H. B., Baier, K., Jha, R., Ahmed, S., Azzam, R. Assessment of impact of urbanization on groundwater resources using GIS techniques – Case study of Hyderabad, India. Int. *J. Environ. Res*. **2014**. 8, 1145–1158.

Wang, J., Gao, Y., Wang, S. Assessing the response of runoff to climate change and human activities for a typical basin in the Northern Taihang Mountain, China. *J. Earth. Syst. Sci*. **2018**, 127, 1−15.

Wang, K., Onodera, S.I., Saito, M., Shimizu, Y. Long-term variations in water balance by increase in percent imperviousness of urban regions. *J. Hydrol.* **2021**, 602, 126767.

Weng, Q. H., Yang, S. H. Managing the adverse thermal effects of urban development in a densely populated Chinese city. *J. of Environ. Manage*. **2004**, 70, 145−56.

Yigzaw, W., Hossain, F. Land use and land cover impact on probable maximum flood and sedimentation for artificial reservoirs: Case study in the Western United States. *J. Hydrol. Eng*. **2016**, 21, 05015022.

Zareian, M.J., Eslamian, S.S., Safavi, H.R. Investigating the effects of sustainability of climate change on the agriculture water consumption in the Zayandeh-Rud River basin. *JWSS-Isfahan. Univ. Technol*. **2016**, 20, 113–128. (In Iranian)

Chapter 2

Study Sites and Analytical Methods

2.1 Location and Description

This study was conducted in three Japanese mountainous catchments (Kubi and Ocho watershed in Osakishimojima island, Kurose River catchment and Saijo watershed, and) and are briefly discussed in this chapter alongside their Methodology (Figure 2.1).

2.1.1 Kurose River catchment and Saijo watershed

The Kurose River catchment (Figure 1A), with a geographic area of approximately 39.5 km^2, is situated between latitude 34°25′30′′N and longitude 132°44′33′′.

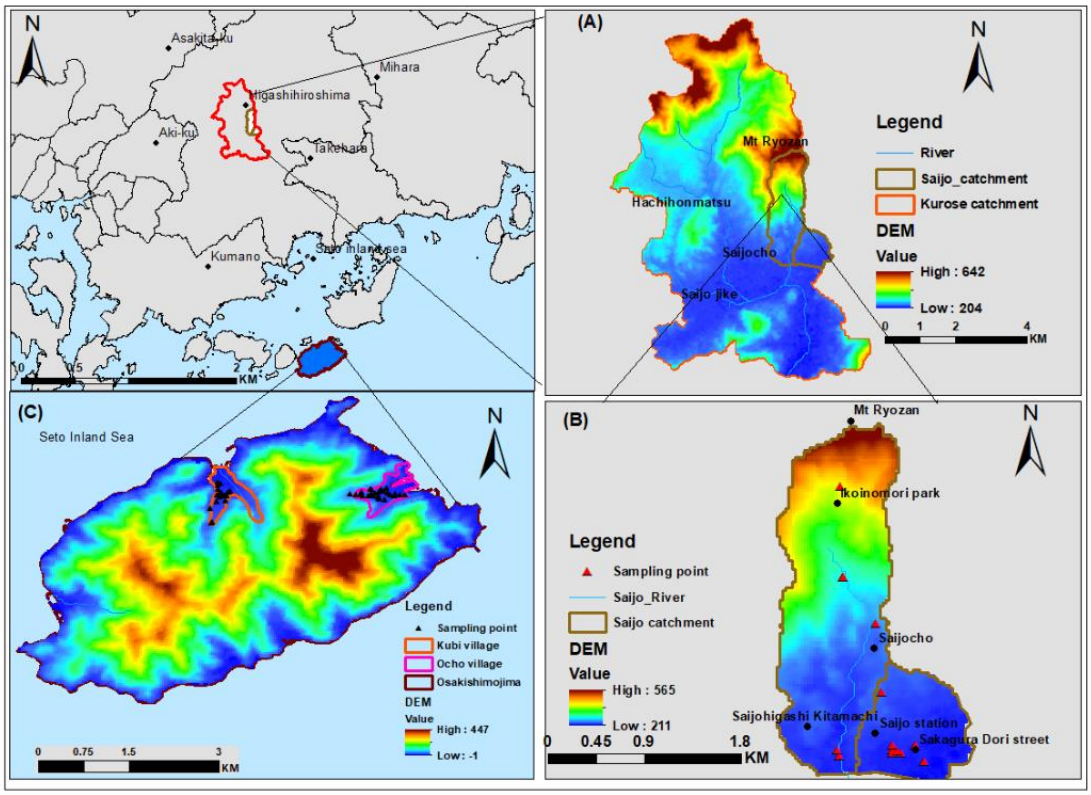

Figure 2.1: Location of study sites in Higashihiroshima city (A) Kurose River Catchment located in center Higashihiroshima city, (B) Saijo Watershed located in eastern Kurose River Catchment, and (C) Osakishimojima Island.

The Saijo watershed or subbasin is located within the Kurose River catchment, hence their climatic conditions and geology are similar. The total population in the former Higashihiroshima city (Figure 2.2) which includes the saijo watershed and Kurose River catchment has doubled over the past three decades, growing from 74,235 persons in the 1980s to approximately 130 thousand persons in late the 2000s at an urbanization rate of 0.25% per decade (Higashihiroshima city report, 2021). Note: urbanization here refers to the gradual increase in the proportion of people living in urban areas and has been calculated as a relative percentage change of the total population from 1980s to 2000s.

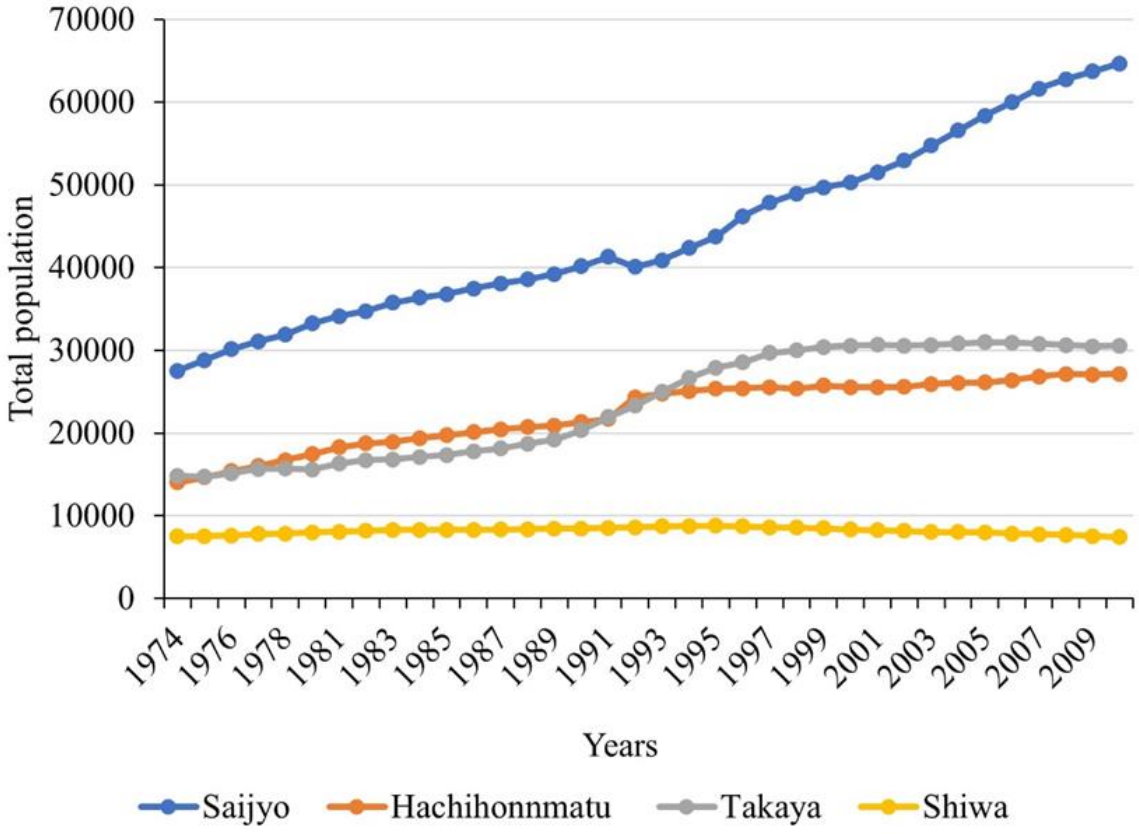

Figure 2.2: Population trend in Higashihiroshima from 1974 in four of its major towns.

Kurose catchment area has undergone land use changes since the 1980s owing to anthropogenic activities (Figure 2.3) with a greater portion of paddy fields converted to residential areas. Also, the Kurose River catchment is characterized by a warm humid climate with mean annual daily temperature varying from 12 °C to 15 °C and mean annual precipitation is approximately 1469 mm. Further detail on the Kurose River Catchment is expatiated on in Chapter 3.

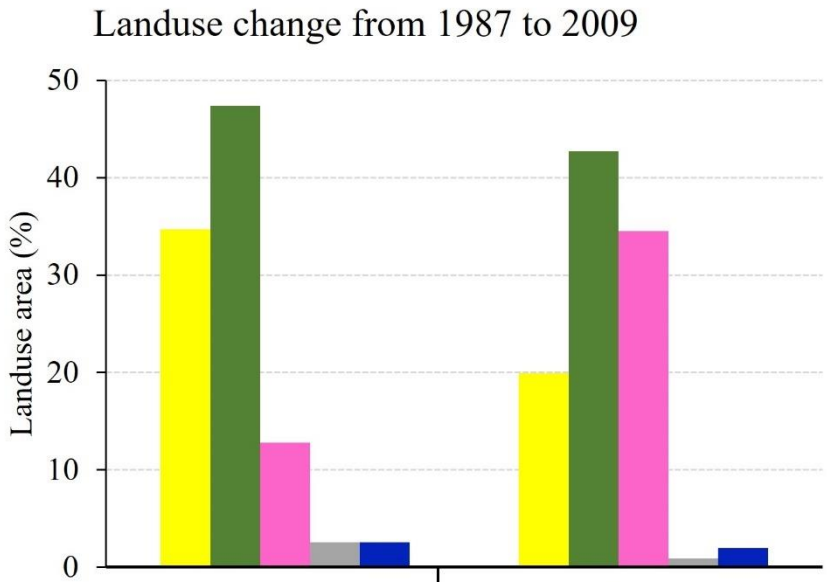

	1987	2009
Rice	34.69	19.94
Forest	47.34	42.7
Residential	12.8	34.53
Other	2.58	0.86
Water	2.59	1.97

Figure 2.3: Land use change from 1987 to 2009 in the Kurose River Catchment.

2.1.2. Osakishimojima Island

Osakishimojima is a small island located along the stretches of the Seto inland sea in Hiroshima prefecture, western Japan (Figure 1.1C) about 10km off the coast of Kure city. Its surface area is about 43 km^2 with geographic coordinates 34º10'24"N and 132°50'3"E. This

modest-sized island is large enough to be lined with steep mountains and narrow valleys yet small enough to be tucked away amid a cluster of other islands. Osakishimojima experiences a warm temperate climate with an annual average temperature of 15.6 ◦C and with an average annual precipitation of approximately 1000mm. The four seasons are distinct with cold weather during the winter and hot weather during summer months.

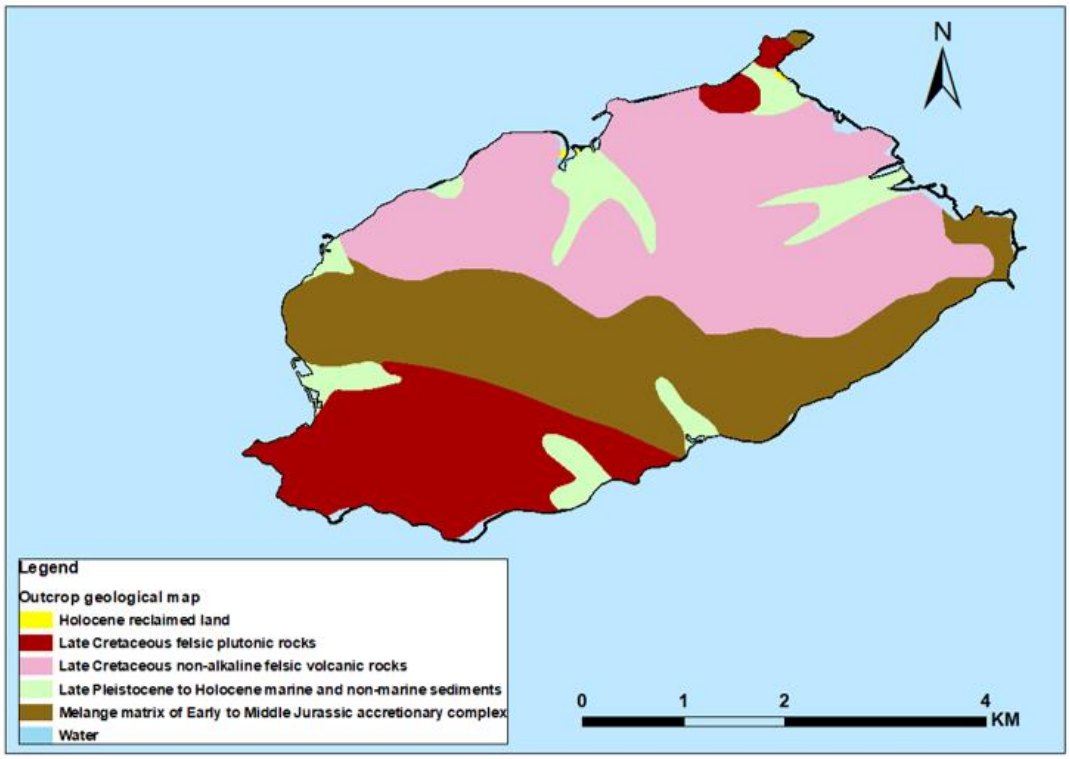

Figure 2.4: Outcrop geological map of Osakishimojima Island.

The geological map (Figure 2.4) of the study area shows that Osakishimojima basin consists of Quaternary deposits that lie on top of a basement made up of igneous rocks. The Quaternary cover consists of Late Pleistocene to Holocene marine and non-marine formations that occupy 8.8% of the land and Holocene reclaimed land that occupies 0.1% of the basin. Among the underlying units, a mélange matrix representing a Middle Jurassic accretionary complex covers 30.7% of the surface whereas 19.7% of the land are covered by Late Cretaceous felsic plutonic rocks and 40.9% are occupied by Late Cretaceous non-alkaline felsic

volcanic rocks. Only 0.1% of water is found on the island surface. Osakishimojima is dominated by forest and agricultural land (Figure 2.5) made up of citrus fields. The island has well-drained soil which makes it perfect to grow citrus rendering it famous for its rich cultivation of Mikan (Japanese mandarin) and lemon. Because of its sheltered location and gentle climate, Osakishimojima is Japan's citrus island taking advantage of the calm air, strong sunlight, light rainfall, and good mountain drainage, which is so important for citrus orchards cultivation.

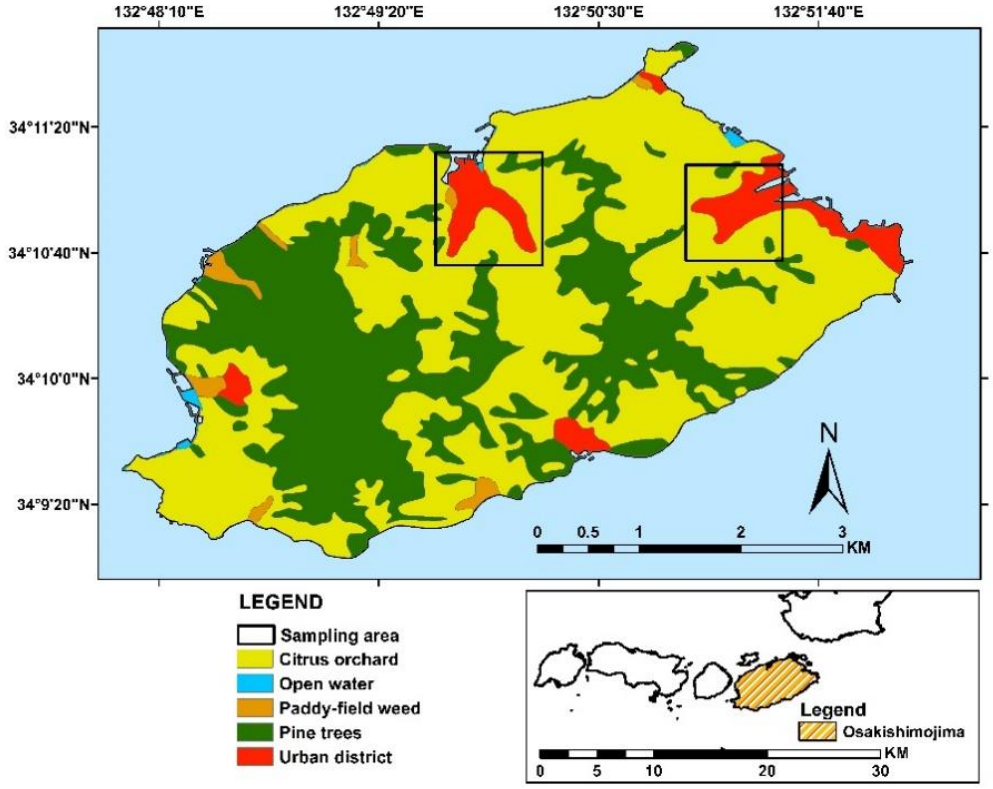

Figure 2.5: Land use of Osakishimojima Island.

2.2 Research Methods

The methods followed in the research process are based on the objectives formulated in Chapter 1 section 1.3. The methodology designed for the research work consists of two major approaches.

1. The hydrochemical approach which consist of pre-fieldwork, fieldwork, and post-fieldwork. This approach has been applied to chapters 3 and 5 to determine groundwater contamination status and proportional contribution rates using nitrogen 15 isotopes and Bayesian micing model

2. The Soil and Water Assessment Tool (SWAT) used in chapter 4 on the Kurose River catchment to estimate the groundwater recharge under the influence of climate change and urbanization will be introduced in this chapter

2.2.1 Hydrochemical approach

2.2.1.1 Pre-field, field, and Post field work

The major task of this phase in the study has been devoted to the review of previous works on the area and literature related to the hydrochemical and environmental tracer methods in hydrological investigations. Apart from the literature review, an archive search SRTM of the study area was also part of the pre-fieldwork. Delimitation and selection of the sample points, acquisition of equipment and preparation of data requirement list and data collection form were the activities conducted before the field trip.

In the present study, a total of 52 water samples were collected from Kubi and Ocho villages in Osakishimojima island in the month of October 2021 while 17 water samples were collected from the Saijo area. These samples are classified as follows:

- Kubi village: One borehole, two rivers and seventeen shallow wells
- Ocho village: two springs and thirty shallow wells
- Saijo town: eleven boreholes, three springs, three shallow wells, and one river

Geographical parameters (latitude, longitude, and altitude) of each sample site were recorded on the field using a hand-held Garmin GPS. The water samples intended for major ions analysis were collected in acid washed into one 250 mL, three 10 mL, and one 100 mL

high-density polyethylene sampling after rinsing three times with the sample and preserved airtight to avoid evaporation. Water samples were filtered through a 0.2μm membrane and stored at −4°C for further hydrochemical and isotopic analyses. Physicochemical parameters including groundwater pH, temperature, electrical conductivity (EC), dissolved oxygen (DO), and oxidation-reduction potential (ORP) were measured on-site using a portable multiparameter water quality meter (pH/COND Meter D-54, HACH LD0101, ORP Meter RM-20P). The values of these parameters were recorded after they were stably displayed. Surface water samples were obtained by submerging the sampling bottles into the water at areas where there is an active, but not turbulent flow. Water was drawn from the open wells using drawing buckets tied with ropes. Static water levels in open wells and boreholes were measured.

Data collected during the pre-fieldwork period and fieldwork are processed and analyzed. The analysis of the samples for major ions, nutrients and Nitrogen 15 isotope has been carried out at the biogeochemistry lab, Hiroshima University and Institute of Geosciences, Yamanachi University. The concentrations of the major cations (Na^+, K^+, Mg^{2+}, and Ca^{2+}) and anions (Cl^-, NO_3^-, and SO_4^{2-}) were analyzed by ion chromatography with conductivity detection on ICS-2100 (Dionex integrion, Thermo Fisher Scientific, Waltham, MA, USA). Alkalinity was analyzed within 12 h of sample collection by acid titration. A volume of 0.02 N sulfuric acid (H_2SO_4) was added to the sample to reach the end point titration (pH 4.5). To evaluate the data quality, the accuracy of the water analysis was checked with the anion-cation balance. The principle of the anion–cation balance is that the sum of the positive ionic (cationic) charges (expressed in meq/L) in a solution should equal the negative ionic (anionic) charges; this because the solution must be electrically neutral. The electroneutrality of the water samples is commonly calculated with the following equation of Hounslow, 1995:

$$Electroneutrality\ (\%) = \frac{\sum(\text{Cations}) - \sum(\text{Anions})}{\sum(\text{Cations}) + \sum(\text{Anions})} x100 \qquad (2.1)$$

According to Appelo and Postma (1999), solutes present in concentrations above 100 mg/l can be determined with an accuracy of better than ± 5 %. For solutes concentrations below 1 mg/l the accuracy is generally not better than ± 10 % and can be poorer. When concentrations are near the detection limit of the method used, and in all determinations of constituents that are near or below the mg/l level, both accuracy and precision are even more strongly affected by the experience and skill of the analyst (Deutsch, 1997).

2.2.1.2 Data Analysis and graphical methods

To meet the objectives fixed for this study, the analysis and interpretation of standard hydrochemical and environmental tracers' data are required in order to determine the distribution, transit time and movement of dissolved species throughout the studied areas, and to investigate hydrological links between groundwater and surface. This was achieved using conventional graphical plots and multivariate statistical techniques which are described below. Various graphical methods have been developed for the visual inspection of the Hydrogeochemical data in order to look for discernible patterns and trends. Piper's trilinear diagram, Stiff diagram, Gibbs diagrams and Wilcox were used to determine water type, degree of mineralization, spatial variation in the chemistry of the water samples and to identify dominant processes and detect grouping of water samples as used by (Fantong et al.,2009; Kamtchueng et al., 2016).

For this study the Gibbs and Piper diagrams were used. The Piper's diagram is a graphical representation of the chemistry of a water sample or samples were cations and anions are shown by separate ternary plots (Piper, 1994). The apexes of the cation plot are calcium, magnesium and sodium plus potassium cations. The apexes of the anion plot are sulphate, chloride and carbonate plus hydrogen carbonate anions. The two ternary plots are then projected onto a diamond (Figure 2.6). The diamond is a matrix transformation of a graph of the anions (sulphate + chloride/ total anions) and cations (sodium + potassium/total cations).

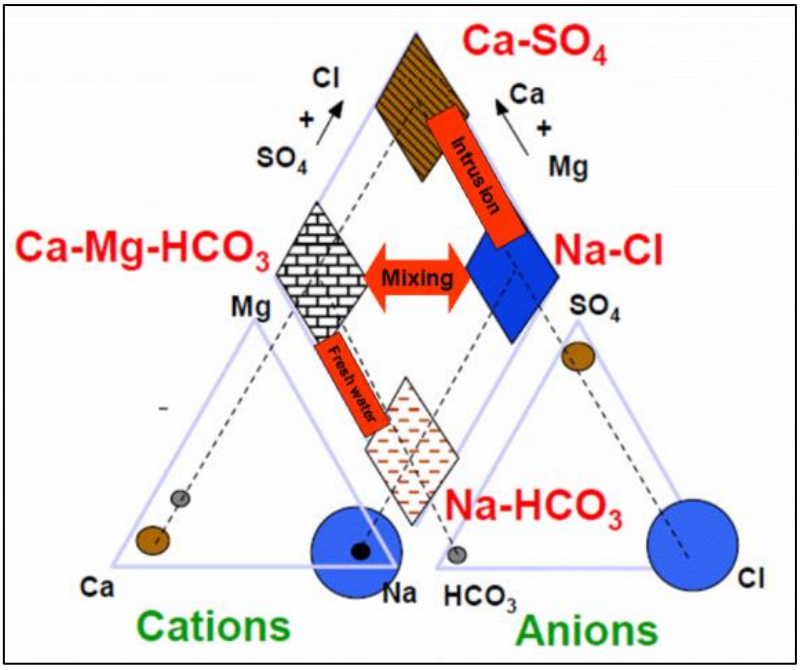

Figure 2.6: Piper diagram; cations and anions are expressed as percentages of total in meq/L.

2.2.1.3 Multivariate statistical method

Multivariate statistical analysis (MSA) consists of a collection of methods that can be used when several measurements are made on each individual or object in one or more samples (Rencher, 2002). Amongst the numerous MSA available, coefficient of determination (R^2). In addition to correlation analysis, principal component analysis (PCA) was used to analyze groups of ions based on similarities or differences in concentrations. SPSS® ver. 23.2 (Statistical Package for Social and Management Science) was used to compute physicochemical parameters in order to produce Statistical tables, correlation analysis and bar graphs.

2.2.2 The Soil and Water Assessment Tool

The SWAT (soil and water assessment tool) model, developed by the USDA Agricultural Research Service, simulates the land phase of the hydrologic cycle in daily time steps. Routines are also included for simulating the detachment of sediments from the

watersheds and their transport through the drainage systems. The SWAT model is designed to route water and sediments from individual watersheds, through the river systems. The model can be used for the assessment of existing and anticipated water uses and water shortages. The model provides a complete accounting of the quantity of water that is supplied to the land by precipitation; enters the streams as surface run-off; is used and returned to the atmosphere by natural vegetation, agricultural crops and evaporation, and that percolates through the root zone and a part returns as groundwater contribution.

SWAT simulates the hydrological cycle of a watershed in two phases, the land phase and the routing phase (Figure 2.7).

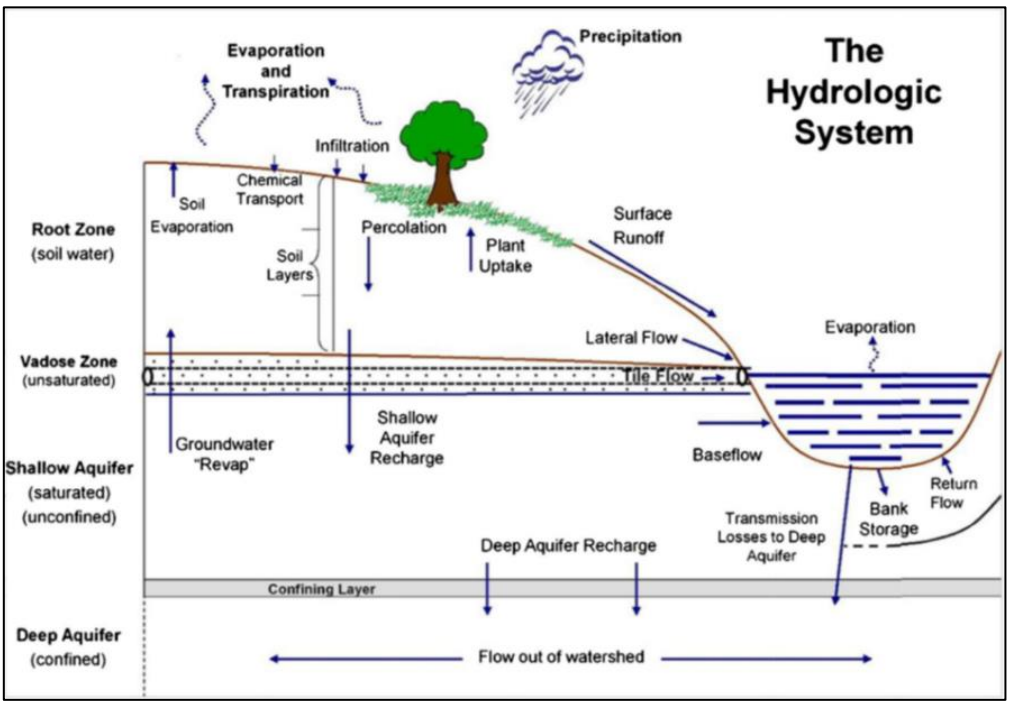

Figure 2.7: Schematic diagram of the hydrological cycle and SWAT simulation processes (Neitsch et al., 20011; Nasiri et al., 2020).

The land phase of the hydrologic cycle controls the movement of water, sediment, nutrient and pesticide loadings to the main channel in each sub-basin. The routing phase of the hydrologic cycle simulates the movement of water, sediments, etc. through the channel network

of the watershed to the outlet. The following sections describe both phases (i.e., the land and routing phases) and their components as simulated by SWAT. However, the description is focused on the relevant components and processes to this current work, so that the parts related to chemical modelling are not described. A full description of all processes in SWAT is given in Neitsch et al. (2011). The main hydrological components simulated in the land phase of the hydrologic process include canopy interception, infiltration, evapotranspiration, lateral subsurface flow, surface runoff, groundwater recharge and streamflow in a watershed. This study focused on the land-phase water balance, where land-use change has its main impact. The water balance governing the land phase of the SWAT hydrological cycle is given by Eq. (2.2), Neitsch et al. (2011):

$$SW_t = SW_o + \Sigma_{i=1}^{t}\left(R_{day} - Q_{surf} - E_a - W_{seep} - Q_{gw}\right) \qquad (2.2)$$

where, SW_t is the final soil water content on day i (mm); SW_o is the initial water content (mm) on day i; t is the time (days); R_{day} is the amount of precipitation on day i (mm); Q_{surf} is the amount of surface runoff on day i (mm); E_a is the amount of evapotranspiration on day i (mm); W_{seep} is the amount of water entering the vadose zone from the soil profile on day i (mm); and Q_{gw} is the total amount of return flow on day i (mm). SWAT offers two methods for estimating surface runoff: the Soil Conservation Service Curve Number (SCS-CN) method and Green and Ampt infiltration method (Green and Ampt, 1911). The SWAT calculates the surface runoff using the SCS curve number method, as shown in Eqs. (2.3) − (2.4) (Soil Conservation Service, 1972).

$$Q_{surf} = \frac{(R_{day} - 0.2S)^2}{(R_{day} + 0.8S)} \qquad (2.3)$$

$$S = 25.4\left(\frac{1000}{CN} - 10\right) \qquad (2.4)$$

where, CN is the curve number for the day and S is the retention parameter. SCS defines CN2 as a moisture condition II curve number, which is referred to as the average moisture condition. CN2 is primarily used as the curved number in SWAT, with daily CN2 adjusted from the moisture condition (Soil Conservation Service Engineering Division, 1986).

The SWAT model calculates evapotranspiration from soil and plants separately and provides three alternative methods for predicting potential evapotranspiration based on available information: (Hargreaves and Samani, 1985; Priestly− Taylor, 1972; Monteith, 1965). The information required for the Penman−Monteith method includes solar radiation, air temperature, wind speed and relative humidity. In the Hargreaves method, only air temperature information is required, and in the Priestley−Taylor method, radiation information, air temperature, and relative humidity are required. For this study, the Penman−Monteith method was used, which is given by Eq. (2.5):

$$E_o = \frac{\delta(ho + S) + \frac{\rho_a \, C_p (e_s - e_a)}{r_a}}{HV \left[\delta + \gamma \left[\frac{r_a - r_c}{r_a}\right]\right]} \qquad (2.5)$$

Where, E_o is evaporation (g m^{-2} s^{-1}), HV is the latent heat of vaporization (J g^{-1}), ho is the net radiation (J m^{-2} s^{-1}), δ is the slope of saturation vapor density function (g m^{-3} C^{-1}), S is the soil heat flux (J m^{-2} s^{-1}), γ is the psychometric constant (g m^{-3} C^{-1}), ρ_a is the air density (g m^{-3}), C_p is the specific heat of air (J g^{-1} C^{-1}), e_s is the saturation vapor density (g m^{-3}), e_a is the air vapour density (g m^{-3}), r_a is the aerodynamic resistance for heat and vapor transfer (s m^{-1}), and r_c is the canopy resistance for vapor transfer (s m^{-1}). Further details of the water balance equation can be found in the SWAT theoretical document (Neitsch et al., 2011).

2.2.2.1 Input data and model setup

SWAT model needs Digital Elevation Model (DEM) data as input for delineating the catchment boundary, sub-catchment, and stream network (Figure 2.8).

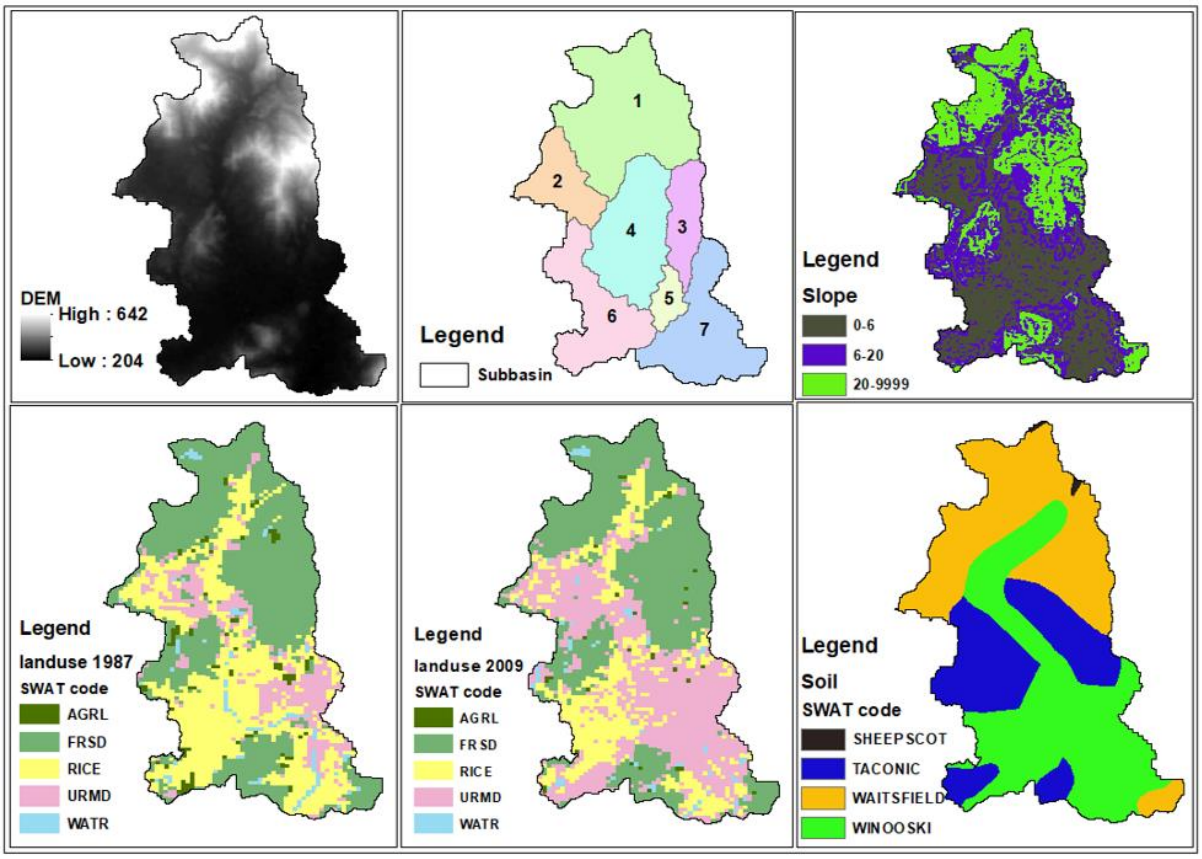

Figure 2.8: Input dataset in to ArcSWAT showing Digital Elevation Model (DEM), subbasins after watershed delineation, slope classes, land use classes and soil classes used in SWAT model for HRU definition.

The DEM, land use data, soil data and climatic data are required as input files for the SWAT. The DEM was used to delineate the watershed into sub-basins, drainage surfaces, stream networks and longest reaches. The topographic data were obtained from the Shuttle Radar Topography Mission of the United States Geological Survey, which has a spatial resolution of 30 m (https://eart hexplorer.usgs.gov/). Land use and soil data were obtained from the Ministry of Land, Infrastructure, Transport, and Tourism of Japan (MLIT), with a spatial resolution of 100 m (https://nlftp.mlit.go.jp/). To assess the effect of land-use change on

groundwater resources, it is necessary to possess data from at least two time periods for comparison. In this study, the 1987 and 2009 land use maps (Figure 2.8), were used for the simulation period of two-time steps, the 1980s (1983−1993) and the 2000s (2004−2007) respectively. The coverage areas of several land use categories and input database codes in the Arc SWAT are presented in Table 2.1.

Table 2.1: Land use classes used in ArcSWAT, area coverage, and comparison of land use change in 1987 and 2009.

Land use type	SWAT Name	1987		2009		Area of change (km^2)	Area of change (%)
		Area (km^2)	% Area	Area (km^2)	% Area	1987-2009	1987-2009
Rice	RICE	13.6	34.7	7.8	19.9	-5.9	-14.8
Agricultural	AGRL	1.0	2.6	0.3	0.9	-0.7	-1.8
Forest	FRSD	18.6	47.3	16.8	42.7	-1.9	-4.7
Residential	URML	5.0	12.8	13.6	34.5	8.6	21.8
Water	WATR	1.0	2.6	0.8	2.0	-0.3	-0.7

A total of five land-use classes (Figure 2.8) were classified from the downloaded Land use files: rice paddy, agricultural land, residential land, forests, water, and other (shrubs and agriculture). Significant land-use changes between the two land use maps were observed in the studied watershed, with three dominant land use categories: forest, rice paddy, and residential land. Four major soil groups were found, either as a single type or in association with other soil groups. The contribution of Grey low land soils (40.3%) in association with brown Regosol (34.1%) were discovered to have dominated the distribution of soil types in the study area (Figure 2.8).

The spatial datasets were converted to SWAT input datasets using ArcSWAT 10.6 (Geographical Information System interface) and the SWAT version 2012 was used for map

production and model set up. Figure 2.9 gives an overview of SWAT model components and phases in the GIS interphase. With respect to residential areas, this study assumed that the residential area is not completely impervious, providing some pervious spaces between the houses that are often used for house yards.

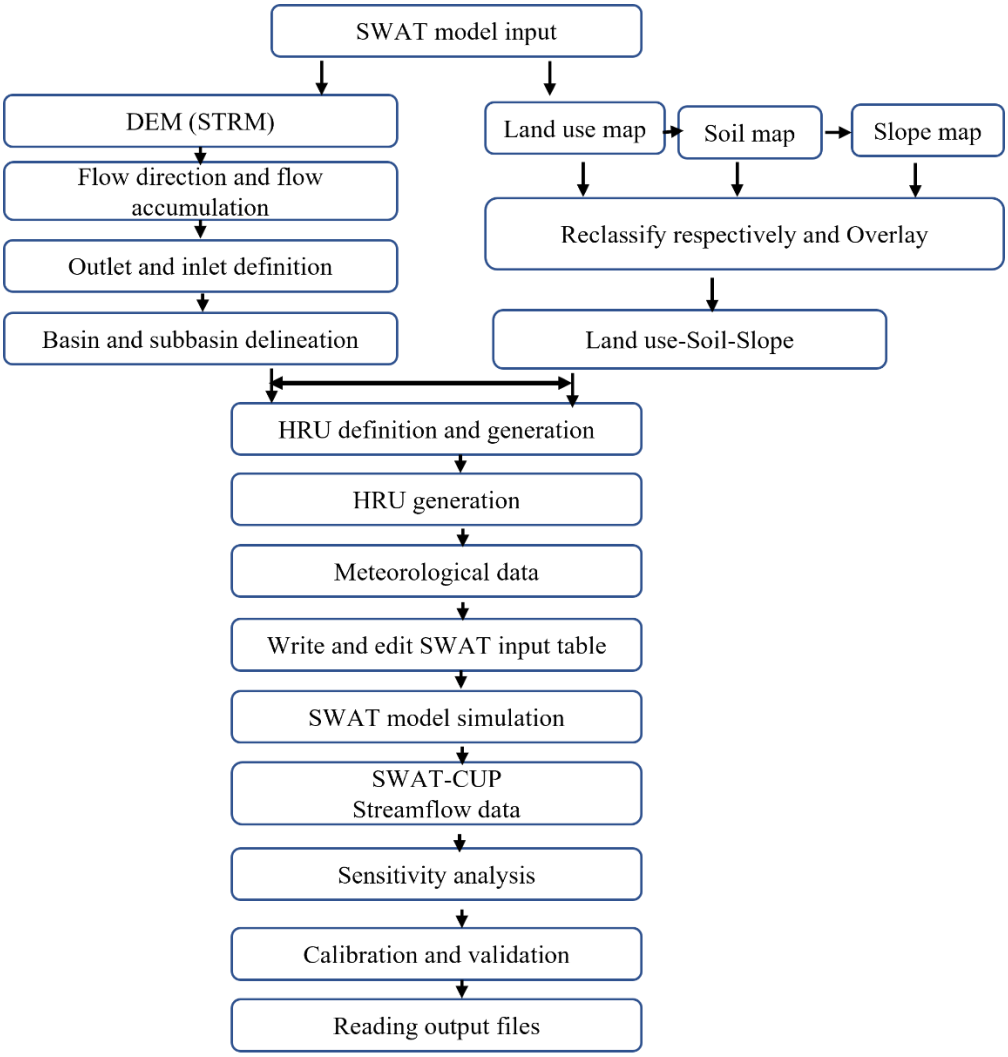

Figure 2.9: Model setup diagram for SWAT model in ArcGIS and ArcSWAT.

Thus, the class Urban Residential Medium Density (URMD) in the SWAT model was used to assign parameters in the residential area (Table 2.1). URMD assumes an average of 38% impervious area in the settlement area (Neitsch et al., 2011), which is like the settlement conditions in the study catchment. To simulate hydrological processes in a watershed, the

SWAT model divides a catchment into sub-catchments and then further divides each sub-catchment into Hydrological Response Units (HRUs) based on a relatively homogenous combination of land use, soil types and slope, for which a land-phase water balance is calculated (Arnold et al., 1998). Seven subbasins (Figure 2.8) were generated for both periods, while 223 and 279 HRUs were created for the years 1980s and 2000s correspondingly.

It should be noted that the irrigation function in SWAT was not activated in this catchment study because of the unavailability of observed data for irrigation and crop yield. Observed meteorological data (daily precipitation, maximum temperature, minimum temperature, wind speed, solar radiation, and relative humidity) were obtained from the National Agriculture and Food Research Organization, Japan (https://www.naro.go.jp/) and were derived from the study catchment. The weather station is located approximately 1 km southwest of the study catchment and is surrounded by paddy fields.

2.2.2.2 Model calibration

Based on the procedure described by Abbaspour (Arnold et al., 2012), parameters to be used for SWAT calibration were identified. Calibration estimates model parameters that cannot be measured directly. This process can be manual or automated, or a combination of both processes while Validation is a comparison between simulation and the observed data on time step with the use of several indexes, and mainly in Nash and Sutcliffe coefficient. The calibration period for the 1980s was selected from 1983 to 1989 and validated from 1990 to 1993. For the 2000s, the calibration period was from 2000 to 2005 and was validated from 2006 to 2007. For each model run, the first three years of simulations were considered model warm-up periods, which were not included in the above periods. Based on the observed flow data collected from the streamflow gauge in the Kurose River, sensitivity analysis, calibration, and validation of the model were performed on a daily time step using Sequential Uncertainty Fitting 2 (SUFI-2) of the SWAT-CUP (Abbaspour et al., 2007). Parameterization was tested to

reduce uncertainty by adjusting some relevant parameters affecting the simulation results. The first parameter ranges were determined based on the minimum and maximum values deduced from the SWAT user manual (Neitsch et al., 2011) and varied iteratively within the allowable ranges until satisfactory agreements between measured and simulated streamflow were obtained for each period. The SUFI-2 algorithm accounts for different sources of parameter, conceptual model, and input data uncertainties (Gupta et al., 2006). Several iterations were performed, where each iteration consisted of 1,000 simulations with narrowed parameter ranges in the subsequent calibration rounds. In addition, daily calibration was performed by manually adjusting the input parameters to attain satisfactory agreement between the simulated and observed discharge data for both periods. Calibration finished only when a group of parameter ranges returned the same fitted parameter values. Depending on the situation, if calibration results are poor, the parameter range may need to be reselected (Table 2.2).

Table 2.2: List of sensitive parameters and optimization ranges included in the final calibration.

		1983-1993		**2000-2007**	
Parameter/file name	**Model description**	**Min**	**Max**	**Min**	**Max**
r_CN2.mgt_URML, URLD	SCS runoff curve number	-0.43	-0.38	-0.1	0.34
r_CN2.mgt_RICE, ARGL	SCS runoff curve number	-0.38	-0.35	-0.33	-0.25
r_CN2.mgt_FRSD	SCS runoff curve number	-0.3	-0.27	-0.2	-0.18
r_CN2.mgt_RNGB, WATR	SCS runoff curve number	-0.4	-0.31	-0.05	0.2
v_ESCO.hru, URML, URLD	Soil evaporation compensation factor	0.05	0.08	0.7	0.9
v_ESCO.hru_RICE, AGRL	Soil evaporation compensation factor	0	0.08	0.7	0.9
v_ESCO.hru_FRSD	Soil evaporation compensation factor	0	0.08	0.4	0.7
v_ESCO.hru_RNGB, WATR	Soil evaporation compensation factor	0	0.08	0.7	0.9
v_ALPHA_BF.gw	Baseflow alpha factor (days)	0.32	0.56	0.32	0.56
v_GW_DELAY.gw	Groundwater delay (days)	0	220	0	220

v_GWQMN.gw	Treshold depth of water in the shallow aquifer required for return flow to occur (mm)	174.5	209.6	174.5	209.62
r__SOL_K.sol	Saturated hydraulic conductivity	-0.28	0.1	-0.29	0.45
r_SOL_AWC.sol	Available water capacity of the soil layer	0.23	0.46	0	0.21
r_SOL_BD. Sol	Moist bulk density	0.25	0.5	0.52	0.77
r_HRU_SLP.hru	Average slope steepness	-0.92	-0.91	-0.96	-0.95
v_CANMX.hru	Maximum canopy storage	25.36	32.09	24.36	25.09
V_RCHRG_DP.gw	Deep aquifer percolation fraction	0.24	0.29	0.28	0.3
V_REVAPMN.gw	Threshold depth of water in the shallow aquifer for "revap" to occur (mm)	30	80	30	80
R_SLSUBBSN.hru	Average slope length	0.7	0.9	0.5	0.7

The simulation accuracy was verified using a validation process. In this process, the model was operated with input parameters set during the calibration process without any further changes, and the results were analyzed using the remaining observation data. In the studied catchment, climate and geological conditions did not change significantly. To avoid differences in results due to parameter changes in this study, a group of parameters that can be used during both time-step was selected. However, some parameters still responded quite differently during calibration in both periods. SWAT output files for (. hru and .sub files) were extracted from SWATOutput.mdb after the final calibration and validation process.

2.2.2.3 Model Evaluation and Statistical methods

To determine the reliability of the simulation results, it is necessary to evaluate their accuracy. In this study, simulations for model calibration were assessed daily, and the following statistical criteria were used to verify the reliability of the results: the coefficient of determination (R^2) and the Nash-Sutcliffe Efficiency (NSE) as shown in Eqs. (2.6) − (2.7) (Nash and Sutcliffe, 1970; Fadil et al., 2011; Singh et al., 2004; Moriasi et al., 2007).

R^2 is the square of the correlation coefficient, which indicates the strength relationship value between the observed and simulated data and can range from 0 to 1 (Santhi et al., 2001). An R^2 value of 1 indicates a perfect alignment between the simulated and observed values whereas an R^2 value of 0 indicates no alignment between the simulated and observed values. However, the weakness of using only the R^2 statistic lies in the fact that the model predictions can be consistently wrong and still result in an R^2 value close to 1 due to systematic over- or under-prediction; thus, the need to use an additional evaluation statistics such as the NSE to accurately determine the model results (Krause et al., 2005). The NSE value is a measure of the predictive power of the model and can range from $-\infty$ to 1. The values of NSE = 1 are the optimal values, and the model with NSE > 0.5 is considered satisfactory (Moriasi et al., 2007).

$$R^2 = \frac{[\sum_{i=1}^{n}(X_i - \overline{X})(Y_i - \overline{Y})]}{\sum_{i=1}^{n}[(X_i - \overline{X})\sum_{i=1}^{n}(Y_i - \overline{Y})^2]} \qquad (2.6)$$

$$NSE = 1 - \frac{\Sigma_{t=1}^{T}(X_o^t - Y_m^t)^2}{\Sigma_{t=1}^{T}(X_o^t - X_o^{-t})^2} \qquad (2.7)$$

where, NSE is the Nash−Sutcliffe model efficiency coefficient; Q_o represents the observation discharge, Q_m is the model discharge, $\bar{Q}_o$ indicates the average of the observation discharge, and Q^t is the discharge at time t.

2.3 References

Abbaspour, K.C., Vejdani, M., Haghighat, S. SWAT-CUP calibration and uncertainty programs for SWAT. Modsim 2007: International Congress on Modelling and Simulation: Land, Water and Environmental Management: Integrated Systems for Sustainability, Christchurch, New Zealand. **2007**.

Appelo, C.A.J., Postma, D. Chemical Analysis of Groundwater, Geochemistry, Groundwater & Pollution. Balkema, Rotterdam. **1999**.

Arnold, J.G., Srinivasan, R., Muttiah, R.S., William, J.R. Large area hydrologic modeling and assessment part i: model development. *J. Am. Water. Resour. Assoc.***1998**, 34, 73–89.

Deutsch, W.J. (1997). Groundwater geochemistry: fundamentals and application to contamination. Boca Raton (Fla.): Lewis Publishers. **1997**

Drever, J.I. The geochemistry of natural waters, 2nd ed. Englewood Cliffs, N.J.: Prentice Hall. **1988**, 402.

Fadil, A.H.R., Abdelhadi, K., Youness, K., Bachir, O.A. (2011). Hydrologic modeling of the bouregreg watershed (morocco) using GIS and SWAT model. *J. Geogr Inf. Syst*. **2011** 3, 279–289.

Fantong, W.Y., Satake, H., Ayonghe, S.N., Aka, F.T. and Asai, K. Hydrogeochemical controls and usability of Groundwater in semi-arid Mayo Tsanaga River Basin, Far North Region, Cameroon. *Environ. Geol*. **2009**, 58, 1281−1294.

Green, W.H., Ampt, G.A. (1911). Studies on soil physics, 1. The flow of air and water through soils. *J. Agric. Sci*. **1911,** 4, 11−24.

Gupta, H.V., Beven, K.J, Wagener, T. Model calibration and uncertainty estimation. In: Encyclopedia of hydrological sciences. **2006**, 11–131.

Hargreaves, G.L., Hargreaves, G.H., Riley, J.P. (1985). Agricultural Benefits for Senegal River Basin. J. *Irrig. Drain. Engr*. **1985**, 111:113−124.

Higashihiroshima city report. Accessed 12, November **2021**. https://www.city.higashihiroshima.lg.jp.

Hounslow, A.W. Water Quality Data: Analysis and Interpretation (1st ed.). CRC Press. **1995**.

Kamtchueng, B. T., Fantong, W.Y., Wirmvem, M. J., Tiodjio, R.E., Takounjou, A.F., Ngoupayou, J. R. N., Kusakabe, M., Zhang J., Ohba T., Tanyileke, G., Joseph V. H. and Akira U. Hydrogeochemistry and quality of surface water and groundwater in the vicinity of Lake Monoun, West Cameroon: approach from multivariate statistical analysis and stable isotopic characterization. *Environ. Monit. Assess*. **2016**, 188, 524.

Krause, P., Boyle, D.P., Bäse, F. Comparison of different efficiency criteria for hydrological model assessment. *Adv. Geosci*. **2005**, 5, 89–97.

Ministry of Land, Infrastructure, Transport, and Tourism of Japan, (**2020)**. Available from: https://nlftp.mlit.go.jp/ (accessed on 10 April 2020).

Monteith, J.L. Evaporation and environment. Symp. *Soc. Exp. Biol*. **1965**, 19, 205– 234.

Moriasi, D.N., Arnold, J.G., Van Liew, M.W., Bingner, R.L., Harmel, R.D., Veith, T.L. Model evaluation guidelines for systematic quantification of accuracy in watershed simulations. *Trans. ASABE*. **2007**, 50, 885–900.

Nash, J.E., Sutcliffe, J.V. River flow forecasting through conceptual models: part I. A discussion of principles. *J. Hydrol*. **1970**,10, 282–290.

Nasiri, S., Ansari, H. & Ziaei, A.N. Simulation of water balance equation components using SWAT model in Samalqan Watershed (Iran). *Arab. J. Geosci*. **2020**, 13, 421.

National Agriculture and Food Research Organization, Japan. **2020** (https://www.naro.go.jp/) (Accessed 9 April 2020).

Neitsch, S.L., Arnold, J.G., Kiniry, J.R., Williams, J.R. Soil and water assessment tool theoretical documentation version 2009. Texas Water Resources Institute 647. **2011**.

Piper, A. M. A. Graphic procedure in the geochemical interpretation of water analyses. *Trans. Am. Geophy. Union*. **1944**, 25, 914–928.

Priestly, C.H.B., Taylor, R.J. "On the Assessment of Surface Heat Flux and Evaporation Using Large Scale Parameters," Monthly Weather Review**. 1972**, 100, 81−92.

Rencher-Arvin, C. Methods of Multivariate Analysis Brigham, Young University 2nd Ed. New York: John Wiley & Sons, Inc. Publication. **2002**.

Santhi, C., Arnold, J.G., Williams, J.R., Dugas, W.A., Srinivasan, R., Hauck, L.M. Validation of the SWAT Model on a Large River Basin with Point and Nonpoint Sources. *J. Am. Water. Resour. Assoc*. **2001**, 37, 1169–1188.

Shuttle Radar Topography Mission of the United States Geological Survey, **2020**. Available from: https://eart hexplorer.usgs.gov/ (accessed on 10 April 2020).

Singh, J., Knapp, H.V., Demissie, M. Hydrologic modeling of the Iroquois river watershed using HSPF and SWAT. *J. Am. Water. Resour. Assoc*. **2004**, 41, 343–360.

Soil Conservation Service (SCS). National Engineering Handbook, Section 4: Hydrology. Department of Agriculture, Washington DC. **1972**,762.

Chapter 3

Social Impacts on Groundwater Nitrate Contamination Status and its Sources on an Island with Intensive Citrus Cultivation

This chapter is an edited version of the article:

Kimbi, S.B.; Onodera, S.-I.;Ishida, T.; Saito, M.; Tamura, M.;Tomozawa, Y.; Nagasaka, I. Nitrate Contamination in Groundwater: Evaluating the Effects of Demographic Aging and Depopulation in an Island with Intensive Citrus Cultivation. Water 2022, 14, 2277.

3.1. Introduction

In recent years, demographic trends have raised concerns with respect to the effects of population growth on water resources. Despite rapid global population growth, population densities are declining in some regions and the proportion of aged people in most developed countries is rising. However, Japan has experienced this demographic transition faster than most Western and Asian countries, with an increasing number of citizens over the age of 65 (Hayashi et al., 2021). However, despite these changes in its demographics, it still faces serious environmental problems related to groundwater pollution, with nitrates being one of the more serious groundwater contaminants (Tase, 1992; Onodera et al., 2011; Haque et al., 2013). Agricultural-related nitrate contamination of groundwater is a widespread problem in many countries, with numerous studies demonstrating a relationship between agriculture and high nitrate concentrations in groundwater. Groundwater contamination is likely to occur when Nitrate (NO_3^-) input into the soil exceeds the consumption capacity of plants, which leads to nitrogen loss to the environment (Agrawal et al., 1999; Noland et al., 2000; Sacchi et al.,2013;

Mcclain., 1994). In Japan, nitrate pollution in groundwater has been associated with intense agricultural production since the 1960s, as chemical fertilizers have increasingly been utilized (Kumazawa, 2002). As a result, nitrogen fertilizer effectiveness has diminished, and the nitrogen remaining in the soil after crop absorption has leached into the groundwater as nitrate. Due to increasing demographic aging as a major socioeconomic problem in many regions in Japan (Hiyashi et al., 2021), the use of chemical fertilizers to maximize production is increasing. Prior studies in Japanese agricultural island were found to have high nitrate levels (Hayashi et al., 2021; Saito et al., 2015; Kimbi et al., 2021), which was associated with intensive cultivation. The widespread use of fertilizers by farmers was believed to be the primary source of groundwater contamination; however, agricultural farmland has varied sources of contamination input. An effective measure for controlling and managing nitrate pollution is to identify the sources of nitrate (Zhang et al., 2014), however NO_3^- pollution comes from diverse sources even in agricultural fields which can be classified into four groups: chemical fertilizers, soil nitrogen, atmospheric deposition, and manure and sewage (Kendall et al., 1998; Bedard-Haughn., 2003; Knapp et al., 2005; Chen et al., 2007., Umezawa et al., 2008; Peralta et al., 2020; Rusydi et al., 2021; Wang et al., 2022). Thus, understanding the different sources of NO_3^- in groundwater is crucial, especially for stakeholders intending to implement groundwater conservation measures (Xue et al., 2008).

In the past, conventional methods for determining groundwater NO_3^- sources relied on the association between land-use types and the variation in groundwater chemical composition (Kou et al., 2021). Based on this method, most nitrate sources were inaccurately identified with a high level of uncertainty. Therefore, a technique was proposed for identifying NO_3^- sources using N and O isotopes (Kohl et al., 1971; Amberger and Schmidt 1987; Kendall et al., 2008). NO_3^- sources are characterized by different isotope signatures that allow them to efficiently trace point and non-point contamination sources in both ground and surface waters. However,

a concern arose in relation to overlapping ranges, which may cause inaccurate nitrate sources to be identified and compromise the usefulness of isotopes alone. As a result, it was determined that $\delta^{18}O_{NO3-}$ could provide additional information for distinguishing nitrate from chemical fertilizers and atmospheric deposition because of its distinctive values compared to those of the overlapping N isotopes (Kendall., 2008). The isotopic compositions of N and O differ among nitrate sources, and their combination with NO_3^- is an effective indicator for tracing the source of groundwater nitrate (Knapp et al., 2005). Several studies have successfully used the double isotope technique to identify the sources of NO_3^- pollution in surface and groundwater after the typical range of $\delta^{15}N\text{-}NO_3^-$ and $\delta^{18}O\text{-}NO_3^-$ for various sources of NO_3^- pollution was reported (Kendall et al., 1998, 2008; Aravena and 1993; Wu et al., 2006; Chen et al., 2009; Liu et al., 2013). Relatively accurate results can be obtained by using these dual isotopes along with conventional tracing methods (Maghdadi et al., 2018). Therefore, the isotopic composition of nitrate can help to distinguish different sources of nitrates in groundwater, such as synthetic or organic fertilizers, human waste/septic system effluents, and soil organic matter.

The Bayesian isotope mixing model has been used to calculate the proportionate contributions of the main nitrate sources in groundwater (Chen et al., 2007; Ji et al., 2017; Parnell et al., 2010; Fu et al., 2019; Yu et al., 2020). Previous studies have successfully used the $\delta^{15}N_{NO3-}$ and $\delta^{18}O_{NO3-}$ and Bayesian isotopic mixing models to determine the proportionate contribution of different nitrate sources (Zhang et al., 2014; Chen et al., 2007; Torres-Martinez et al., 2020). The results revealed that by using a Bayesian "fingerprint" for pollution activities, the SIAR model could predict the probability distribution of the proportional NO_3^- contribution source. Nitrogen and oxygen isotopes can be used in conjunction with traditional methods to identify nitrate sources, and stable isotope analysis in R software (SIAR) can quantify the contributions of various sources of nitrate groundwater contamination to protect the environment of intensive agricultural areas (Kimbi et al., 2021; Yu et al., 2020). Nitrate

contamination of groundwater and surface water in Osakishimojima Island is a cause for concern, as a previous study (Kimbi et al., 2021) has linked the elevated nitrate concentrations in water sources to the nitrogenous fertilizers used in citrus farms. Sometimes, the nitrate levels have been observed to exceed the World Health Organization's (WHO, 2017) recommended guideline for maximum NO_3^- (50 mg/L) in drinking water or Japan's recommended guideline for maximum NO_3^-–N concentration (10 mg/L) in water supplies. Hence, exploring the spatial variation of NO_3^- and its sources in two study sites with different extents of areas under cultivation could provide insights into the sources contributing to NO_3^- pollution on this island, which would help in the effective management of groundwater sources, particularly considering that the island has a declining and aging population.

The aims of this investigation were: (1) to demonstrate how the dual isotope approach ($\delta^{15}N\text{-}NO_3^-$ and $\delta^{18}O\text{-}NO_3^-$) can be used to determine the dominant sources of nitrates in the shallow groundwater of a small island and (2) to evaluate the influence of social aspects such as population aging and depopulation on NO_3^- concentrations in groundwater.

3.2 Location and description of the study area

This study was conducted in Osakishimojima (34°10'24" N, 132°50'3" E), a small island located in the Seto Inland Sea in Hiroshima Prefecture, western Japan (Figure 3.1), about 20km WSW from Kure City. Two neighboring villages and watersheds, Ocho in the eastern of the island and Kubi in the northern were compared. The population of Kubi and Ocho is approximately 413 and 830 in 2021, respectively (Kure city report, 2021) and the average age of farmers is 76 and 73, respectively (Japan Agricultural Cooperative, 2022). Osakishimojima has a warm temperate climate with all four seasons, including cold winters and hot summers. The annual average air temperature is 15.6 ℃, and the average annual precipitation is approximately 1100 mm. The land use of Osakishimojima Island includes citrus orchards, pine

forests, residential areas, paddy weeds, and water bodies, with area proportions of 56.69 %, 36.46 %, 5.56 %, 0.82 %, and 0.4 9%, respectively (Kimbi et al., 2021). Land use data were obtained from another study (Ministry of Land, Infrastructure, Transport, and Tourism of Japan, 2021), with a spatial resolution of 100 m and detailed classification carried out using google earth to suit the purpose of this research.

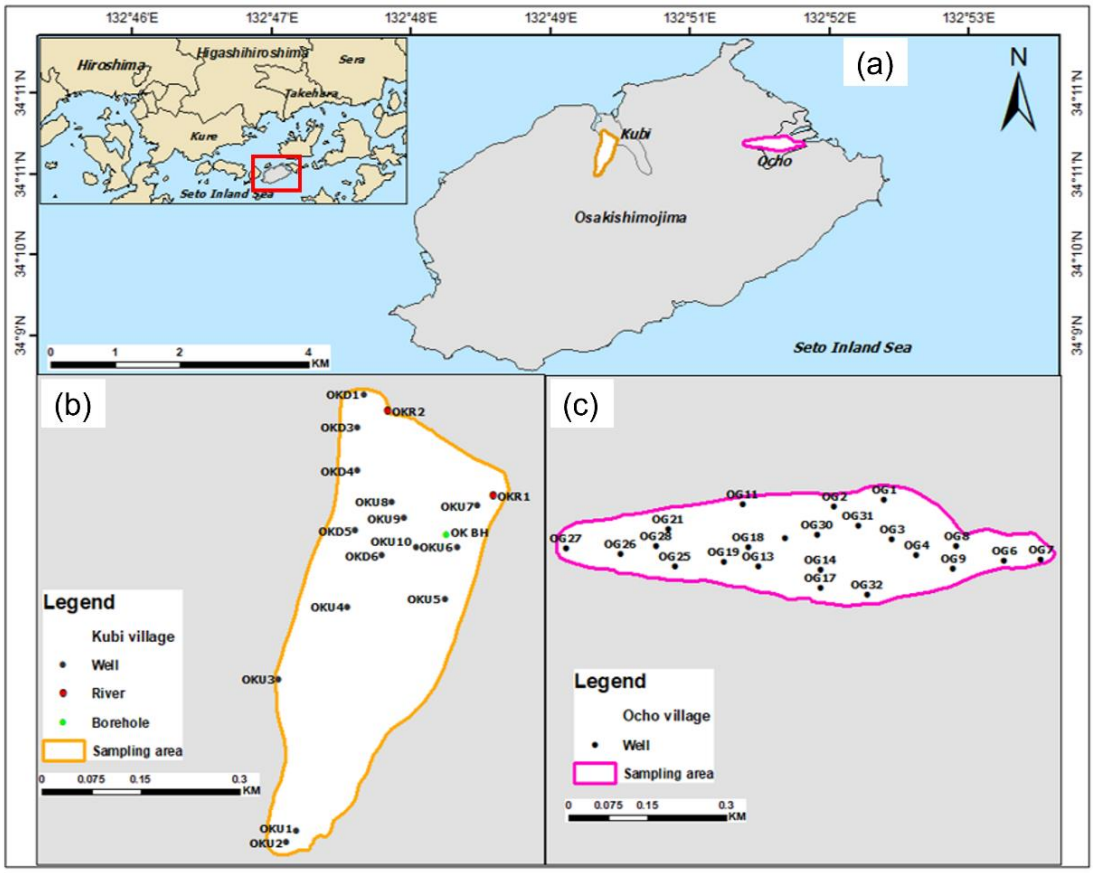

Figure 3.1: (a) Location map of Osakishimojima Island in the Seto Inland Sea showing the sampling points in (b) Kubi village and (c) Ocho village.

Agricultural land in Ocho and Kubi is approximately 1.6 km^2 and 0.6 km^2, respectively, and has decreased by 37% and 46% over the last 10 years (Ministry of Land, Infrastructure, Transport, and Tourism of Japan, 2021). In comparison, citrus orchards, and residential areas in the lowlands of Ocho and Kubi are 35.2% and 56.7%, and 45.4% and 43.3%, respectively (Figure 3.2). The residential areas in the region mainly consist of scattered villages with low

urbanization levels and substandard sewage treatment facilities. In addition, the village of Ocho has a higher building density and greater surface area than Kubi village (low housing density which are randomly distributed). General information on farmer choice of fertilizer, and information pertaining to farmer agricultural practices in each village were determined based on oral discussion with some farmers and from the areas agricultural company, however no formal interviews were conducted in the study sites during the sample survey.

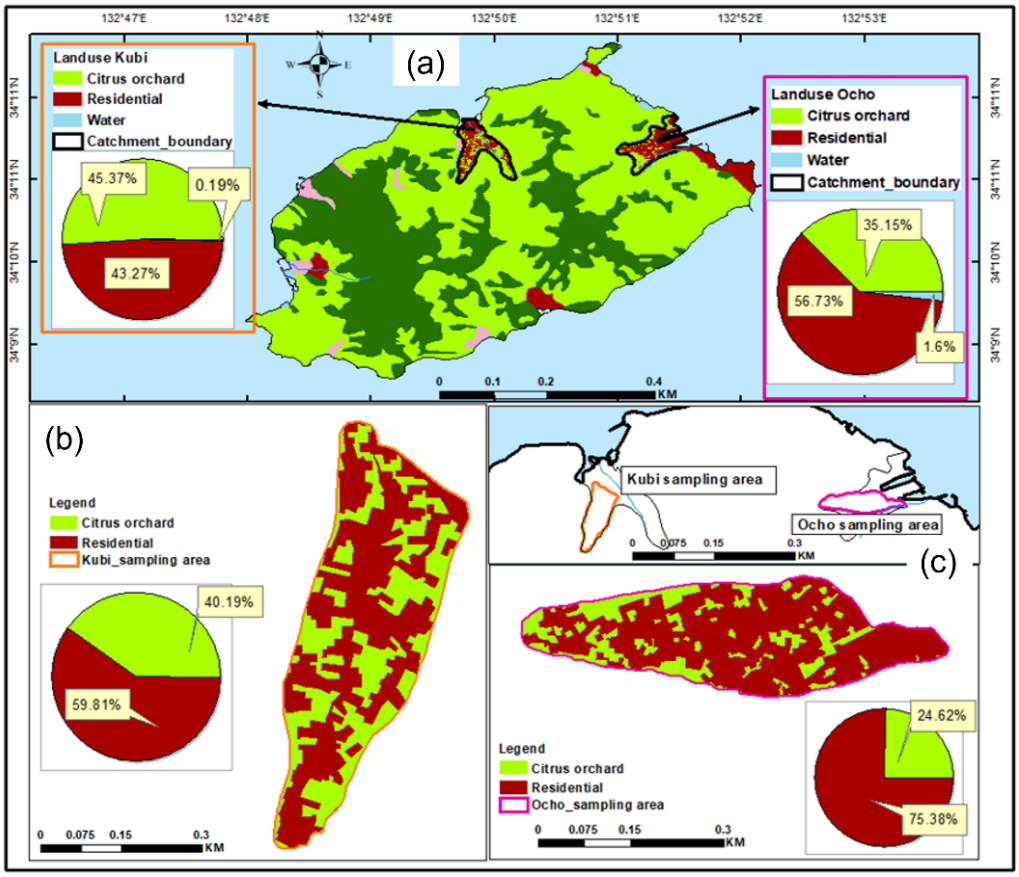

Figure 3.2: Land use of Osakishimojima, showing proportions of citrus orchards and residential areas in (a) Kubi and Ocho lowland areas, (b) Kubi sampling area, and (c) Ocho sampling area.

In addition, hydrogeological data for the study sites were unavailable; thus, only the geological outcrops were examined. The main geological features of Osakishimojima Island are Late Cretaceous non-alkaline felsic volcanic rocks and rhyolites (Figure 2.4). They are

found on mountain slopes, and Late Pleistocene to Holocene marine and non-marine formations cover the basement rocks in the lowland.

3.3 Materials and Method

3.3.1 Sample collection

Fifty-two water samples were collected in the study area in October 2021, which included 32 sites comprising of 2 springs and 30 shallow wells in Ocho area and 20 sites of 1 observation and production borehole, 2 rivers, and 17 shallow wells in Kubi, respectively (Figure 3.1). The sampling location, depth, and utilization information for each sampling site were determined from GPS coordinates. All wells chosen for groundwater sampling were commonly used for domestic and/or agricultural purposes; these wells had a mean depth of 10.8 m and 4.84 m in the Kubi and Ocho villages, respectively. The groundwater pH, temperature, electrical conductivity (EC), dissolved oxygen (DO), and oxidation- reduction potential (ORP) were measured on-site using a portable multiparameter water quality meter (pH/COND Meter D-54, HACH LD0101, ORP Meter RM-20P). All samples were collected from a 0.5–1 m depth below the water level in the wells using a high-density polyethylene sampler and filtered through a 0.2 μm membrane into one 250 mL, three 10 mL, and one 100 mL high-density polyethylene sampling bottles. After filtration, the samples were stored at 4 °C and subsequently transported to the laboratory, where they were frozen at −4 °C until further hydrochemical and isotopic analyses. The contents of the main cations, Na^+, K^+, Mg^{2+}, and Ca^{2+}, were analyzed by ion chromatography with conductivity detection on an ICS-2100 (Dionex integrion, Thermo Fisher Scientific, Waltham, MA, USA). Analytical precisions for cations were set at <0.2 % for Na^+ and < 0.1% for Ca^{2+}; Mg^{2+} and K^+ while for anions, <0.1 % for NO_3^-, Cl^- and <0.2 % for SO_4^{2-}. HCO_3^- was determined within 12 hours of sample

collection by acid titration from a volume of 0.02 N H_2SO_4 added to the sample to reach its titration endpoint, marked by a pH of 4.5. Dissolved organic carbon (DOC) was determined using a total organic carbon analyzer (Total Organic Carbon analyzer, SHIMADZU, Hiroshima University, Japan). The analyses of major ions and DOC were conducted at the Biogeochemistry Laboratory, Hiroshima University, Japan.

Isotope analyses were performed at the Institute of Geosciences, Yamanachi University, using a stable isotopic ratio mass spectrometer (MAT 253, Thermo Fisher Scientific, Waltham, MA, USA). Chemical reduction (cadmium and azide reduction) was used to quantify $\delta^{15}N_{NO3}$ and $\delta^{18}O_{NO3}$, respectively (Mcllvin and Altabet, 2005; Tu et al., 2016). Briefly, to eliminate nitrite, the samples were treated with a 2.5 mmol/L sulfamic acid solution. The NO_3^- in the samples was then quantitatively converted to gaseous nitrous oxide (N_2O) using a two-step reduction process. First, NO_3^- was reduced to nitrite with spongy cadmium, then nitrite was converted to nitrous oxide with an azide/acetic acid buffer, and finally, the $\delta^{15}N$ and $\delta^{18}O$ of N_2O were determined. The stable isotope ratios of $\delta^{15}N$ and $\delta^{18}O$ were given in delta value (δ) and per mil (‰) notation in comparison to international standards as follows (Kendall et al., 1998):

$$\delta_{sample}(‰) = [(R_{sample}/R_{standard}) - 1] \times 1000 \quad (3.1)$$

where R_{sample} and $R_{standard}$ are the $^{15}N/^{14}N$ and $^{18}O/^{16}O$ ratios of the samples and standards for $\delta^{15}N$ and $\delta^{18}O$, respectively. The $\delta^{15}N$ values were reported relative to N_2 in atmospheric air (AIR), and the $\delta^{18}O$ values relative to Vienna Standard Mean Ocean Water (VSMOW). The precision values for $\delta^{15}N$ and $\delta^{18}O$ were ±0.3 ‰ and ±0.4 ‰, respectively. Two representative samples of organic and chemical fertilizer were collected from local farmers in Kubi village in January 2022 for analysis as end-member samples. The solid samples were transported to the laboratory for air-drying and then fully ground for chemical and isotopic analyses. The solid samples were converted to N_2 by high-temperature redox reactions,

and $\delta^{15}N\text{-}N_2$ was measured using an isotopic ratio mass spectrometer. The precision for $\delta^{15}N$ was ±0.3 ‰.

3.3.2 Source apportionment calculation

The Stable Isotope Analysis in R (SIAR) software program was used to develop the mixing model. The system model used in SIAR can be expressed by defining a set of *N* mixture measurements on *J* isotopes with *K* source contributors, the mixing model can be expressed as follows (Kendall et al., 2008):

$$X_{ij} = \sum_{k=1}^{k} P_k\left(P_{jk} + C_{jk}\right) + \varepsilon_{jk}$$

$$S_{jk} \sim N\left(\mu_{jk}, \omega_{jk}^2\right) \qquad (3.2)$$

$$C_{jk} \sim N\left(\lambda_{jk}, \tau_{jk}^2\right)$$

$$\varepsilon_{jk} \sim N\left(O, \partial_j^2\right)$$

where X_{ij} is the isotope value *j* of mixture *i*, in which *i*=1, 2, 3, …, *I* and *j*=1, 2, 3, …, *J*; S_{jk} is the source value *k* of isotope *j* (k=1,2,3, …, *K*), and is normally distributed with a mean value μ_{jk} and a standard deviation ω_{jk}; P_k is the proportion of source *k*, which is estimated using the SIAR model; C_{jk} is the fractionation factor for isotope *j* of source *k,* and is normally distributed with a mean value λ_{jk} and a standard deviation τ_{jk}; and ε_{ij} is the residual error representing the additional unquantified variation between individual mixtures, and is normally distributed with a mean value of 0 and a standard deviation σ_j. Details of this model were described in previous studies (Mcclain et al., 1994; Jackson et al., 2009).

A Bayesian model was applied to determine the potential NO_3^- contribution from each of four sources for Kubi and Ocho villages: $\delta^{15}N\text{-}NO_3^-$ in manure and sewage (M&S), chemical fertilizer (CF), and organic fertilizer (OF); and soil nitrogen (SN) x (k=4). The end-member

isotopic compositions for the three sources were used (j=3) in the model setup. SN and M&S samples were not analyzed in the study area, so the SN values from (Kendall et al., 2008; Fadhullah et al., 2020; Fu et al., 2019; Yu et al., 2020) were compared with the CF samples, and since they showed similar ranges; they were identified as one source CF_SN in this study. Meanwhile, the M&S values were obtained from the literature and used in the model as an additional source. We considered M&S as a suspension of water and solid waste from humans and animals transported by sewers, and OF exclusively as a mixture of chicken litter and sawdust**.** Although discrete samples of individual $\delta^{15}N\text{-}NO_3^-$ sources in the study area were measured, the limited number obtained may induce a biased model outcome. Alternatively, the mean values of $\delta^{15}N\text{-}NO_3^-$ isotopes (μ_{jk}) and associated SDs (ω_{jk}) of different M&S were acquired by consulting previously published data (Kendall et al., 2008; Fu et al., 2019; Fadhullah et al., 2020; Yu et al., 2020), whereas CF and OF were obtained from the Kubi area.

3.3.3 Statistical Method

Statistical analysis was performed to determine the NO_3^-−N relationship with DOC and the major ions using scattered plot, which was demonstrated by the coefficient of determination (R^2). In addition to correlation analysis, principal component analysis (PCA) has been used to analyze groups of ions based on similarity or difference in concentration. SPSS® ver. 23.2 (SPSS Inc., Chicago, USA) was used to analyze the groundwater chemical data in this study. A PCA can explain most of the variability in a data set with fewer variables than the original dataset, so parameters with similar loadings in the same PC group may have similar contribution sources or geochemical behavior (Huang et al., 2018a; Zhang et al., 2019). PCA was used to identify the primary groundwater contamination indicators using Kaiser's varimax rotation method, adopting only PCs with eigenvalues greater than one. An inverse distance weighting method (IDW) was also performed using ArcMap 10.6 to show the spatial distribution of NO_3^-−N and $\delta^{15}N\text{-}NO_3^-$ in Kubi and Ocho groundwaters

3.4 Results and Discussion

3.4.1 General hydrochemistry

The hydrochemical compositions of Kubi and Ocho are summarized in Table 3.1. The results showed that the pH of groundwater was near neutral in Kubi (6.4 to 7.5, mean pH 6.8). The pH values of the river water sample were neutral to alkaline (7.9 to 8.6) and higher than the groundwater pH values, which may be due to the strong evaporation of the surface water. In Ocho village, groundwater was slightly acidic to alkaline with pH values ranging from 6.2 to 8.5 with a mean of 6.7. All samples had moderate EC values varying from 106.3 to 472 µS/cm, (mean 306.7 µS/cm) in Kubi and 164.9 to 479 µS/cm (mean 308.5 µS/cm) in Ocho. Total dissolved solids (TDS) were approximated from EC following the equation (Evangelou, 1998):

$$TDS\ \left(\frac{mg}{L}\right) = 0.64\ x\ EC\left(\frac{\mu S}{cm}\right) \qquad (3.3)$$

The DOC levels of groundwater in Kubi ranged from 2.5 to 13.33 mg/L (mean 5.1 mg/L), while those in Ocho ranged from 1.6 to 7.0 mg/L (mean 3.5 mg/L). The DO ranged from 1.1 mg/L to 8.6 mg/L with a mean of 4.9 in the wells in Kubi, while those in Ocho ranged from 0.8 mg/L to 9.1 mg/L with a mean value of 3.4 mg/L. All but one sample from Kubi had DO values above 2 mg/L, whereas in Ocho, nine samples had values less than 2 mg/L. Also, observed DO levels were higher in naturally occurring springs (mean 9.2 mg/L in Kubi and 8.6 mg/L in Ocho). Hence, groundwater samples in Ocho had the potential to undergo denitrification processes as opposed to those in Kubi. Ca^{2+} was the most dominant cation in both study areas and ranged from 7.8 – 38.1 mg/L in groundwater samples and from 9.8 mg/L − 35.5 mg/L in surface water samples in Kubi while in Ocho area, concentrations ranged from 0.5 mg/L – 4.6 mg/L in surface water and from 8.8 mg/L − 50.8 mg/L in groundwater samples.

Table 3.1: Statistical characteristics of the hydrochemical compositions of the groundwater and surface water sources in Kubi and Ocho village.

	Kubi village								Ocho village					
	Spring (n = 1)	River (n = 2)			Wells (n = 17)			Borehole (n = 1)	Spring (n =2)			Wells (n = 30)		
Parameters	**Min/Max**	**Min.**	**Max.**	**Ave.**	**Min.**	**Max.**	**Ave.**	**Min/Max**	**Min.**	**Max.**	**Ave.**	**Min.**	**Max.**	**Ave.**
pH	7.3	7.9	8.6	8.3	NM	7.4	6.8	7.5	7.5	7.5	7.5	6.2	8.5	6.8
Temp	19.1	23.7	24.7	24.2	18.1	26.7	21.2	19	17.6	23.6	20.6	19.2	28.3	22.3
EC	185.7	206	274	240	107	465	314.8	472	133	217	175	165	479	308.5
TDS	118.9	131.9	175.4	153.6	68.5	297.6	201.5	302.1	85.2	138.9	112	105.6	306.6	105.6
DO	9.2	8.3	9	8.7	1.1	8.7	5	6.1	7.7	9.5	8.6	0.8	9.1	3.5
DOC	3.6	3.8	5.3	4.6	2.5	13.3	5.1	4.1	NM	3.5	3.5	NM	7	3.3
Cl^-	14.7	9.4	11.1	10.3	7.6	34	11.9	13.4	4.6	10.9	7.8	4.1	37.5	11.9
$SO42^-$	22.9	30.5	50.4	40.5	22.1	75.3	44.4	80.7	4.5	22.9	13.7	–	145.1	37.7
NO_3^-	7.1	12.4	34.2	23.3	14.9	74.5	41.5	70.3	2.7	13.7	8.2	3.5	66.4	21.7
NO_3^-–N	1.7	2.9	7.8	5.4	3.4	16.9	9.5	15.9	0.7	3.1	1.9	0.8	15.1	5
HCO3	7.2	50.6	61.2	55.9	–	121.6	48.6	39.1	4	9.3	6.7	4.5	150.2	64.2
Na^+	21	16.3	18.3	17.3	9.4	32.5	15.7	31.4	–	5.5	2.8	9.4	57.6	18.6
K^+	2.2	3.2	3.6	3.4	0.7	6.9	4.1	1	3.2	8.4	5.8	0.3	10.5	4.1

$Mg2^{+}$	9.8	8.2	10.7	9.5	7	17.8	11.5	17.8	1.4	25.8	13.6	4.9	22.2	10
$Ca2^{+}$	24.6	22.3	30	26.2	20.4	48.4	31.7	44.8	−	4.6	4.6	−	50.8	28.8

Note: *n* = number of samples; SD = standard deviation; − = below detection limit; NM = not measured, ionic concentrations, DOC and DO = mg/L; EC = µS/cm; Temp = ^{O}/C

Magnesium concentrations ranged from 1.6 mg/L − 15.3 mg/L in groundwater samples and 4.5 – 14.4 mg/L in surface water in Kubi whereas in Ocho village, these concentrations where much lower, varying from 4.9 mg/L – 22.2 mg/L in groundwater samples (Table 3.1). Ca^{2+} and Mg^{2+} can contaminate groundwater through ion exchange when minerals dissolve in rocks, or when fertilizers run off and leach into the groundwater. According to (Earle, 2019), soils containing $CaCO_3$ and $CaSO_4$ may increase Ca^{2+} levels in groundwater by leaching, whereas (Keesari et al., 2016) suggests agricultural runoff and sewage disposal may lead to high Mg^{2+} levels. The most abundant anion in the water samples in both villages is HCO_3^-.

In in Kubi, HCO_3^- in river samples ranged from 50.6 mg/L – 61.2 mg/l with a mean value of 55.9 mg/L while concentrations in wells ranged from 14.2 mg/L – 121.6 mg/L with a mean of 45.3 mg/L (Table 3.1). HCO_3^- concentrations in Ocho ranged of 4.5 mg/L – 64.2 mg/l in wells and from 4 mg/L to 9.25 mg/L in spring samples. Cl^- values varied from 4.2 to 14.7 mg/L with a mean value of 9.41 mg/L in Kubi while values varied from 4.1 to 37.5 mg/L with a mean value of 11.59 mg/l in Ocho village. The average concentration of dissolved species in the samples in both villages was in the sequence of $Ca^{2+} > Na^+ > Mg^{2+} > K^+$ for the cations and $HCO_3^- > SO_4^{2-} > NO_3^- > Cl^-$, for the anions.

The chemical compositions of water samples of both Kubi and Ocho village were identified and classified using the trilinear plot (Figure 3.3). The major groundwater facies in Kubi area were mainly $Ca{-}HCO_3$ and $Ca{-}SO_4$ water type constituting 55 % and 45 % of the water samples, respectively. Meanwhile, the Trilinear analysis for Ocho village suggest that 59% of water samples are composed of $Ca{-}HCO_3$ water type while 42% of water samples plotted in the zones of $Ca{+}Mg{-}SO_4$ or $CaMg{-}Cl$ water types. Groundwater samples from both areas showed freshwater signatures with higher percentages in the $Ca{-}HCO_3$ zone, however

they show susceptibility to anthropogenic contamination as they evolve between Ca-HCO_3 and Ca+Mg−SO_4 or CaMg−Cl types.

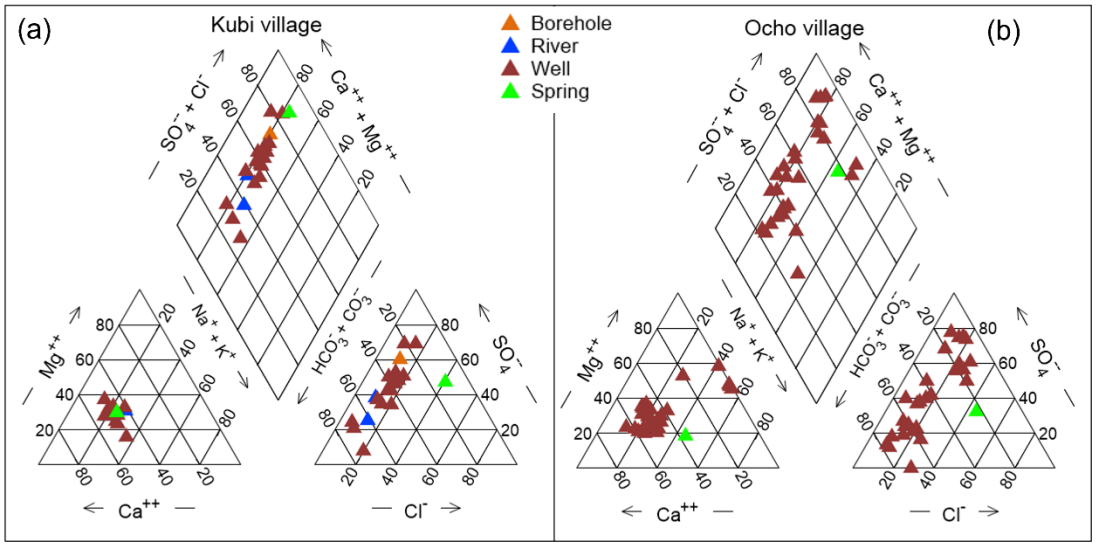

Figure 3.3: Piper diagram of surface water and groundwater in (a) Kubi and (b) Ocho (Adopted after Piper, 1944).

3.4.2 Spatio-temporal variations in the NO_3^-−N concentration

Nitrate concentration can characterize the degree of groundwater nitrate contamination. When the nitrate nitrogen (NO_3^-−N) concentration exceeds 3 mg/L, it is deemed to be affected by human factors (Amber and Schmidt, 1987). A mean value of 6.7 mg/L and a median value of 6.5 mg/L were observed in Kubi, with NO_3^-−N concentrations ranging from 0.5 mg/L to 13 mg/L. Approximately 33.4 % of groundwater samples had NO_3^-−N concentrations below 5 mg/L, 47.7% of samples ranged between 5 mg/L − 10 mg/L and 19.1% of samples have concentrations above 10 mg/ L. Meanwhile, NO_3^-−N concentrations in Ocho varied from 0.7 mg/L −15.1 mg/L with a mean and median value of 4.8 mg/L and 4.5 mg/L respectively. These concentrations were much lower than those of Kubi. In Ocho village, over 62.5% of the groundwater samples had NO_3^-−N concentrations less than 5 mg/L 31.3% of the samples had

concentrations between 5 and 10 mg/L, and 6.2% of the samples had NO_3^-–N concentrations above 10 mg/L.

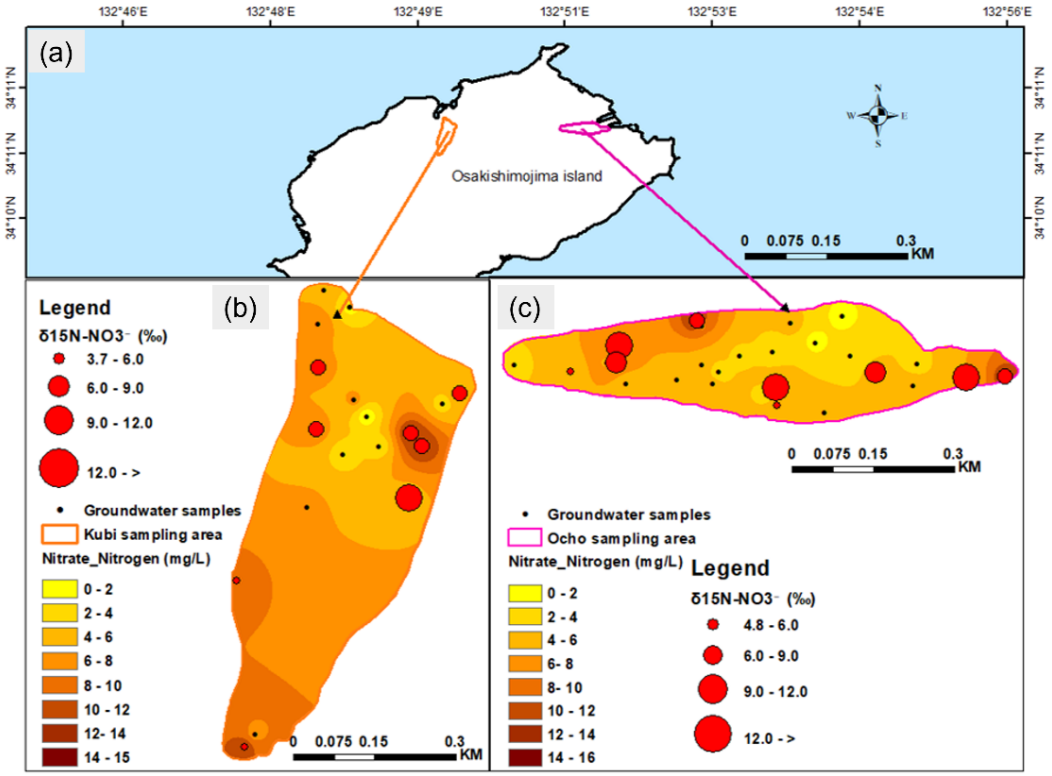

Figure 3.4: (a) Osakishimojima Island. Spatial variation of NO_3^-–N and $\delta^{15}NO_3^-$–N concentrations in groundwater of (b) Kubi and (**c**) Ocho villages.

The observed higher values of NO_3^-–N concentrations in Kubi village was likely attributed to differences in land use pattern and contribution from difference in fertilizer application by farmers which coincides with the spatial distribution of agricultural areas in the study sites. From Figure 3.4b, most of the higher concentrations of NO_3^-–N are located upstream of the lowland area which is directly below the upland citrus cultivation zone.

Leaching of chemical fertilizers into the groundwater, which are subsequently transported downstream, could be responsible for the elevated NO_3^-–N concentrations in Kubi. In contrast, Ocho village had lower NO_3^-–N concentrations, with some sampling points showing relatively high NO_3^-–N concentrations, including upstream, midstream, and downstream sampling points (Figure 3.4c). Groundwater contamination was likely caused by

organic fertilizer inputs or leakages from the septic systems. The NO_3^-–N concentration was observed to be between 3 and 8 mg/L at well depth between 4 and 6 m (Figure 3.5).

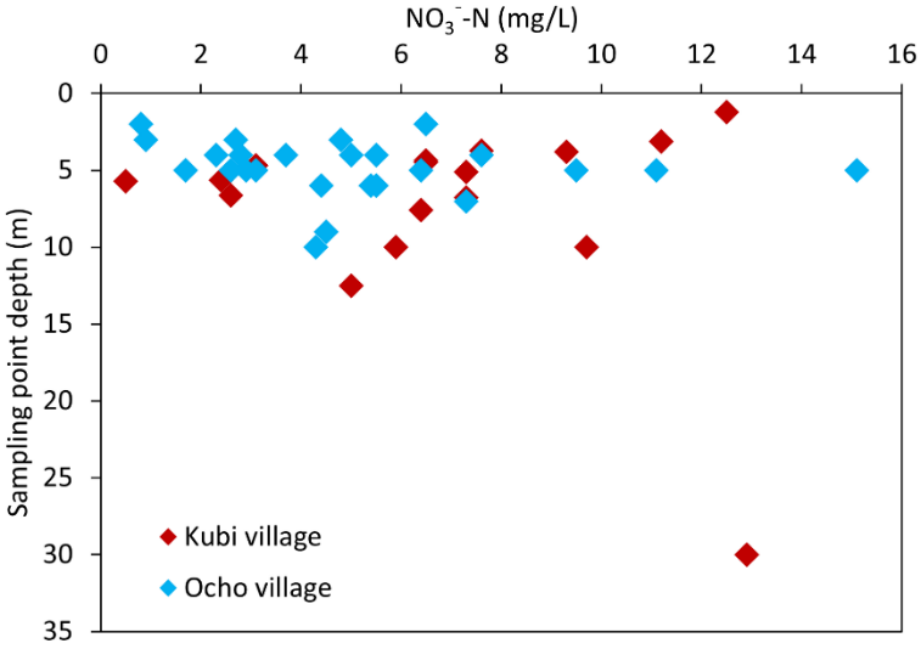

Figure 3.5: NO_3^-–N (mg/L) concentration vs. well depth in shallow wells in Kubi and Ocho villages.

A pattern can be observed in Kubi with groundwater NO_3^-–N concentrations gradually increasing from deeper depths to shallower depths but for some few samples showing higher concentrations even at deeper depths. This may reflect variations in NO_3^-–N residence time in the groundwater system. The topography and hydrogeological properties of the aquifer might equally be influencing the distribution of groundwater contaminants (Lasagna et al., 2019), however, this relationship could not be confirmed in this study because of unavailability of data. In Ocho, NO_3^-–N concentrations didn't change much with depths with most samplings plotting at 5 m depth.

3.4.3 Relationship between NO_3^-–N and water chemical parameters

A correlation coefficients between measured parameters for all groundwater samples in Kubi and Ocho are presented in Table 3.2. According to the statistical significance levels,

most of these correlations are valid and reasonably accurate. In Ocho village, NO_3^-–N was positively correlated with SO_4^{2-} (r = 0.69, p < 0.01), Na^+ (r = 0.72, p < 0.01), Mg^{2+}(r = 0.6, p < 0.01), Ca^{2+} (r = 0.48, p < 0.05) and EC (r =0.6, p < 0.01) meanwhile in Kubi village NO_3^-–N was positively correlated with SO_4^{2-} (r = 0.88, p < 0.01), Na^+ (r = 0.68, p < 0.01), Mg^{2+}(r = 84, p < 0.01), Ca^{2+} (r = 0.8, p < 0.05) and EC (r =0.6, p < 0.01).

Table 3.2: Correlation matrix between measured parameters in Kubi and Ocho villages.

	NO_3^-–N	Cl^-	HCO_3^-	SO_4^{2-}	Na^+	K^+	Mg^{2+}	Ca^{2+}	EC	DOC
Kubi village (n =19)										
NO_3^-–N										
Cl^-	0.17									
HCO_3^-	-0.2	-0.37								
SO_4^{2-}	.88**	0.15	-0.15							
Na^+	.68**	.67**	-0.21	.66**						
K^+	-0.18	-0.14	-0.21	-0.45						
Mg^{2+}	.84**	0.38	-0.13	.93**	.77**	-0.12				
Ca^{2+}	.80**	0.35	0.06	.85**	.74**	-0.02	.94**			
EC	.63**	0.11	0.32	.66**	.60**	-0.07	.73**	.71**		
DOC	0.37	-0.28	-0.36	0.29	-0.02	-0.04	0.21	0.1	0.16	
Ocho village (n=23)										
NO_3^-–N										
Cl^-	0.38									
HCO_3^-	0.08	.59**								
SO_4^{2-}	.69**	0.33	0.00							
Na^+	.72**	.59**	0.28	.82**						
K^+	-0.08	0.00	0.05	-0.16	-0.12					
Mg^{2+}	.60**	.56**	0.25	.82**	.80**	-0.18				
Ca^{2+}	.48*	.54**	0.21	.74**	.62**	0.12	.85**			
EC	.60**	.67**	0.34	.67**	.66**	-0.27	.72**	.72**		
DOC	-0.03	-0.23	0.15	-0.12	-0.12	0.32	-0.26	-0.25	-0.16	

* Correlations significant at p = 0.05

** Correlations significant at p = 0.01

The relatively high concentration of NO_3^-–N in the Kubi groundwater was consistent with the significantly elevated concentrations of major cations and anions Mg^{2+} and Ca^{2+} and SO_4^{2-} (Figure 3.6).

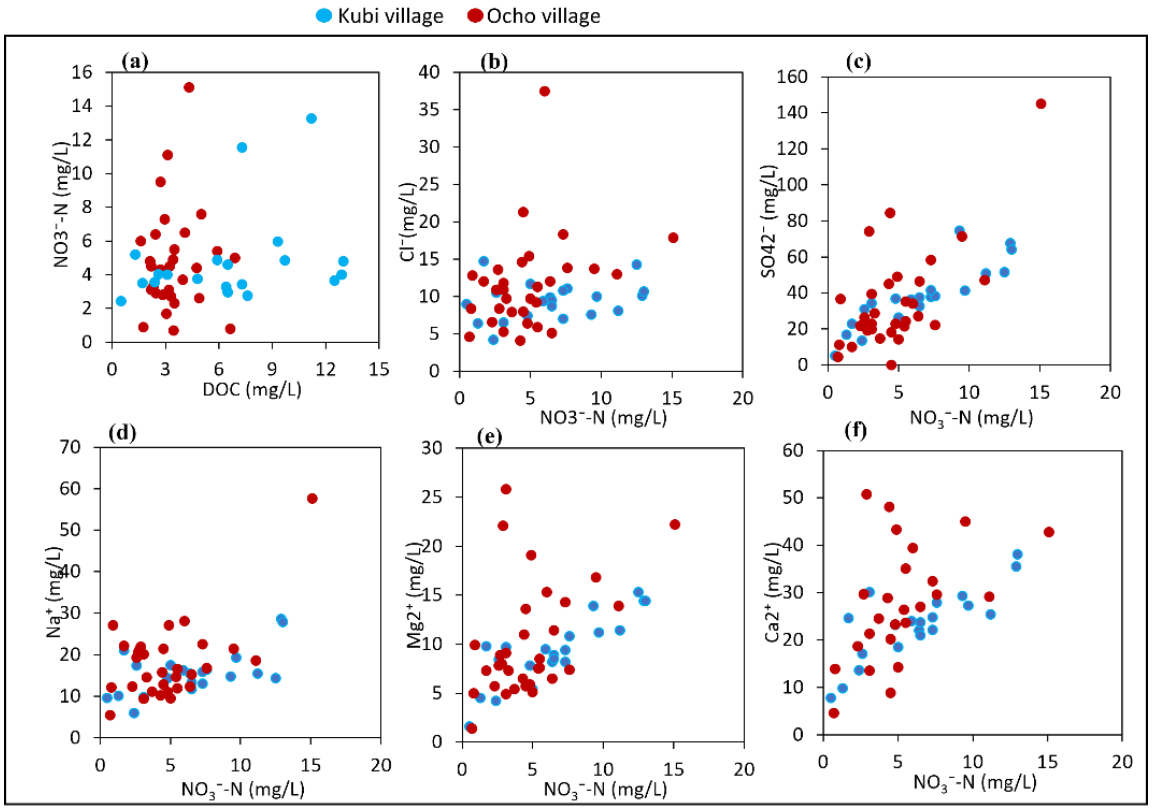

Figure 3.6: Relationship between NO_3^-–N and (a) DOC, (b) Cl^-, (c) SO_4^{2-}, (d) Na^+, (e) Mg^{2+}, and (f) Ca^{2+}.

There was a weak positive association among NO_3^-–N, DOC, and Cl^- in both Kubi and Ocho villages. In the absence of a geological chloride source, nitrate and chloride are frequently utilized as indicators of anthropogenic groundwater contamination because of their positive correlations. While chloride is a conservative tracer that does not normally undergo biological transformation in groundwater, the denitrification process can reduce the nitrate concentration in groundwater (Rivett et al., 2008; Korom,1992). Thus, the presence of this process in the groundwater samples from Kubi and Ocho might have reduced the degree of correlation between the parameters shown in Figure 3.6.

Furthermore, the positive relationship between NO_3^-–N and SO_4^{2-} could be due to the use of chemical fertilizers such as $(NH_4)_2SO_4^{2-}$ (Babiker et al., 2004). A positive relationship has been suggested among NO_3^-, Mg^{2+}, and Ca^{2+} (Fu et al., 2019), indicating that they are

derived from chemical fertilizers, such as $CaCO_3$ and $MgCO_3$. In Kubi, concentrations of NO_3^-–N showed strong significant positive correlations with SO_4^{2-} ($R^2 = 0.76$, $p < 0.01$) as opposed to Ocho, which presented a weak significant positive relationship ($R^2 = 0.45$, $p < 0.01$). This agrees with earlier studies by (Cuoco et al., 2015; Rufini et al., 2019) affirming, there exist a correlation between SO_4^{2-} and NO_3^- concentrations in groundwater, indicating that locations with high SO_4^{2-} concentrations also have high NO_3^- concentrations. More chemical fertilizers may be used in Kubi since the chemical fertilizer derived component was higher in Kubi than Ocho. The observed higher values of NO_3^-–N concentrations in Kubi village were likely attributed to differences in the type of fertilizer used by farmers and the proportion applied to the area under cultivation, which coincides with the spatial distribution of agricultural areas in the study sites. Other researchers (Nakagawa et al., 2016) found that the application of $CaCO_3$ fertilizer to their research site generated a positive association between NO_3^- and Ca^{2+}. Similarly, in Kubi village ($R^2 = 0.63$, $p < 0.01$), there was a considerable positive correlation between NO_3^-–N and Ca^{2+} compared to that in Ocho ($R^2 = 0.22$, $p < 0.01$), confirming inputs from chemical fertilizers. K^+ showed no correlation with NO_3^-–N in both study sites.

3.4.4 Principal component analysis results

A three-factor model controlled the groundwater chemistry of in Kubi, and the cumulative variance by the three PCs was 73.2% (Table 3.3). In Kubi, PC1 explained 40.9 % of the total variation, with positive loadings of 6 variables in the order $Mg^{2+} > SO_4^{2-} > NO_3^-$–N > Na^+> TDS > Ca^{2+} (Table 3.3). A strong positive loading of Mg^{2+}, and SO_4^{2-} and a moderate positive loading of Ca^{2+} and TDS suggest increased mineralization of groundwater water from natural sources, whereas a strong positive loading of NO_3^-–N indicates anthropogenic pollution from agricultural activities such as fertilizer usage, manures, and land use (Egbi et al., 2019). Several studies (Earle, 2009; Yadav et al., 2002; Huang et al., 2018a) have linked domestic sewage and agricultural fertilizers to the occurrence of Na^+, Mg^{2+}, K^+, SO_4^{2-}, NO_3^- and Cl^-.

Thus, PC1 was denoted by infiltration of agricultural fertilizer and domestic sewage. PC2, accounting for 19.5% of the total variance, showed a moderate positive loading for DO and a moderate negative loading for K^+.

PC3 explained 13% of the total variance with moderate loadings of pH. The groundwater chemistry of Ocho was also controlled by a three-factors model, and the cumulative variance explained by the three PCs was 67.8% (Table 3.3). PC1, accounting for 38.2% of the total variance, showed strong loadings of SO_4^{2-} and NO_3^-–N, and moderate loadings for Ca^{2+}, Mg^{2+}, and Na^+. Although these variables can be interpreted as anthropogenic contamination from agricultural fields, their loadings were lower in comparison to PC1 in the Kubi area, possibly due to difference in rate of leaching and residence time of contaminants in the groundwater system.

Table 3.3: Principal component (PC) loadings of 11 chemical variables in the groundwater samples of Kubi and Ocho.

PCs Kubi village (21 samples)				PCs Ocho village (32 samples)			
Variables	**PC1**	**PC2**	**PC3**	**Variables**	**PC1**	**PC2**	**PC3**
pH	-0.098	0.396	***0.663***	pH	-0.088	-0.242	***0.768***
TDS	***0.783***	-0.379	0.309	TDS	0.542	***0.686***	0.141
DO	-0.209	***0.766***	0.105	DO	0.035	***-0.726***	0.382
NO_3^-–N	***0.903***	-0.05	-0.119	NO_3^-–N	***0.815***	0.058	-0.033
Cl^-	0.407	0.398	-0.528	Cl^-	0.376	***0.723***	0.067
SO_4^{2-}	***0.914***	-0.018	-0.001	SO_4^{2-}	***0.922***	0.041	-0.067
HCO_3^-	-0.117	-0.603	0.574	HCO_3^-	-0.131	***0.798***	-0.002
Na^+	***0.823***	0.394	0.117	Na^+	***0.683***	0.517	-0.047
K^+	-0.167	***-0.747***	-0.375	K^+	-0.109	-0.144	***-0.787***
Mg^{2+}	***0.917***	-0.099	-0.13	Mg^{2+}	***0.719***	0.124	0.055
Ca^{2+}	***0.673***	-0.051	0.29	Ca^{2+}	***0.754***	-0.023	0.102
Eigen value	4.5	2.2	1.5		4.3	2	1.3
EV	40.9	19.5	13		38.2	18	11.7
CV	40.9	60.3	73.2		38.2	56.2	67.8

EV: Explained variance (%); CV: Cumulative % of variance; Bolding and Italics numbers: PC loadings that are significant at (> 0.65)

PC2 explained 18% of the total variance with moderate positive loadings on 3 variables (HCO_3^-, Cl and TDS) and a negative loading on DO. We can consider that, the dissolution of carbonate rocks by water-rock interaction was responsible for the loading of HCO_3^- while Cl^- contributing source was from domestic sewage. The third PC, which accounts for 11.7% of the total variance in Ocho village, had moderate positive and negative loadings for pH and K, respectively. The results from PC indicate that natural processes involving mineral components and anthropogenic contamination from fertilizers and domestic sewage are the main processes affecting groundwater chemistry in Kubi and Ocho.

3.4.5 Distribution characteristics of stable isotopes

Ten samples from Kubi (1 river, and 9 well samples) and nine well samples from Ocho were analyzed $\delta^{15}N\text{-}NO_3^-$ and $\delta^{18}O\text{-}NO_3^-$ (Table 3.4). Samples were selected primarily on the bases of nitrate levels and spatial distribution to represent each study site. The $\delta^{15}N\text{-}NO_3^-$ values of Osakishimojima Island showed high variability in the Kubi and Ocho villages (Figure 3.3). In Kubi village, the $\delta^{15}N\text{-}NO_3^-$ values of groundwater samples ranged from 3.7 ‰ to 13.3 ‰, with a mean value of 6.7 ‰, and the $\delta^{18}O\text{-}NO_3^-$ values ranged from -1.0 ‰ to 2.8 ‰, with a mean value of 1.5 ‰. Similarly, in Ocho village, the $\delta^{15}N\text{-}NO_3^-$ values ranged from 4.9 ‰ to 26.0 ‰, with a mean value of 11.4 ‰, and the $\delta^{15}N\text{-}NO_3^-$ values ranged from 0.1 ‰ to 14.9 ‰, with a mean value of 5.3 ‰ (Table 3.4).

Table 3.4: Isotopic data (‰) of sampled groundwater in Kubi and Ocho areas, October 2021.

Kubi village				Ocho village			
Sample	**Type**	**$\delta^{15}N\text{-}NO_3^-$**	**$\delta^{18}O\text{-}NO_3^-$**	**Sample**	**Type**	**$\delta^{15}N\text{-}NO_3^-$**	**$\delta^{18}O\text{-}NO_3^-$**
OKR1	River	7.2	2.1	OG4	Well	9.9	2.6
OK BH	Borehole	6.5	1.2	OG6	Well	26	14.9
OKU2	Well	3.7	2.4	OG7	Well	6.6	1
OKU3	Well	5.1	0.8	OG11	Well	8.6	2.6

OKU5	Well	13.3	2.2	OG14	Well	15.2	3.3
OKU6	Well	6.8	1.4	OG17	Well	5.2	0.7
OKU11	Well	5.3	-1	OG21	Well	14.5	14.7
OKD2	Well	6.8	2.8	OG24	Well	12	7.7
OKD4	Well	6.5	1.4	OG26	Well	4.9	0.1
OKD5	Well	6.1	1.6	Min		4.9	0.1
Min		3.7	-1	Max		26	14.9
Max		13.3	2.8	Mean		11.4	5.3
Mean		6.7	1.5	STDev		6.7	5.9
STDEV		2.6	1.1				

A relatively high value of $\delta^{15}N\text{-}NO_3^-$ (26 ‰) in sample OG6 may suggest other controlling processes in the catchment area, such as denitrification, however since the sample size was small, it was excluded from further analysis to avoid bias estimation, especially in the SIAR model. The mean values of $\delta^{15}N\text{-}NO_3^-$ and $\delta^{18}O\text{-}NO_3^-$ in Kubi village were significantly lower than those in Ocho village. This was contrary to the spatial distribution of NO_3^-−N concentrations (Figure 3.3). The reason is that more chemical fertilizers with lower isotopic values and faster leaching rate were used for citrus cultivation in Kubi than in Ocho. In general, the leaching rate is determined by the degree of water solubility of a fertilizer in combination with the amount of soil water at any time, soil type, porosity, and compaction (Soil Health, 2013). Kubi and Ocho have the same soil type and soil properties, but due to the differences in their choice of fertilizer, variations in NO_3^-−N concentrations may arise. Highly soluble fertilizers dissolve quite rapidly into the soil and since plants can only absorb a certain amount of nutrition at a time, a greater percentage of the fertilizer simply leaches through the soil into the groundwater. The nitrate sources were identified from the cross-plot of $\delta^{15}N\text{-}NO_3^-$ and $\delta^{18}O\text{-}NO_3^-$ (Figure 3.7).

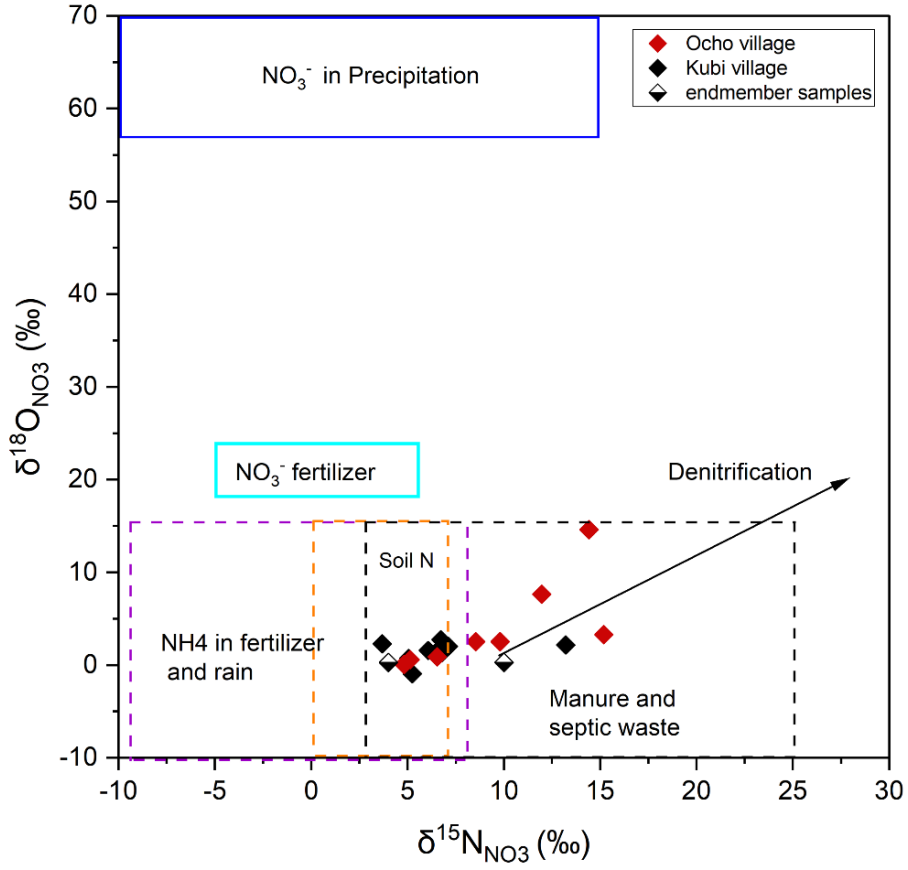

Figure 3.7: Nitrate isotopic signatures for sampling points in Kubi and Ocho with typical nitrate endmembers (adapted from Kendal et al.,2008).

Most of the data points were plotted in the range of synthetic fertilizer and soil nitrogen in Kubi village, while in Ocho village, points were plotted mainly in the manure and sewage domain. This suggests that the major inputs of NO_3^- are from synthetic fertilizer in Kubi, whereas in Ocho, they are mainly from organic fertilizer. The groundwater chemistry in Figure 3.6 and Table 3.3 suggests that more chemical fertilizer is used in Kubi than in Ocho, which explains the significant differences in the isotopic values between the sites. Additionally, higher $\delta^{15}N\text{-}NO_3^-$ concentrations may have been derived from sewage systems, whose end-member samples were not measured in this study.

Ocho has a higher housing density than Kubi (Figure 3.2), and since the area is a rural depopulating and aging community, the sewage system may be poorly managed with possible

contamination from leakages through worn out pipes into the groundwater system. According to (Kure City Water Works and Sewerage Bureau, 2021). Kubi has a local waste treatment plant while Ocho depend solely on septic treatment tanks. Given the density in ocho, sewer discharge into the groundwater is more likely. The difference in the age structure and population size influences farming practices, such as the method of fertilizer and pesticide application and the application schedule, which are important processes for quality crop yields. Chemical fertilizers are water soluble which makes them readily available for plant uptake than organic fertilizers thus, aged farmers prefer to use chemical fertilizers that are more cost-effective, less time consuming, and more convenient for maximum crop yield. However, because the nutrient requirements for plant growth, productivity, and fruit quality fluctuate seasonally, the split fertilization method is commonly utilized in citrus farming (Morgan et al., 2020).

While this strategy is acceptable and reduces inorganic N leaching while boosting N use efficiency (Moe et al., 2014), it necessitates the utilization of an additional labour force, which is unsuitable for Kubi and Ocho as the population is both declining and aging (Kure city report, 2021; Japan Agricultural Cooperatives, 2022) with a limited crop-production labour force. In studies conducted in China by (Moe et al., 2014; Zhou et al., 2017), the association between fertilization application methods, population ageing, and restricted labour force has been observed. However, given that Kubi farmers tend to use more fertilizer may possibly be because of their lower population size when compared to Ocho (Kure city report, 2021). Since the decreasing population has a reduced labor force which drives farmers towards the choice of using chemical fertilizers to increase crop yields even with the low work force to perform proper farming methods.

Also, the proportion of area under cultivation may influence the quantity of fertilizer applied, subsequently contributing to elevated NO_3^-−N. As observed in Figure 3.2, Kubi has

approximately 40.2 % of its total area occupied by orchard fields, which is twice the coverage area than that of Ocho village even thou at the catchment scale Ocho has almost thrice agricultural land than Kubi (Ministry of Land, Infrastructure, Transport, and Tourism of Japan, 2021), the pathways of nitrate in the two study sites may be different. Nevertheless, the overlapping $\delta^{15}N\text{-}NO_3^-$ and $\delta^{18}O\text{-}NO_3^-$ values of the different sources hinder the quantitative estimation of their contributions. Some samples showed trends towards denitrification in Ocho; however, we could not confirm the occurrence of this process because the used sample size in this study was relatively small (n = 9). Furthermore, a previous study reported related investigations and concluded that the link among $\delta^{15}N$, $\delta^{18}O$, and NO_3^- is a complex web in which all environmental settings should be considered to accurately distinguish between different biogeochemical processes (Chen et al., 2007). Hence, biological, and geochemical processes may be occurring simultaneously in Ocho village which results in the shift in $\delta^{15}N$ and $\delta^{18}O$ levels.

3.5 Source apportionment of NO_3^-

The proportional contributions of NO_3^- sources in groundwater were identified using the SIAR model. Two isotopes (J = 2) ($\delta^{15}N\text{-}NO_3^-$ and $\delta^{18}O\text{-}NO_3^-$) and three potential sources (K = 3) (OF, CF_SN, and M&S) were used to estimate the contributions of NO_3^- sources in Kubi and Ocho village. The $\delta^{15}N\text{-}NO_3^-$ and $\delta^{18}O\text{-}NO_3^-$ of groundwater samples (Table 3.4) and sources (both mean and SD in Table 3.5) were input into the SIAR model

Table 3.5: The δ15N and δ18O values of various nitrate sources.

Source	**$\delta^{15}N$ (‰)**		**$\delta^{18}O$ (‰)**	
	Mean	**SD**	**Mean**	**SD**
[b]SN	4.4	0.7	2.85	0.2
[a]CF	4	0.3	2.85	0.4
[a,b]CF_SN	4.2	0.5	2.9	0.3

[a]OF	10	0.3	2.85	0.4
[b]M&S	19	0.3	-12.51	0.4

[a] Theoretical values analyzed, and [b]data sources (Kendall et al., 2008; Fahullah et al., 2020; Fu et al., 2019; Yu et al., 2020).

Sewage was not measured in the study area; however, considering the residential area in one of the study sites, we applied the literature value for the model, while atmospheric deposition was not considered. Furthermore, the fractionation factor C_{jk} was set to zero because we did not investigate to determine its value. The results of source apportionment are shown in Figure 3.8.

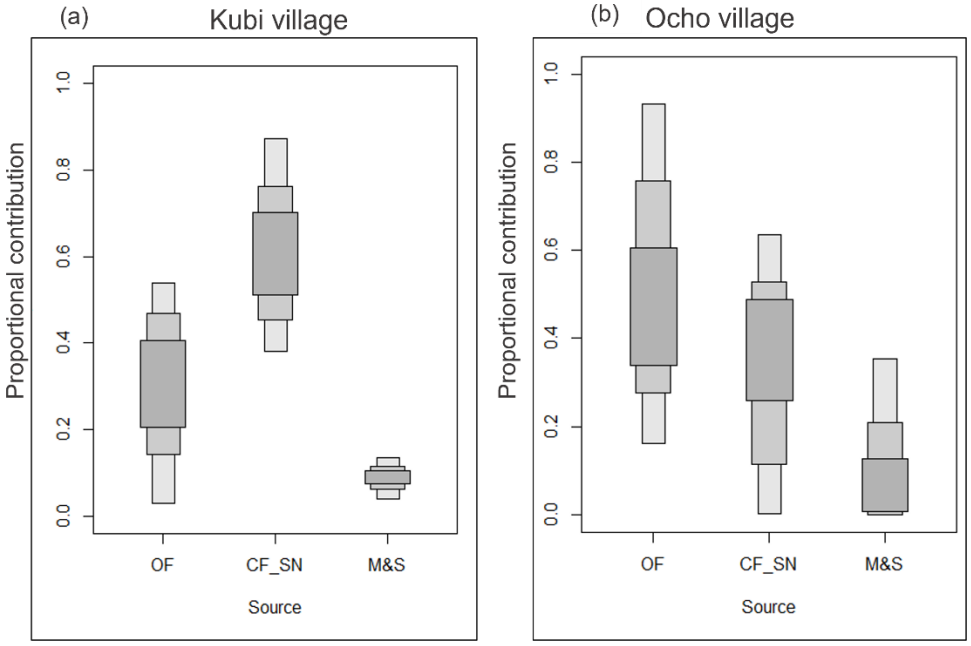

Figure 3.8: Spatial proportional contributions of NO_3^- sources estimated using SIAR in (a) Kubi and (b) Ocho villages. Boxplots illustrate the 50th, 75th and 95th percentiles from dark to light.

The source contributions showed significant spatial variation under similar cropping systems with different land-use proportions. The dominant NO_3^- pollution source in Kubi village was CF_SN, which contributed 60.1 %, followed by OF, which contributed 30.1 %, and M&S, which contributed 9.8% (Figure 3.8). An increase in the fertilizer source

contribution in the research area could also be due to the irrigation system. According to another study conducted by (Lui et al., 2013), higher yields from irrigated crops are generally associated with higher nitrogen fertilizer applications, increasing the risk of N loss to the environment. In Ocho village, the proportional contribution decreased in the following order: M&S (10.9 %) < CF_SN (38.5 %) < OF (50.7 %).

The results of NO_3^- source apportionment with SIAR in Ocho corresponded with our field investigation and the land use distribution shown in (Figure 3.2). Residential areas in Ocho are more concentrated than those in Kubi and have a low urbanization level due to depopulation. Contamination from old and poorly maintained drainage systems is highly probable. According to (Kure City Water Works and Sewerage Bureau, 2021), 70% of the resident' wastewater for Kubi is treated by a local wastewater treatment plant while the remaining 30% is treated by septic tank whereas in Ocho all waste is treated by septic tanks. The difference between the waste management system may explain the differences in NO_3^-–N concentrations in each area. Hence, chemical fertilizer is mainly used in Kubi and organic fertilizer in Ocho (Figure 3.7). However, due to differences in wastewater treatment systems, Ocho has higher values of sewage and manure contributions than Kubi (Kure City Water Works and Sewerage Bureau, 2021), but this impact is not so high when compared to organic fertilizer input, so we conclude that the main source of nitrate pollution is organic fertilizer. Additionally, Kubi's proportional input of manure, sewage, and chemical fertilizer suggests a high rate of leaching that may differ from Ocho village and result in a higher concentration of nitrates in the ground-water system.

In summary, chemical fertilizers are mainly used in Kubi and organic fertilizers are used in Ocho (Figure 7). Due to differences in the wastewater treatment systems, Ocho has higher values of sewage and manure contribution than Kubi (Kure City Water Works and Sewerage Bureau, 2021) but its impact is not as high as that of organic fertilizer input; therefore,

we concluded that the main source of nitrate pollution is organic fertilizers. Additionally, large quantities of manure, sewage, and chemical fertilizers are used in Kubi, suggesting a high rate of leaching, resulting in a higher concentration of nitrates in the groundwater system. Table 3.6 demonstrates the relationship between social factors and groundwater nitrate–nitrogen contamination in Kubi and Ocho villages, with Kubi having a smaller population and agricultural area and a higher concentration of NO_3^-–N levels, primarily due to chemical fertilizers. Compared to Kubi village, Ocho village had lower NO_3^-–N levels despite having a larger population, and the organic fertilizers used in agricultural areas were the primary source of contamination.

Table 3.6: A summary of social aspects and groundwater NO_3^-–N contamination status in Kubi and Ocho villages.

Social Information	**Units**	**Kubi Village**	**Ocho Village**	**Key References**
Population		413	830	Kure city population Statistics, 2021
Average farmer age	Years	76	73	JA Yukata, 2022
Agricultural land	km^2	0.6	1.6	MLIT, 2021
Sewage treatment coverage	%	70	0	Kure City Water Works and Sewerage Bureau, 2021
Summary of NO_3^-–N concentration				Figure 3.4
Average NO_3^-–N concentration	mg/L	6.6	4.8	
<5	%	33.3	62.5	
5–10	%	47.7	31.3	
>10	%	19	6.2	
Main NO_3^-–N contribution ratio				Figure 3.8
Chemical fertilizer	%	60.1	38.4	
Organic fertilizer	%	30.1	50.7	
Manure and sewage	%	9.8	10.9	

3.6 Summary

Japan's society has undergone major social change, including increased population aging and depopulation, but it still faces serious environmental problems due to groundwater pollution. Intensification of fertilizer use in agricultural activity constitute one of the major factors contributing to elevated nitrate levels in Japanese groundwater resources. However, other factors may also contribute to pollution, such as land use, the proportion of cultivation and farming methods. We investigated the impact of population aging and depopulation on groundwater nitrate contamination on a western Japanese island that has extensive citrus farming. In comparison to the eastern Ocho village, where the average age of farmers is 73 years, the northern Kubi farmers are slightly older on average, at 76 years, and agricultural land decreased by 46% over the past ten years, from 2005 to 2015. Ocho had 830 residents, which was twice as many as Kubi. In comparison to Ocho, which had an average NO_3^-−N concentration of 4.8 mg/L (37.5% of water samples > 5 mg/L), Kubi village had a higher average NO_3^-−N concentration of 66.7 mg/L (66.7% of water samples > 5 mg/L). The proportional contribution for each NO_3^-−N source using SIAR (endmember method) showed that chemical fertilizer (60.1%) was the main contributing NO_3^-−N source in Kubi, while in Ocho, Organic fertilizer (50.7 %) was the major contributors, with minor contributions observed from sewage. These source distributions were associated to social aspects such as depopulation and population aging and to a greater extent land use type. It was suspected that a considerable quantity of chemical fertilizers applied by the older farmers in Kubi leads to inefficient nitrogen uptake by the plants, resulting in more leaching, which contaminates the groundwater more in Kubi than in Ocho.

3.7 References

Agrawal, G.D., Lunkad, S.K., Malkhed, T. Diffuse agricultural nitrate pollution of groundwaters in India. *Water. Sci. Technol*. **1999**, 39, 67–75.

Amberger, A., Schmidt, H.L. Natürliche Isotopengehalte von Nitrat als Indikatoren für dessen Herkunft. Geochim. Cosmochim. Acta **1987**, 51, 2699–2705. (In German).

Aravena, R., Robertson, W. Use of multiple isotope tracers to evaluate denitrification in groundwater: Case study of nitrate from a large-flux septic system plume. Ground Water **1998**, 36, 975–982.

Babiker, I.S. Mohamed, M.A.A., Terao, H., Kato, K., Ohta, K. Assessment of groundwater contamination by nitrate leaching from intensive vegetable cultivation using geographical information system. *Environ. Int*. **2004**, 29, 1009–1017.

Bedard-Haughn, A., van Groenigen, J. W., van Kessel, C. Tracing 15 N through landscapes: Potential uses and precautions. *J. Hydrol*. **2003**, 272, 175–190.

Chen, F.J., Jia, G.D., Chen, J.Y. Nitrate sources and watershed denitrification inferred from nitrate dual isotopes in the Beijiang River, south China. *Biogeochemistry*. **2009**, 94, 163–174.

Chen, J., Taniguchi, M., Liu, G., Miyaoka, K., Onodera, S., Tokunaga, T., Fukushima, Y. Nitrate pollution of groundwater in the Yellow River delta, China. *Hydrogeol. J.* **2007**, 15, 1605–1614.

Cuoco, E., Darrah, T.H., Buono, G., Verrengia, G., de Francesco, S., Eymold, W.K., Tedesco, D. Inorganic contaminants fromdiffuse pollution in shallow groundwater of the Campanian plain (southern Italy). Implications for geochemical survey. *Environ. Monit. Assess*. **2015**, 187, 46.

Earle, S. Physical Geology, 2nd ed.; BC Open Textbook Project; BC campus: Victoria, BC, USA, **2019**. Available online: https://books.google.co.jp/books?id=lSwwywEACAAJ (accessed on 3 May 2022).

Egbi, C.D., Anornu, G., Appiah-Adjei, E.K., Ganyaglo, S.Y., Dampare, S.B. Evaluation of water quality using hydrochemistry, stable isotopes, and water quality indices in the Lower Volta River Basin of Ghana. *Environ. Dev. Sustain*. **2019**, 21, 3033–3063.

Evangelou, V.P. Environmental Soil and Water Chemistry; Wiley: New York, NY, USA, **1998**.

Fadhullah, W., Syahirah Yaccob, N., Syakir, M.I., Akmal, M.S.,Yue, F.-J., Li, S.-L. Nitrate sources and processes in the surface water of a tropical reservoir by stable isotopes and mixing model. *Sci. Total Environ*. **2020**, 700, 134517.

Fu, X.M., Sun, Y.Y., Su, J., Zheng, M.X., Xi, B.D., Qian, G.R. Source of nitrate in groundwater based on hydrochemical and dualstable isotopes. *China Environ. Sci*. **2019**, 39, 3951–3958.

Haque, S.J.; Onodera, S.; Shimizu, Y. An overview of the effects of urbanization on the quantity and quality of groundwater in South Asian megacities. *Limnology*. **2013**, 14, 135–145.

Hayashi, K., Shibata, H., Oita, A., Nishina, K., Ito, A., Katagiri, K., Shindo, J., Winiwarter, W. Nitrogen budgets in Japan from 2000 to 2015: Decreasing trend of nitrogen loss to the environment and the challenge to further reduce nitrogen waste. *Environ. Pollut*. **2021**, 286, 117559.

Huang, G., Liu, C., Sun, J., Zhang, M., Jing, J., Li, L. A regional scale investigation on factors controlling the groundwater chemistry of various aquifers in a rapidly urbanized area: A case study of the Pearl River Delta. *Sci. Total Environ*. **2018**, 625,510–518.

Jackson, A.L., Inger, R., Bearhop, S., Parnell, A. Erroneous behaviour of MixSIR, a recently published Bayesian isotope mixing model: A discussion of Moore & Semmens (2008). *Ecol. Lett*. **2009**, 12, E1–E5.

Japan Japan Agricultural Cooperatives (JA), Yutaka, Hiroshima, **2022**. Yutaka Town Population Statistics (2005–2021) and Yutaka.

Ji, X.L.; Xie, R.T.; Hao, Y.; Lu, J. Quantitative identification of nitrate pollution sources and uncertainty analysis based on dual isotope approach in an agricultural watershed. *Environ. Pollut*. **2017**, 229, 586–594.

Keesari, T.; Ramakumar, K.L.; Chidambaram, S.; Pethperumal, S.; Thilagavathi, R. Understanding the hydrochemical behavior of groundwater and its suitability for drinking and agricultural purposes in Pondicherry area, South India—A step towards sustainable development. *Ground. Sustain. Dev*. **2016**, 2, 143–153.

Kendall, C. Tracing nitrogen sources and cycling in catchments. In Isotope Tracers in Catchment Hydrology; Kendall, C., McDonnell, J.J., Eds.; Elsevier Science: Amsterdam, The Netherlands. **1998**, 519–576.

Kendall, C., Elliott, E.M., Wankel, S.D. Tracing anthropogenic inputs of nitrogen to ecosystems. In Stable Isotopes in Ecology and Environmental Science; Michener, R.H., Lajtha, K., Eds.; Blackwell: Oxford, UK, **2008**, 375–449

Kimbi, S.B., Onodera, S., Nozaki, S., Tomozawa, Y., Wang, K., Rusydi, A.F., Saito, M. Impact of citrus agriculture on the quality of water resource in as small steep Island, Seto Inland Sea, Japan. *GEOMATE J*. **2021**, 20, 109–114.

Knapp, A.N., Sigman, D.M., Lipschultz, F.N. Isotopic composition of dissolved organic nitrogen and nitrate at the Bermuda Atlantic time-series study site. *Glob. Biogeochem. Cycles*. **2005**, 19, GB1018.

Kohl, D.H., Shearer, G.B., Commoner, B. Fertilizer nitrogen: Contribution to nitrate in surface water in a Corn Belt Watershed. *Science*. **1971**, 174, 1331–1334.

Korom, S.F. Natural denitrification in the saturated zone: A review. *Water Resour. Res*. **1992**, 28, 1657–1668

Kou, X., Ding, J., Li, Y., Li, Q., Mao, L., Xu, C., Zheng, Q., Zhuang, S. Tracing nitrate sources in the groundwater of an intensive agricultural region. *Agric. Water Manag*. **2021**, 250, 106826.

Kumazawa, K. Nitrogen fertilization and nitrate pollution in groundwater in Japan: Present status and measures for sustainable agriculture. *Nutr. Cycl. Agroecosystems.* **2002**, 63, 129–137.

Kure City Water Works and Sewerage Bureau, **2021**. Business Plan 2020. Pages: 110, Japanese. Available online: https://www.city.kure.lg.jp/site/jougesui/about-jigyougaiyou.html (accessed on 10 May 2022).

Kure City. Population Statistical Data (Basic Resident Register). **2021**. (In Japanese). Available online: https://www.city.kure.lg.jp/soshiki/36/people.html (accessed on 10 May 2022).

Lasagna, M., de Luca, D.A. Evaluation of sources and fate of nitrates in the western Po plain groundwater (Italy) using nitrogen and boron isotopes. *Environ. Sci. Pollut. Res*. **2019**, 26, 2089–2104.

Liu, T., Wang, F., Michalski, G., Xia, X.H., Liu, S.D. Using 15N, 17O, and 18O to determine nitrate sources in the Yellow River, China. *Environ. Sci. Technol*. **2013**, 47, 13412–13421.

Mcclain, M., Richey, J., Pimentel, T. Groundwater nitrogen dynamics at the terrestrial-lotic interface of a small catchment in the Central Amazon Basin. *Biogeochemistry.* **1994**, 27, 113–127.

McIlvin, M.R., Altabet, M.A. Chemical conversion of nitrate and nitrite to nitrous oxide for nitrogen and oxygen isotopic analysis in freshwater and seawater. *Anal. Chem*. **2005**, 77, 5589–5595.

Meghdadi, A., Javar, N. Quantification of spatial and seasonal variations in the proportional contribution of nitrate sources using a multi-isotope approach and Bayesian isotope mixing model. *Environ. Pollut*. **2018**, 235, 207–222.

Ministry of Land, Infrastructure, Transport, and Tourism of Japan. **2021**. Available online: https://nlftp.mlit.go.jp/ (accessed on 8 April 2022).

Moe, K., Yamakawa, T., Thu, T.T.P., Kajihara, Y. Effects of pretransplant basal and split applications of nitrogen on the growth and yield of Manawthukha rice. *Commun. Soil Sci. Plant Analysis.* **2014**, 45, 2833–2851.

Morgan, T.K., Kadyamakeni, M.D., Zekri, M.; Schumann, W.A., Vashisth, T., Obreza, A.T., Ferrarezi, S.R. 2021–2022 Florida Citrus Production Guide: Nutrition Management for Citrus Trees; UF/IFAS: Polk, FL, USA. **2020**.

Nakagawa, K., Amano, H., Asakura, H., Berndtsson, R. Spatial trends of nitrate pollution and groundwater chemistry in Shimabara City, Nagasaki Prefecture, Japan. *Environ. Earth Sci*. **2016**, 75, 1–17

Nolan, B., Stoner, J. Nutrients in groundwaters of the conterminous United States, 1992–1995. *Environ. Sci. Technol*. **2000**, 34,1156–1165.

Onodera, S. Subsurface pollution in Asian megacities. In Groundwater and Subsurface Environments: Human Impacts in Asian Coastal Cities; Springer: Berlin/Heidelberg, Germany. **2011**; pp. 159–184.

Parnell, A.C., Inger, R., Bearhop, S., Jackson, A.L. Source partitioning using stable isotopes: Coping with too much variation. PLoS ONE. **2010**, 5, e9672.

Peralta, E.M., Batucan, L.S., De Jesus, I.B.B., Triño, E.M.C., Uehara, Y., Ishida, T., Kobayashi, Y., Ko, C.Y., Iwata, T., Borja, A.S., et al. Nutrient loadings and deforestation decrease benthic macroinvertebrate diversity in an urbanised tropical stream system. *Limnologica*. **2020**, 80, 125744.

Piper, A.M. A graphic procedure in the geochemical interpretation of water analyses. *Eos Trans. Am. Geophys. Union*. **1944**, 25, 914–923.

Rivett, M.O., Buss, S.R., Morgan, P., Smith, J.W.N., Bemment, C.D. Nitrate attenuation in groundwater: A review of biogeochemical controlling processes. *Water Res*. **2008**, 42, 4215–4232.

Rufino, F., Busico, G., Cuoco, E., Darrah, T.H., Tedesco, D. Evaluating the suitability of urban groundwater resources for drinking water and irrigation purposes: An integrated approach in the Agro-Aversano area of Southern Italy. *Environ. Monit. Assess*. **2019**, 191, 768.

Rusydi, A.F., Onodera, S., Saito, M., Hyodo, F., Maeda, M., Sugiantiuyo, K., Wibawa, S. Potential sources of ammonium-nitrogen in the coastal groundwater determined from a combined analysis of nitrogen isotope, biological and geological parameters, and land use. *Water*. **2021**, 13, 25.

Sacchi, E., Acutis, M., Bartoli, M., Brenna, S., Delconte, C.A., Laini, A., Pennisi, M. Origin and fate of nitrates in groundwater from the central Po plain: Insights from isotopic investigations. *Appl. Geochem*. **2013**, 34, 164–180.

Saito, M., Onodera, S., Okubo, K., Takagi, S., Maruyama, Y., Jin, G., Shimizu, Y. Effects of physical and morphometric factors on nutrient removal properties in agricultural ponds. *Water Sci. Technol*. **2015**, 72, 2187–2193.

Soil Health, **2013**. Leaching Characteristics of Organic Fertilizers. Lebanon Turf Cumberland ST. Lebanon. Available online: https://www.lebanonturf.com/education-center/soil-health (accessed on 9 June 2022).

Tase, N. Groundwater contamination in Japan. Environ. Geol. Water Sci. **1992**, 20, 15–20.

Torres-Martínez, J.A., Mora, A., Knappett, P.S.K., Ornelas-Soto, N., Mahlknecht, J. Tracking nitrate and sulfate sources in groundwater of an urbanized valley using a multi-tracer approach combined with a Bayesian isotope mixing model. *Water Res*. **2020**, 182, 115962.

Town Farmer Age and Population Statistics (1970–2005), Unpublished Data in Japanese. **2022**. Available online: https://www.city.kure.lg.jp/ (accessed on 10 May 2022).

Tu, Y., Fang, Y.T., Liu, D.W., Pan, Y.P. Modifications to the azide method for nitrate isotope analysis. *Rapid. Commun. Mass. Spectrom*. **2016**, 30, 1213–1222.

Umezawa, Y., Hosono, T., Onodera, S., Siringan, F., Buapeng, S., Delinom, R., Yoshimizu, C., Tayasu, I., Nagata, T., Taniguchi, M. Sources of nitrate and ammonium contamination in groundwater under developing Asian megacities. *Sci. Total. Environ*. **2008**, 404, 361–376.

Wang, K., Onodera, S., Saito, M. Evaluation of nitrogen loading in the last 80 years in an urbanized Asian coastal catchment through the reconstruction of severe contamination period. *Environ. Res. Lett*. **2022**, 17, 014010.

WHO. Guidelines for Drinking-Water Quality: First Addendum to the Fourth Edition; WHO: Geneva, Switzerland, **2017**.

Wu, D.D.; Jiang, Y.H.; Jia, J.Y.; Cai, H.S. Analyses of pollution source of nitrogen in groundwater with δ^{15}N-NO_3^- and δ^{18}O-NO_3^- in Changzhou. *Hydrogeol. Eng. Geol*. **2006**, 3, 11–15.

Xue, D.M., Botte, J., Baets, B.D., Accoe, F., Nestler, A., Taylor, P., Cleemput, O.V., Berglund, M., Boeckx, P. Present limitations and future prospects of stable isotope methods for nitrate source identification in surface- and groundwater. *Water Res*. **2009**, 43, 1159–1170.

Yadav, R.K., Goyal, B., Sharma, R.K., Dubey, S.K., Minhas, P.S. Post-irrigation impact of domestic sewage effluent on composition of soils, crops and ground water—A case study. *Environ. Int*. **2002**, 28, 481–486.

Yu, L., Zheng, T., Zheng, X., Hao, Y., Yuan, R. Nitrate source apportionment in groundwater using Bayesian isotope mixing model based on nitrogen isotope fractionation. *Sci. Total Environ*. **2020**, 718, 137242.

Zhang, F., Huang, G., Hou, Q., Liu, C., Zhang, Y., Zhang, Q. Groundwater quality in the Pearl River Delta after the rapid expansion of industrialization and urbanization: Distributions, main impact indicators, and driving forces. *J. Hydrol*. **2019**, 577, 124004.

Zhang, Y., Li, F., Zhang, Q., Li, J., Liu, Q. Tracing nitrate pollution sources and transformation in surface- and ground-waters using environmental isotopes. *Sci. Total. Environ*. **2014**, 490, 213–222.

Zhou, Z.J., Shen, Y.Z., Du, C.W., Zhou, J.M., Qin, Y.S., Wu, Y.J. Economic and soil environmental benefits of using controlled-release bulk blending urea in the North China plain. *Land. Degrad. Dev*. **2017**, 28, 2370–2379.

Chapter 4

Simulation of daily streamflow with SWAT illuminates the impact of land-use change with urbanization and climate change on groundwater recharge over the last three decades

This chapter is an edited version of the article:

Kimbi, S.B., Wang, K., Onodera, Shin-I., Kaihotsu, I., Shimizu, Y. Simulation of daily streamflow with SWAT illuminates the impact of land-use change with urbanization and climate change on groundwater recharge over the last three decades (**To be submitted**) Journal of Environmental science and Technology

4.1 Introduction

Urbanization is a major social change that refers to the gradual increase in the proportion of people living in urban areas and how each society manages this change, and globally, 54% of the population resides in cities, and that number is projected to increase from 60% to 92% by the year 2050 (Ritchie and Rose, 2018). Urbanization is a major social change that refers to the gradual increase in the proportion of people living in urban areas and how each society manages this change (NLM, 2014). In decades, the increase in urbanization has resulted in major challenges in freshwater distribution, with a noticeable impact on the quality and quantity of water sources (Nasiri et al., 2020; Onodera 2011; Doveri et al., 2015; Wakode et al., 2014). Urbanization processes results in significant topographic and vegetational changes, ultimately affecting groundwater resources and the environment (Hamel et al., 2013;

Gatwaza et al., 2016). These changes have been recognized as significant issues affecting catchment water balances both globally and at watershed scales (Haase, 2009; Yigzaw and Hossain, 2016; Kundu et al., 2017; Terskii et al., 2017; Oudin et al., 2018). In addition to anthropogenic impact on watershed hydrology, climate change has been identified as one of the major stressors on water resource sustainability, and to a larger extent, the combination of these stressors has major implications on the water cycle (Zareian et al., 2016; Zhang et al., 2018; Chen and Bofu, 2013). Precipitation and temperature cycles, which have become increasingly unpredictable due to climate change, impact water resources both spatially and temporally (Petersen-Perlman et al., 2017). In fact, according to a report by (Climate Service Center, 2018), the average temperatures have increased by 0.04°C over the last decade while the total annual rainfall has increased by 12% over the three decades. These, combined changes will increase the occurrence and intensity of rainfall events with corresponding adverse effects such as increase floods and droughts events (Gibson et al., 2005). This will certainly have a huge impact on the environment, as changes in urbanization, climate, and land cover will have undesirable effect on the water balance of a given region, subsequently affecting the quantity and quality of freshwater entering the ground. Understanding the impact of environmental factors on hydrological processes calls for the application of hydrological models that can simulate changes in the water cycle over time and space and quantify the impacts of these changes on renewable freshwater availability for multiple sectoral water use (Chung et al., 2010; Flörke et al., 2018). Compared to other modelling techniques, hydrological models are more effective for planning and developing integrated approaches to water resources management, as they are capable of directly estimating water balance components and analyzing human influences with more accurate and useful results (Naef et al., 2002). In addition, these models can be used to assess past as well as possible future impact scenarios at the catchment scale.

Water balance provides an overview of the availability of water in the watershed and to appropriately manage these water resources, it is important to quantify the components of hydrologic processes. The assessment of water balance using hydrological models is a common method used to analyze the effects of land-use changes, climate change, and urbanization processes on watershed hydrology. Several models have been used to study hydrological aspects in watersheds such as the Hydrologic Engineering Centres–River Analysis System (Thakur et al., 2017), Tank model (Ou et al., 2017) and Soil and Water Assessment Tool (Arnold et al., 2012). Among these models, Soil and Water Assessment Tool (SWAT) is a continuous semi-distributed hydrological model that has been used widely for assessing the impacts of land-use change on hydrological processes and simulates agricultural watershed management practices (Moriasi et al., 2007; Francesconi et al., 2016), helps to evaluate and quantify surface and groundwater flow in various watersheds (Vazquez-Amabile and Engel., 2008), assesses the impact of climate and land-use changes under different management practices (Singh and Gosain, 2011; Kundu et al., 2017; Ridwansyah et al., 2020) and is used in various climatic areas of the worldwide ranging from a semi-arid climate (Baker and Miller, 2013; Shivhare et al., 2014; Sellami et al., 2016 Suryavanshi et al., 2014) in humid and tropical regions (Faramarzi et al., 2013; Nguyen and Kappas et al., 2015). Fiseha et al. (2014) applied SWAT to understand the hydrological responses to climate change in the Upper Tiber River basin daily and the SWAT has also been used to understand the water balance in watershed under various climatic and socioeconomic conditions (Neitsch et al., 2011; Wang and Xia., 2010; Nasiri et al., 2020). Considering the changes brought about by urbanization and climate on the water cycle, it is important to study these impact on local water resources, especially on available groundwater sources in the surrounding area (Wakode et al., 2018). Several continental and regional scale studies have shown the net effect of urbanization processes on

water quality (Onodera et al., 2011; Morris et al., 2003). However, quantifying this resource is difficult because a variety of data is needed, which is often lacking or limited.

Historically, groundwater has been a reliable source of water in Japan. As the country's industrialization and urbanization rates increased, however, regional as well as local water demands grew. Several studies have illustrated a decrease in groundwater recharge because of urbanization because surface sealing prevents infiltration and increases runoff (Rose and Peter, 2001), while other studies indicate an increase in groundwater recharge due to reduced evapotranspiration (Hooker et al., 1999; Barron et al., 2013). In general, studies on groundwater recharge have shown that it is difficult to estimate the recharge process because each region has a different climate and environment. Higashihiroshima has experienced rapid urbanization with significant changes on its land use pattern since the 1980s. Although the impact of urbanization and climate change on groundwater resources has been extensively explored, studies on its spatial variability for long-term groundwater recharge remains poorly understood at the regional level. As a result, for long-term groundwater water resource management, a thorough understanding of the changes in hydrological processes occurring due to socio-economic changes (urbanization) and climate change at the catchment scale is required. To identify approaches that would minimize the impacts of these changes on the available groundwater environment, estimating groundwater recharge is essential for gaining an insight into changes in climatic conditions and land use over time on the spatiotemporal distribution of groundwater recharge (Zomlot et al., 2015).

Hence, we assessed the spatial variation in groundwater recharge under the effects of urbanization and climate change, based on water balance components using SWAT over the last three decades, in western Japan. Observed daily streamflow simulation were conducted based on two representative time steps 1980, and 2000s to demonstrate the impact of anthropogenic activities on hydrological processes at the catchment scale. Because SWAT can

output both direct and relative impact of urbanization effect, these results will provide a better understanding of groundwater resource availability and implication for future management at the regional scale.

4.2 Study catchment

The Kurose River catchment (Figure 4.1), with a geographic area of approximately 39.5 km^2, is situated between latitude 34°25′30′′N and longitude 132°44′33′′E in Higashihiroshima City, Hiroshima prefecture and with an elevation between 204 m to 642 m above sea level.

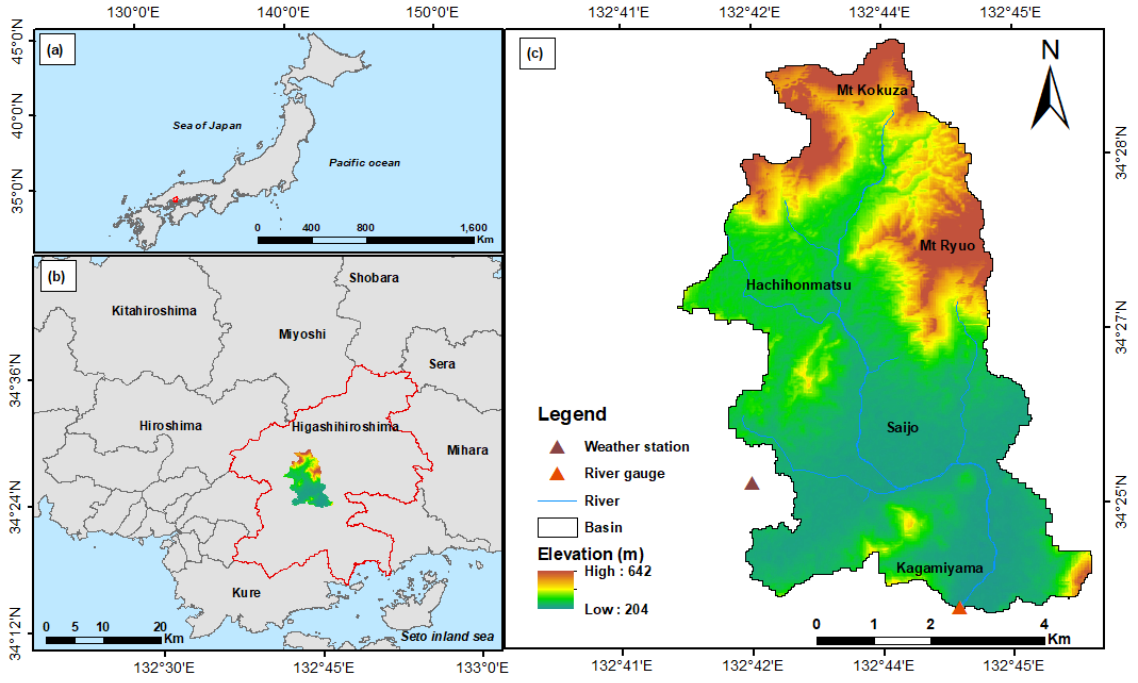

Figure 4.1: (a) Location of Higashihiroshima in Japan, (b) location of Kurose in Higashihiroshima, (c) location of Kurose River catchment in Higashihiroshima city showing meteorological station and river guaging station.

The catchment area has undergone significant anthropogenic changes since the 1980s evident by increase population, changes in land use pattern and increased climatic variations within the catchment. Land-use change is obvious within the catchment, whereby areas

dominated by paddy fields in the 1980s have been gradually converted from natural wetlands/rice paddies to medium and low-density residential areas over the last three decades (Figure 4.2).

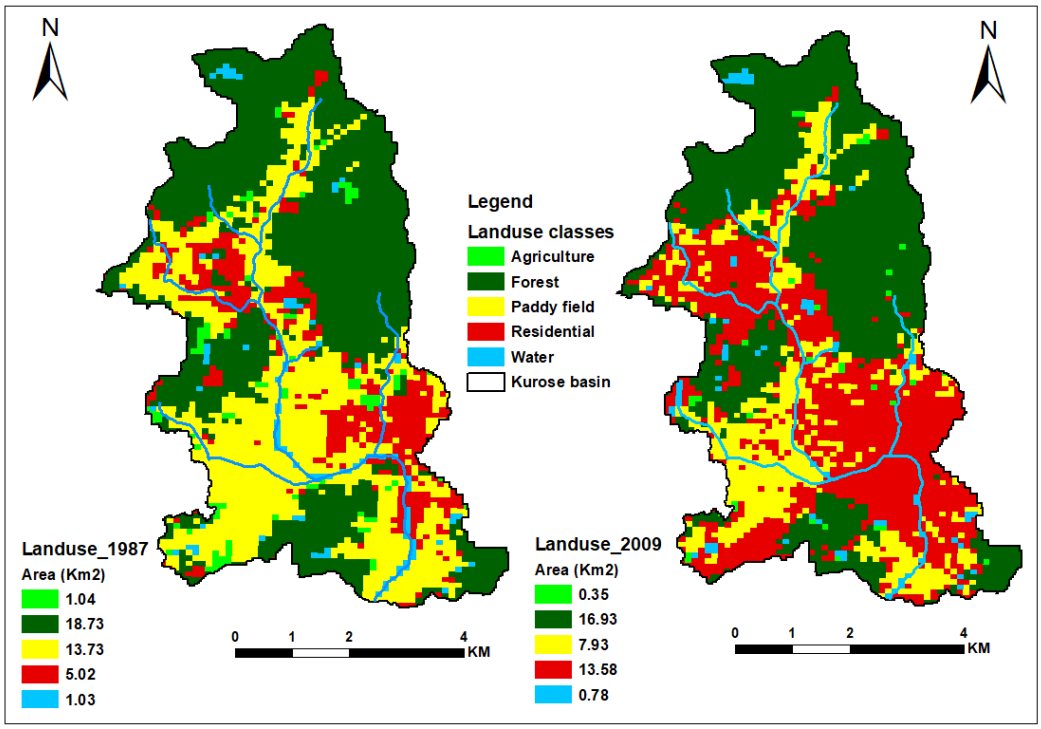

Figure 4.2: Land use map and areal extents of land use classes (Km^2) for the years 1987 representing the 1980s period and 2009 representing the 2000s period in the Kurose River catchment.

For instance, in the 1980s, the area's forest covered over 18.6 km^2, accounting for approximately 47.3% of the catchment area; paddy fields covered 13.6 km^2, which accounted for 34.7%. Rural residential areas covered only 5 km^2 representing 12.8% of the total catchment area (Figure 4.2). By the 2000s, residential areas had increased to 13.6 km^2, accounting for 34.5% of the total catchment area with an urbanization rate of approximately 7.4% per decade (Figure 4.2). However, paddy fields and forest areas decreased by 14.8% and 4.7%, respectively (Table 4.1). From the 1970s to the 2010s, the catchment's total population increased from 72,741 to 128,744, constituting an increase of approximately 76.9%. It should be noted that the relocation of Hiroshima University in the late 1970s to an area southeast of

the study region may be a major contributing factor to the rapid urbanization rate within the study area. The Kurose River, with a length of approximately 43 km, is the mainstream in the catchment, flowing from the northwest to the southeast through the urban and agricultural areas of Higashihiroshima City into the Seto Inland Sea. The Kurose River catchment is characterized by a warm humid climate with mean annual daily temperature varying from 12 °C to 15 °C (Japan Meteorological Agency 2021). The mean air temperatures (1979 − 2010) increased at a rate of 0.4°C per decade (Figure 4.3a) across the study area, suggesting an increasing trend in evaporative potential during the past three decades.

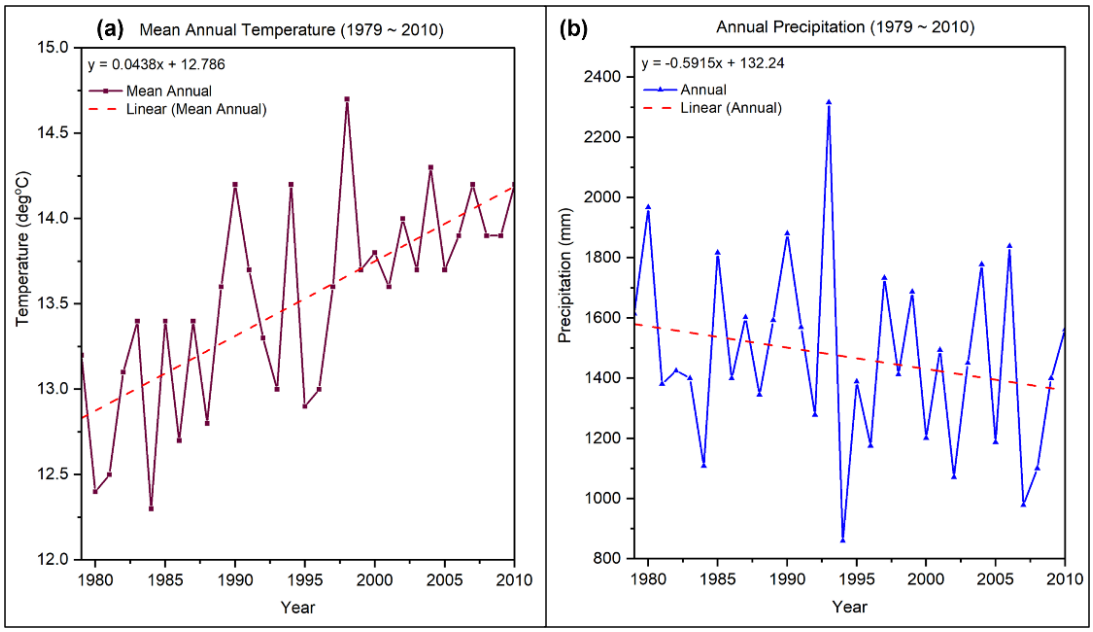

Figure 4.3: (a) Average annual air temperature and (b) average annual precipitation from 1979−2010 in the Kurose River catchment.

The mean annual precipitation over the last three decades (1979 − 2010) was approximately 1469 mm and there exists a clear difference in rainfall pattern between the four seasons in the watershed (Figure 4.4). A considerable amount of rainfall (about 80%) and most of the annual rainfall is received during one rainy season from June to August, and low precipitation from December to February (Figure 4.4). Precipitation within the study area showed a decreasing trend of 6.9 mm per decade (Figure 4.3b). The observed decline in rainfall

patterns coupled with rising temperatures due to urbanization may have a dramatic effect on the water resources in the catchment. Therefore, it is of utmost importance to understand the hydrological responses in the catchment under the aforementioned factors to ensure effective and sustainable management of water resources.

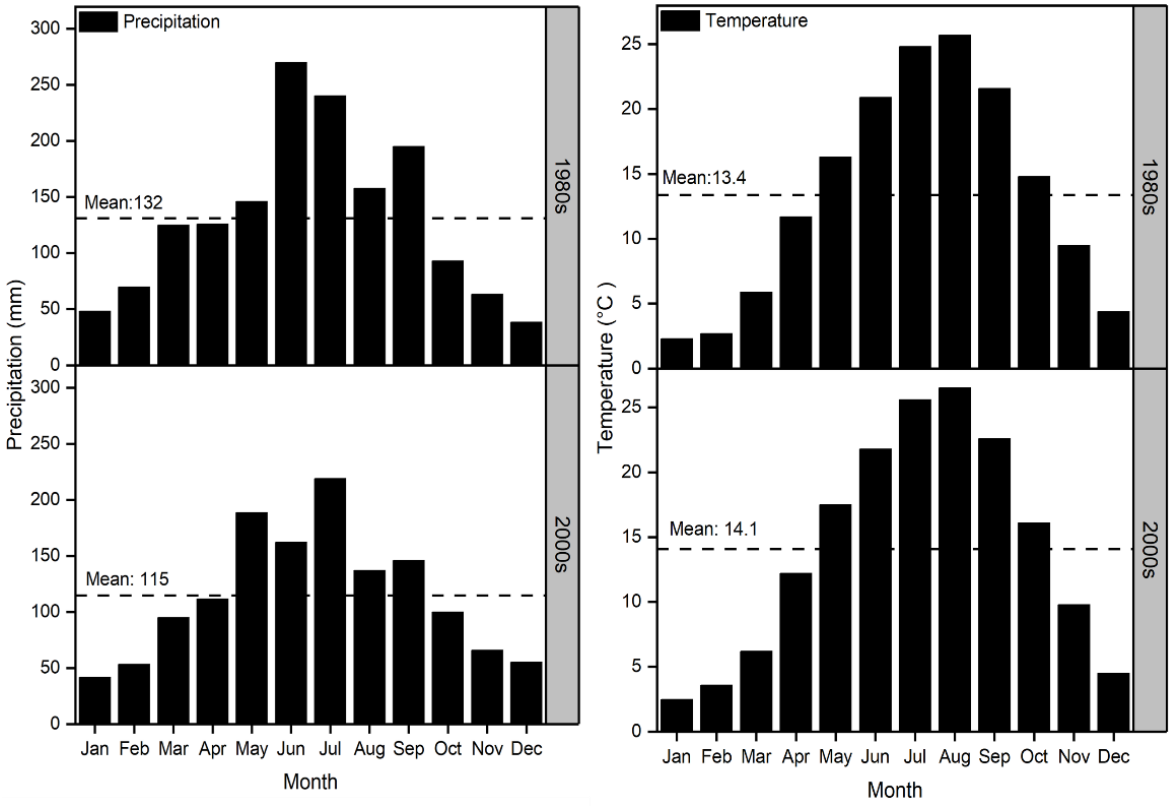

Figure 4.4: (a) Average monthly precipitation and (b) average temperature in the 1980s and 2000s in Kurose River catchment.

The depth to static water level measurements from boreholes within the research catchment was used to generate groundwater depth map. In total, 30 static water level measurements were used for the interpolation of the groundwater depth grid map also known as groundwater flow net, with most of them centred in the northeast and central areas for the years 1974 and 2000. The Inverse Distance Weighted (IDM) interpolation method was employed in this study because it provides consistent results with known values.

An outcrop geological map of the study area (Figure 4.5) reveals that the Kurose catchment is largely composed of Quaternary sediments, such as alluvial fan, terrace, and paleolake deposits. These fluvial deposits consisting of Middle Pleistocene to Holocene marine and non-marine sediments possibly represent the Saijo Formation, which lies unconformably on top of a granitic basement.

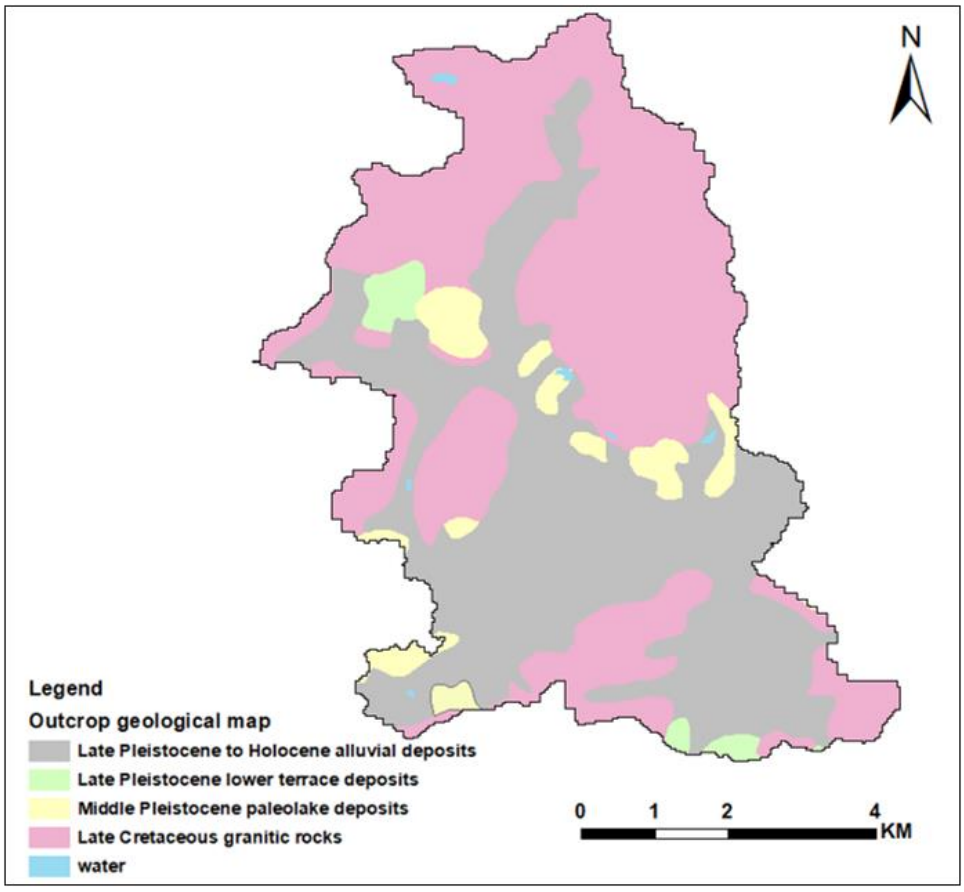

Figure 4.5: An outcrop geological map of Kurose River catchment.

The Hiroshima Granite that intruded in the Late Cretaceous period and which is distributed in southwestern Japan in the Chugoku and northern Shikoku areas (Kagami et al.,1988).

4.3 Materials and Methods

4.3.1 Soil and Water Assessment Tool (SWAT)

SWAT is a hydrological modelling program based on the watershed scope developed by the Agricultural Research Service of the United States Department of Agriculture (USDA-ARS) for predicting the impact of land management practices on water, sediment, and agricultural chemical yields in large and complex watersheds with varying soil, land use and management conditions over long periods (Arnold et al., 2012; Wallen et al., 2015). SWAT has been employed to model watersheds at various scales for different purposes. For example, Singh et al. (2013) applied SWAT to the Tungabhadra catchment in India for the measuring stream flow and reported a result in which the observed and simulated data had excellent correlation during the monthly calibration time step.

Similarly, Chekol et al. (2007) used the SWAT model for assessing the spatial distribution of water resources and analyzed the impact of different land management practices on the hydrologic response and soil erosion in the Upper Awash River Basin watershed, Ethiopia. Although SWAT has mainly been documented in regional studies, some studies have equally highlighted its successful applicability to various small-sized watersheds. Tudose et al. (2021) applied SWAT to a small mountainous forested watershed of 184 km^2 in central Romania and obtained satisfactory performance and results with a lower uncertainty of model results in replicating river discharge compared with observed discharge; Shrivastava et al. (2004) tested the SWAT model on a small watershed of 17.31 km^2 on both daily and monthly basis for estimating surface runoff and sediment yield and obtained satisfactory results. Marcon et al. (2011) evaluated a 4.5 km^2 watershed area of the Atlantic Forest biome in southern Brazil and obtained a good fit at the monthly scale but unsatisfactory results for daily calibration.

According to Gassman et al. (2007) and Daloglu et al. (2014), the main advantage of SWAT is its capability to run simulations for watersheds without extensive monitoring data, and it can predict changes in hydrological parameters under different management practices and physical environmental factors. This makes it suitable for evaluating the water balance allocation and climatic changes in watersheds worldwide. A detailed Model setup procedure has been discussed in chapter 2 section 2.2.2.

4.3.2 Model evaluation, statistical methods, and scenario setup

Model evaluation and statistical methods has been detailed out in chapter 2.2.2.3 HRU files for specific land-use types were extracted and necessary statistical calculations were performed on the chosen hydrological components to determine the influence of land use and climate change on water balance in the Kurose River catchment. Further visualization of the datasets was performed using ArcGIS software version 10.6.1. The relationship between precipitation and simulated groundwater recharge in all HRUs were expressed through linear regression and by applying a linear equation (Eq 4.1) to the observed dataset, as follows:

$$y = b + kx \qquad (4.1)$$

where, y is the simulated groundwater recharge in the HRU (mm); x is the observed precipitation (mm); k is the slope of the line signifying the groundwater ratio, and b is the intercept.

In addition, we developed three future scenarios utilizing climate and land use data from the 2000s as baseline data to determine the influence of either land use change or climate change on the water balance in the current watershed. To test the influence of land use in scenario 1, we used a land use scenario in which 15% of paddy land was converted to residential land while climate data remained constant. To exclude the influence of land use change in scenario 2, we chose a climatic scenario with a 13 % decrease in precipitation and a 0.7°C

increase in temperature. The allocated values for land use change and climate change are average values between the 1980s and 2000s time step.

4.4 Results and Discussion

4.4.1 Evaluation of the main parameters and the simulation accuracy

Nineteen parameters from the SWAT theoretical document affecting streamflow were identified through sensitivity analysis (Table 2.2). The most sensitive hydrological parameters were used for the model calibration and validation processes. Surface runoff parameters such as CN2.mgt, SOL_AWC.sol, SOL_K.sol and CH_K2.rte were more effective parameters to change in streamflow. Baseflow parameters such as ALPHA_BF.gw, GWQMN.gw, REVAPMN.gw, RCHRG_DP.gw, GW_delay.gw, and GW_REVAP.gw were found to be the most sensitive parameters for all subbasins. To correct the delay in daily peak values, r_HRU_SLP.hru and r_SLSUBBSN.hru, which affect lateral flow, were considered in the calibration process. In this study, the SCS runoff curve number (CN2. mgt) was found to be the most sensitive parameter for estimating surface runoff based on discharge simulation results. Studies have demonstrated the sensitivity of CN2.mgt in estimating surface runoff in calibration (Can et al., 2015). The curve number parameter CN2 controls how much water infiltrates into the soil and how much runoff is generated by overland flow, a high CN2 value results in less infiltration and more runoff. Land use classes affected the curve number significantly during model calibration. As for ESCO.hru, it was sensitive to actual evapotranspiration. The performance of SWAT model was evaluated by comparing the observed and simulated discharge data (Figure 4.6). The simulated and observed streamflow hydrograph indicated that the model captured the patterns of hydrologic variability during both at calibration and validation periods, which proved the SWAT model to be capable of simulating the hydrologic processes in the Kurose basin. A comparison of the observed and simulated flow discharge during the calibration and validation periods for the 1980s and the

2000s can be seen with the recommended statistical performance ratings adapted from Moriasi et al. (2007). The results suggest that the model can, be used to predict average annual river flow values. The statistical evaluators showed a good correlation between the annually observed and simulated river discharges as follows: According to R^2 and NSE, the model results for both calibration and validation were good. The statistical evaluation of the model is presented in Table 4.1.

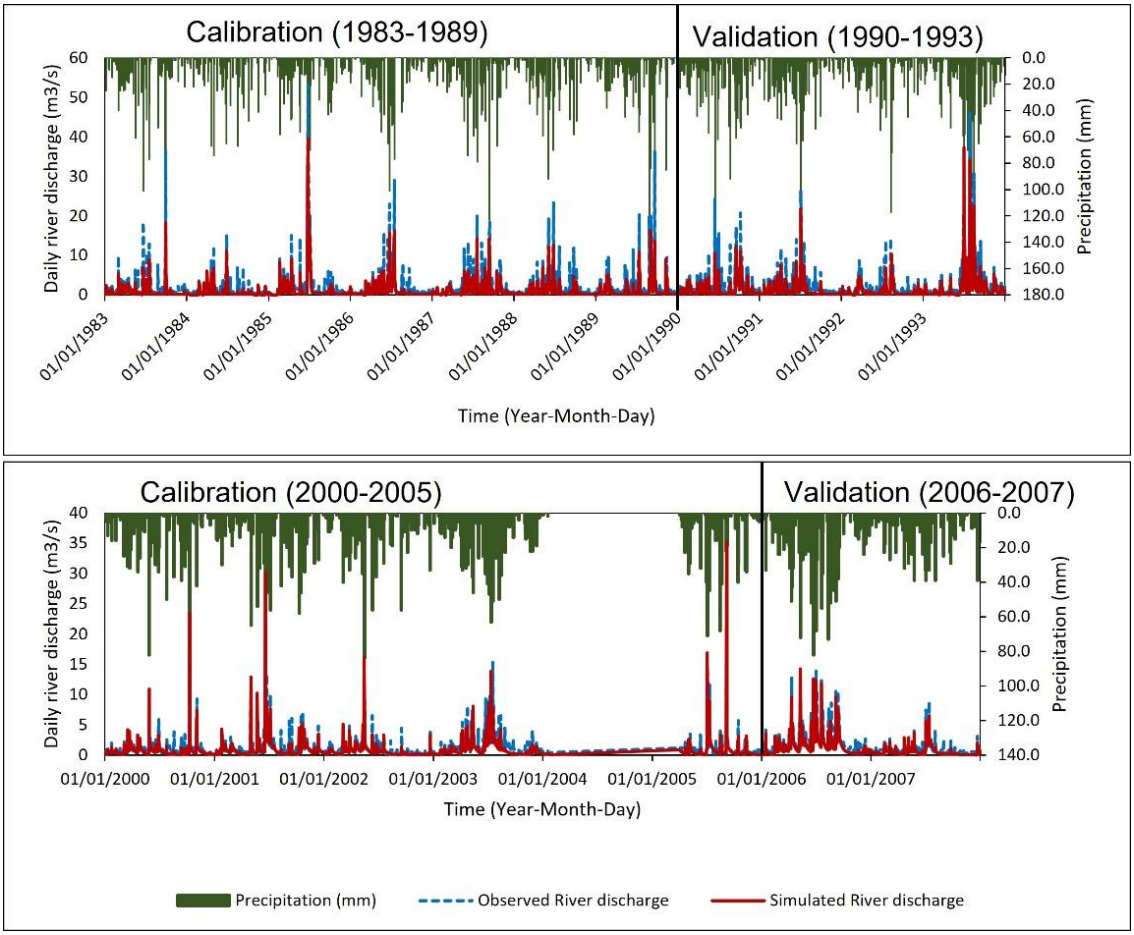

Figure 4.6: Comparison of the observed and simulated daily streamflow in the Kurose River catchment area. Straight lines represent the border of the year for calibration and validation for the 1980s and 2000s period.

Table 4.1: Daily calibration and validation statistics of the SWAT model in the Kurose River catchment.

Period	Period range	R2	NSE
1980s (calibration)	1980-1989	0.79	0.71
1980s (validation)	1990-1993	0.83	0.78
2000s (calibration)	2000-2005	0.74	0.65
2000s (validation)	2006-2007	0.85	0.74

Good model performance was obtained for the 1980s, with NS and R^2 values of 0.71 and 0.79 for the calibration period. Meanwhile for the 2000s, a satisfactory to very good performance rating was obtained with NS and R^2 values of 0.65 and 0.74, respectively. The same parameters also require validation in the simulation to confirm their viability. During the validation period, the R^2 and NSE values were much higher. Overall, based on a visual inspection of the time series graphs (Figure 4.6), the SWAT model can be considered an appropriate tool for simulating the hydrological variability of watershed management in the Kurose Basin.

4.4.2 Variation in water balance from the 1980s to 2000s

4.4.2.1 Water balance in a catchment scale

In the Kurose River catchment, the simulated water balance components included surface runoff (SurfQ), lateral flow (LatQ), groundwater discharge (GW_Q), groundwater recharge to the deep aquifer (DA_RCHG), and actual evapotranspiration (ET) are presented as mean annual values (Figure 4.7a) and calculated as relative percentages of average annual rainfall. The mean annual precipitation in the catchment area was 1573 mm/yr and 1374.9 mm in the 1980s and 2000s, respectively. The estimated DA_RCHG decreased considerably from 184.5 mm in the 1980s to 120.2 mm in the 2000s, which correspond to approximately 43.8% and 30.2% of the annual mean precipitation. The mean annual SurfQ values for the 1980s and

2000s were given by 91.7 mm and 212.6 mm which correspond to approximately 5.9% and 15.5% of the mean annual rainfall, respectively (Figure 4.7a). The recent 2000s yielded higher SurfQ and lower GW_RCHG compared to the earlier years due to urbanization driven processes within the catchment, such as land cover alteration. CN2 has been identified as one of the most influential parameters that affect surface runoff (Arnold et al., 2012) and is influenced by land use and soil type. The 1980s had a lower average curve number of 47.4, indicating a reduction in surface runoff, as the land-use and soil type combination is less resistant to infiltration and favours recharge by precipitation.

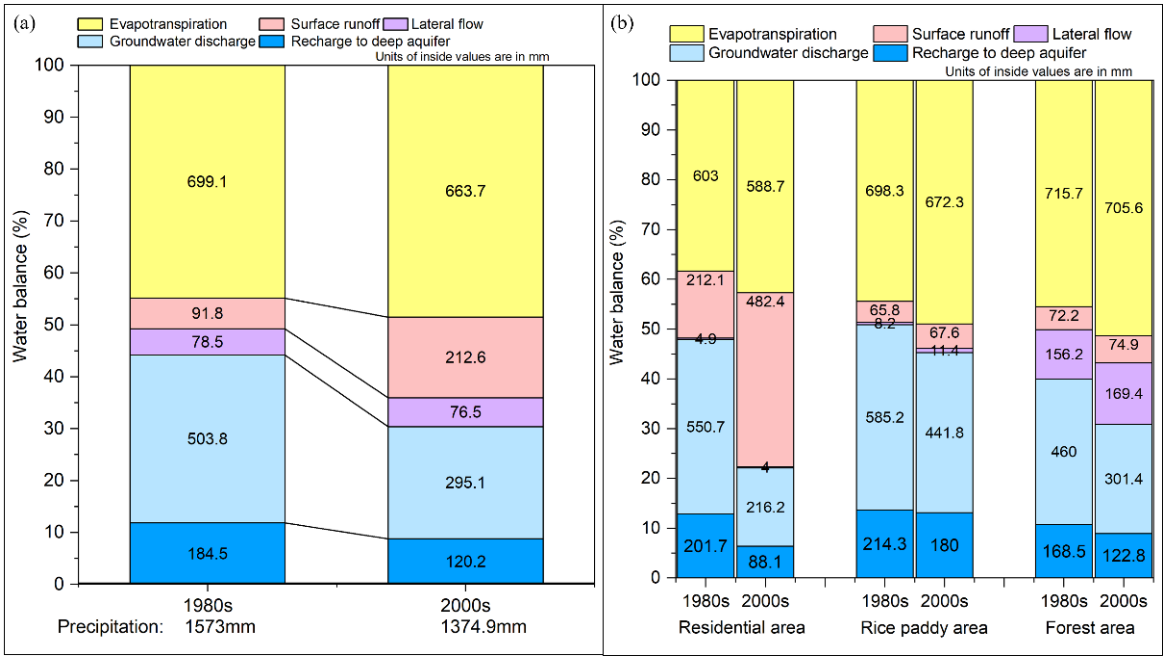

Figure 4.7: Average annual water balance ratio in the 1980s and 2000s in (a) catchment scale and (b) per land use unit in the Kurose River catchment.

By the 2000s, the average curve number had increased to 65.6 as a result of an increase in impervious surfaces as the land-use and soil type combination became more resistant to infiltration and favoured higher overland. Many researchers have documented the increase of surface runoff resulting from urbanization (Phuong, Thong, Ngoc, Chuong, 2014; Tao et al., 2015). Approximately 699.1 mm and 663.7 mm of water was lost through ET from the basin

in the 1980s and 2000s, respectively. This accounted for approximately 44% and 48% of the catchment's annual precipitation, which can be attributed to a decline in precipitation and evaporative surfaces under increasing urbanization processes (Figure 4.7a). The study area has experienced substantial urbanization in the last two decades, which has resulted in the transformation of forests, paddy fields, and agriculture areas into residential, commercial, industrial, and transportation land. The water balance under changing land use (Figure 4.2) changed significantly from the 1980s to the 2000s, with the most noticeable change being an increase in surface runoff and a decrease in groundwater recharge (Figure 4.7a). Based on these results and those of Gatwaza et al. (2016), Marhaento et al. (2017), and Wang et al. (2021), surface runoff is most sensitive to land-use change, and increasing urban areas result in a greater ratio between surface runoff and streamflow with a diminishing ratio of groundwater flow. In addition, the lateral flow also showed few changes, less than 1%, whereas the groundwater contribution to streamflow decreased by 10% from 503.7 mm in the 1980s to 295.1 mm in the 2000s.

4.4.2.2 Water balance in land use unit

The results of the model simulation clearly show the strong impact of land use change on the water balance in the Kurose watershed at the basinal scale. Hence, we compared the variation in the mean annual water balance components for three dominant land uses (rice paddy fields, forest areas, and residential areas) for each period (the 1980s and 2000s) in the catchment area. The estimated mean groundwater recharge for the three land use types showed a difference in magnitude, as shown in (Figure 4.7b). In the forest area, the mean annual recharge amounted to 167 mm (10.7% of mean annual precipitation) in the 1980s and 9 mm (122% of mean annual precipitation) in the 2000s, whereas the mean annual recharge in the residential area was higher in the 1980s than in forest area with a value of 199 mm (12.8% of precipitation), but with a lower value of 88 mm (6.5% precipitation) in the 2000s. Much greater

mean annual groundwater recharge occurred in the paddy field, where total recharge amounted to 212.2 mm (13.5% of precipitation) and 180 mm (13.1% of precipitation) for the 1980s and 2000s, respectively (Figure 4.7b). The striking decrease in groundwater recharge in the residential area as compared to the other land uses between the two periods can be explained by the significant increase in residential area in the catchment area from 12.8% in the 1980s to 34.5% in the 2000s, with over 45% of paddy field area being converted to residential areas (Figure 4.2) in response to urbanization and expansion of rural settlements. Infiltration is reduced in urban areas due to the substitution of natural vegetation by impervious surfaces (Miguez and Magalhães, 2010). According to Takie et al. (2016), natural ecosystems have higher water infiltration capabilities than urban soils, which is largely due to their high level of surface imperviousness. The result is that urban soils do not infiltrate water into the subsoil, thereby reducing recharge rates.

Rice paddy areas had the highest groundwater recharge among the three land use types, with little variation in both periods. The fact that rice paddy fields are naturally flooded by precipitation as well as artificially irrigated makes them good contributors to groundwater recharge. Several studies have found that wetlands increase groundwater recharge compared to forests and other land-use types (Owuor et al., 2016; Takehide et al., 2020). Furthermore, the groundwater recharge in the residential area was much higher in the 1980s than the forest recharge in both periods. In this study, residential areas were not recognized as completely impervious land, but rather as having a fraction of vegetation cover. Furthermore, in the 1980s the residential area had a smaller surface area, with a larger portion of bare soil and vegetation (Figure 4.2), allowing it to capture more infiltrating rainfall for groundwater recharge than the forested area, which is limited by forest canopy interception (Fan et al., 2014). As a result, recharge values in forest areas were lower than those in rice paddy fields. Meanwhile in comparison to residential and rice paddy areas, much more soil water is discharged by lateral

flow in the soil profile. Accordingly, surface runoff in residential areas increased considerably in the 2000s as compared to the 1980s, i.e. from 212.1 mm to 482.4 mm (Figure 4.7b); whereas changes in rice paddy and forest areas were insignificant. Based on these results, several other studies have characterized urban areas as impervious areas that promote surface runoff and inhibit infiltration (Jat et al., 2009; Miguez and Magalhães, 2010). Soils in natural environments, such as rice paddies and forests, allow water to slowly infiltrate the soil through the process of stemflow when precipitation is not intercepted and evaporated. This water can be used by vegetation to increase groundwater saturation, reduce runoff, and recharge the groundwater system, whereas in residential areas, sealed and compacted soils are unable to absorb and retain moisture, and the capacity for groundwater percolation is limited (Coutu and Vega, 2007; Tashie et al., 2016). Therefore, in the case of storm events in the catchment, surface runoff will dramatically increase with a higher risk of flooding due to increased sealing of ground surfaces with concrete (Brath et al., 2006) and groundwater contamination due to leakage from drainage pipes and industrial effluent (Baier Azzam and Strohschon, 2014).

The average annual evapotranspiration results indicate that the ET values were higher in the 1980s than in the 2000s across the three land-use types, with forest ET values being much higher than those of paddy areas and residential areas. In the forest area, ET values varied from 715.7 mm in the 1980s to 705.6 mm in the 2000s, amounting to approximately 46% and 52% of mean annual rainfall. In the paddy area, the mean annual ET amounted to 698.3 mm (45%) for the 1980s and 672.3 mm (49%) for the 2000s. Much lower ET values were recorded in the residential area, where mean annual ET amounted to 603 mm (39% of mean annual rainfall) and 5887 mm (43% of mean annual rainfall) for the 1980s and 2000s, respectively. Generally, in the 2000s, the ET ratios were higher than those in the 1980s, which reflects the change in climatic conditions in the catchment due to natural or anthropogenic causes. According to Lipczynska-Kochany. (2018), climate change has the potential to alter both the

quantity and quality of groundwater by altering ET, precipitation patterns, and air temperature. As such, an increase in precipitation intensity and frequency would contribute to runoff and an increase in ET rates owing to global warming, which might be the case in the Kurose catchment area.

Additionally, there has been a noticeable influence of climate change effect on the groundwater recharge and ET rate, accompanied by an 11.8% decrease in annual precipitation values and a 0.8% increase in mean temperatures over the last two decades (Figure 4.7a and b). In addition, the observed lower ET values in the residential area compared to the forest and paddy land use are due to lower soil moisture availability as evaporative surfaces decrease with surface sealing (Li et al., 2004).

4.4.2.3 Average monthly groundwater recharge

At both the average monthly catchment scale and per land use unit, recharge in the 2000s was significantly lower than in the 1980s. According to the simulated monthly recharge, there was a clear seasonal trend, with major recharge occurring during the wet summer and autumn (Figure 4.8).

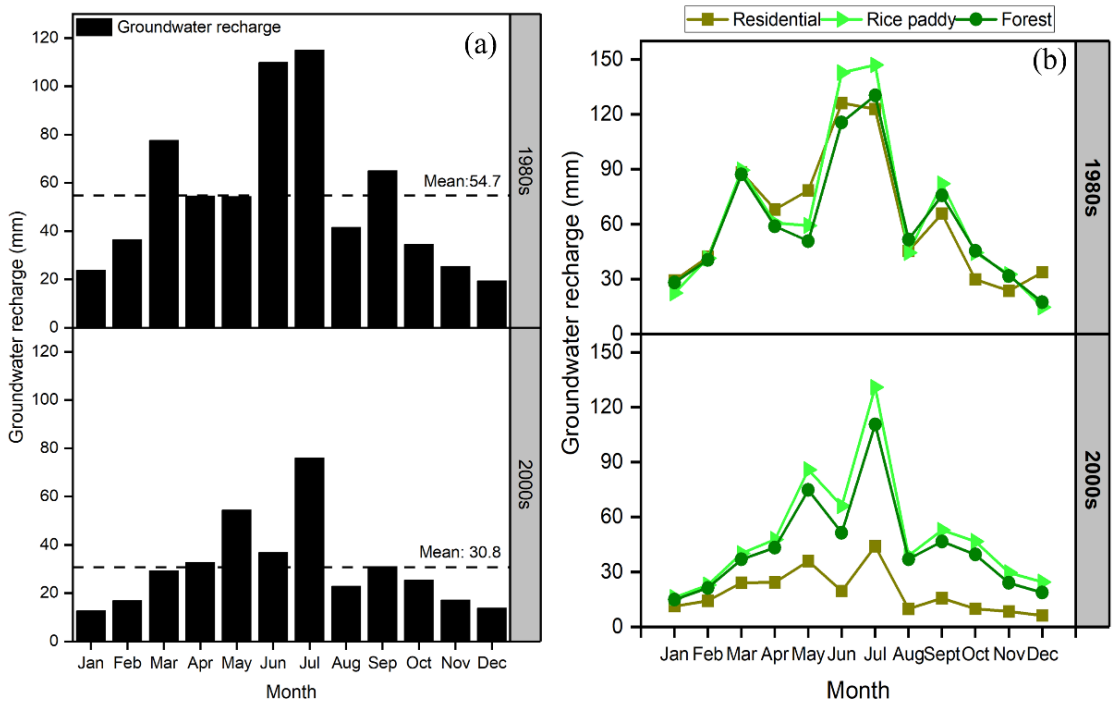

Figure 4.8: Monthly variation in groundwater recharge in (a) basin scale and (b) per land use unit in the Kurose River catchment.

The peaks of groundwater recharge coincide well with those of precipitation, in which precipitation replenishes soil moisture and creates groundwater recharge. Although the annual recharge average from the three land uses amounted to 184.5 mm and 120.2 mm in the 1980s and 2000s, respectively, the monthly average recharge distribution showed remarkable variations for the two periods having minimum and maximum values in January and July both in the 1980s and 2000s (Figure 4.8). The monthly average recharge estimates for the 1980s ranged from 23.7 mm to 270 mm, representing approximately 19% − 48% of the monthly average net precipitation; whereas for the 2000s, mean monthly recharge values varied from 36.4 mm to 191 mm, representing 12% − 67% of the net monthly rainfall. In both periods, the higher recharge value can be associated with the transition from winter to spring, which is characterized by higher temperatures above freezing and precipitation. In the 1980s, significant groundwater recharge occurred in the summer months of June and July, and in the early autumn months of September due to frequent summer rainfall events and typhoons, resulting in substantial replenishment of soil moisture by rainwater (Figure 4.3b and Figure 4.8a). In the 2000s, most recharge occurs in the late spring month of May and the mid-summer month of July, which coincide with the rainfall patterns shown in Figure 4.3b.

These observed changes in precipitation and recharge patterns could be due to the changing climatic conditions in the catchment, with the general increase in temperature and evapotranspiration leading to more intense precipitation events that promote more surface runoff than recharge. Such occurrences have been observed in the study catchment in recent years. The temporal recharge patterns for the three land uses were similar because of similar rainfall patterns, but the magnitude of recharge was different (Figure 4.8b). Rice fields had the highest groundwater recharge in the 1980s and 2000s (147.1 mm and 130.9 mm, respectively),

followed closely by forest land use (130.3 mm in the 1980s and 110 mm in the 2000s) in the summer month of July, while residential groundwater recharge was much lower 123 mm and 43.9 mm in the 1980s and 2000s respectively, due to the above environmental conditions.

4.4.2.4 Groundwater recharge ratios in three decades

The annual precipitation and groundwater recharge per land use were compared between the two periods (Figure 4.9). Groundwater recharge increased considerably with precipitation in all land uses during both time steps with R^2 values >0.95, in the forest and rice paddy land use; while in the residential area, R^2 was 0.99 and 0.87 for the 1980s and 2000s respectively (Figure 4.9). Direct recharge occurs from precipitation reaching the land surface.

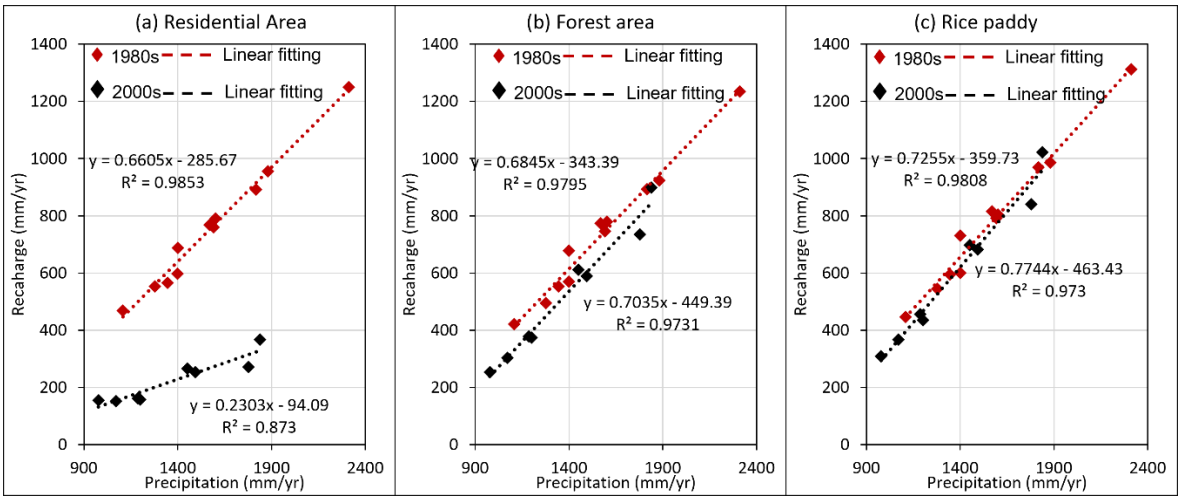

Figure 4.9: Scattered plot showing relation between annual groundwater recharge and annual precipitation in (a) residential area, (b) forest area, and (c) rice paddy for the 1980s and 2000s.

In rice paddy and forest areas, a similar trend in gradient was observed with little change in slope value (k) for both the 1980s and 2000s, which may reflect their similar recharge characteristics such as high infiltration capacity due to more permeable surfaces. Whereas, in the residential area, the obvious disparity between the gradient in the 1980s and 2000s is an indication of the influence of different contributing factors to groundwater recharge other than precipitation.

The recharge ratio (0.66) and gradient in the residential area were similar to those in the forest (0.68) and rice paddy areas (0.7), as expected. During this period, the residential area was smaller, with more vegetative surfaces and water permeable pavements which had a high infiltration capacity and increased groundwater recharge by reducing surface runoff. By the 2000s, the residential area had doubled, alongside paved surfaces and rooftops, which diverted precipitation, leading to reduced infiltration with higher surface runoff. Hence, the intensification of urbanization processes in the 2000s resulted in a substantial decrease in the recharge ratio from 0.66 in the 1980s to 0.23 in the 2000s. This data illustrates the direct impact of urbanization on groundwater recharge in the catchment and its temporal distribution. The annual average precipitation and groundwater recharge over a period of 20 years and their percentages based on precipitation varied among the three land uses (Table 4.2).

Table 4.2: Estimated groundwater recharge at average precipitation in the catchment.

	Mean Annual (mm)	**% Based on rainfall**	**Mean Annual (mm)**	**% Based on rainfall**	**Mean Annual (mm)**	**% Based on rainfall**
Land use	Residential		Forest		Rice paddy	
Precipitation	1400		1400		1400	
1980s	639.03	45.7	614.91	44	655.97	46.9
2000s	228.33	16.4	535.51	38.3	620.73	44.4

Approximately 46.9 and 44.4% of the total precipitation was recharged in the paddy areas in the 1980s and 2000s, respectively. In the forest area, 44% and 38.3% of the total precipitation was infiltrated as groundwater recharge, whereas in the residential area, the recharge rate was greatly reduced with given values of 45.7% and 16.7% of the total precipitation. The average annual groundwater recharge was highest in the paddy areas, with values ranging from 656 mm in the 1980s to 620.8 mm in the 2000s, amounting to a decrease rate of 2.5%. The high recharge values are due to uncovered land and permeable soils, that are mostly waterlogged throughout the year. In the Kurose River catchment, paddy areas are the

highest recharge zones; therefore, conservation of these areas is of utmost importance for future sustainability of groundwater recharge.

4.4.3 Spatial Variation of groundwater recharge

The outcomes of the SWAT model simulation revealed that changes in land use had an impact on groundwater recharge (Figure 4.10) over the last 30 years. The mean annual recharge was estimated at 689 mm (50% of annual mean rainfall) and 416 mm (40% of annual mean rainfall) in the 1980s and 2000s, respectively.

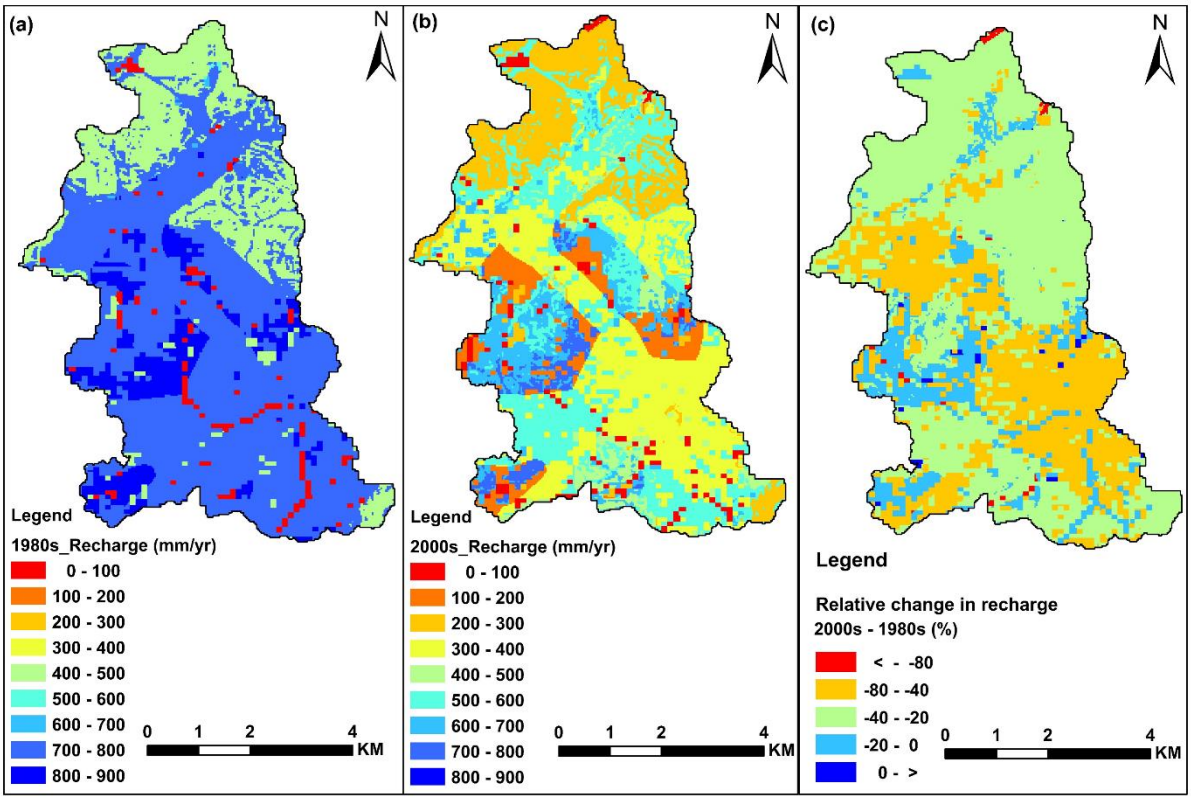

Figure 4.10: Average annual distribution of groundwater recharge in the (a) 1980s, (b) 2000s; (c) relative change between 2000s and 1980s with different land use patterns.

In the 1980s, over 80% of the catchment area (the center and southern parts) had recharge values greater than 700 mm which was dominated by paddy fields, as compared to

the northern areas, which were dominated by forest vegetation and showed relatively lower values. By the 2000s, 44.4% of total paddy field area had been converted to residential areas, accounting for a drastic loss in recharge. This drastic decrease in groundwater recharge in the Kurose catchment over the past two decades shows a response to anthropogenic disturbances and closely depicts the changes in land use in the catchment area (Figure 4.2). In the Kurose catchment, it can be stated that groundwater recharge is reduced by the urbanization processes. In agreement with this study, Hardison et al. (2009) also indicated that recharge decreases in urbanized areas as surface sealing increases, which prevents infiltration while increasing surface runoff as compared to the natural environment. Contrary to these results, a study by Minnig et al. (2018) showed that highly urbanized watersheds exhibited higher groundwater recharge than predominantly rural watersheds due to a reduction in evapotranspiration and an increase in water main and sewer leakage. The considerable variation in the spatial pattern of groundwater recharge rates in the Kurose catchment appeared to be primarily dominated by land use with minor contributions from geology, topography, and soils. The southern and central part of the catchment is dominated by permeable alluvial sediments (Figure 4.5) which can be considered as the primary source of recharge to the aquifer and due to their fertile soils, they are used for the rice paddy farming. In addition, the central and southern parts of the catchment showed relatively higher recharge because of the presence of perennial streams from the western and eastern escarpment, which, in addition to the faults, can facilitate recharge to the aquifer. The major sources of groundwater recharge for the unconsidered sediment aquifer may be subsurface seepage from fractures openings or seepage from runoff generated from precipitation in the highlands and infiltration from rainfall that occurs in the alluvial plains.

The spatial analysis of groundwater level maps (Figure 4.11) depicts that the groundwater level is shallower in the southern region as compared to the northern part of the study area and the maximum depth to groundwater level is observed in the north-western part

of the study area in both the 1970s and 2000s. This agrees with the groundwater recharge map in (Figure 4.9) which recorded higher recharge values in the southern and central parts of the study area. This is because, in areas where the groundwater table is high, the soil is already saturated and any infiltrating water seeps out as lateral flow to streams and rivers. The difference in groundwater level between the year 2000 and 1974 shows that over 76% of the catchment area had a decline in groundwater depth between 0.1m to 2m. The dwindling precipitation from the 1970s to recent years (Figure 4.2b) equally has a decreasing effect on the groundwater recharge in the study area which leads to comparative decline in groundwater level in the 2000s.

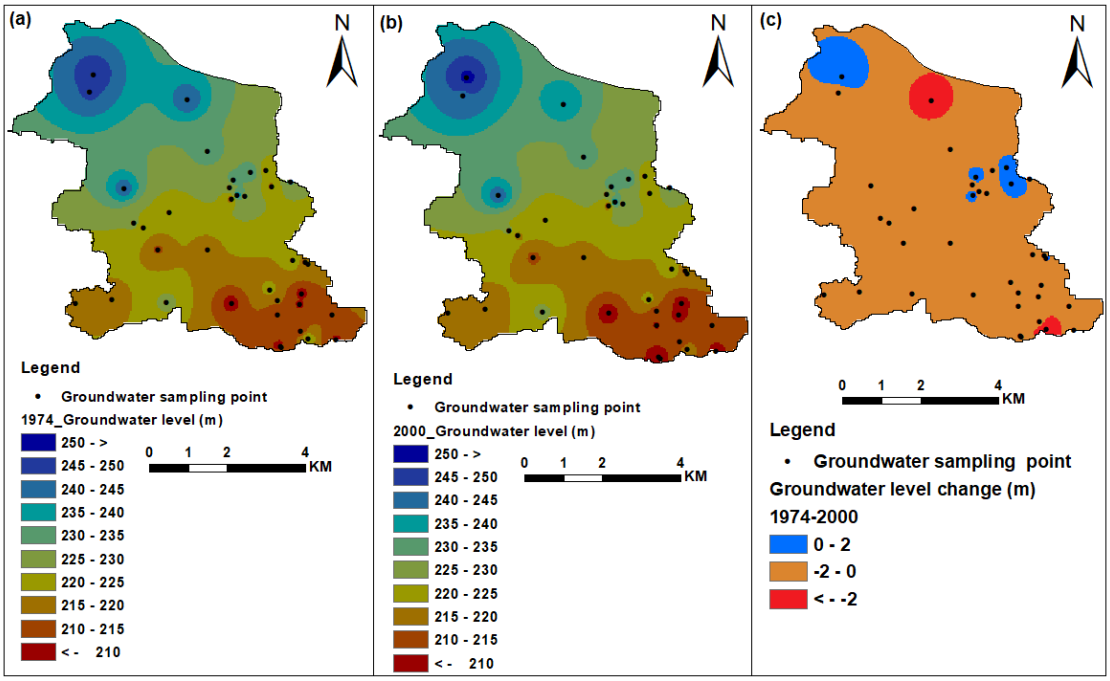

Figure 4.11: Spatial distribution of groundwater level in the year (a) 1974, (b) 2000, and (c) groundwater level change from the 1974 and 2000 in the Kurose River catchment.

In addition, from the groundwater level maps its indicative that areas with high water levels act as discharge zones because they lose water to nearby rivers and streams compared to areas with low water levels which may constitute recharge zones at higher elevations.

4.4.4 Relative urbanization effect (spatial variation in forest ET: 1980s − 2000s)

By increasing infiltration rates and reducing surface runoff, forests can increase groundwater recharge (Lv et al., 2019; Wang et al., 2022). However, forests can also reduce recharge through an increase in ET, which increases with tree age and temperature. Also, a linear relationship between forest age and ET has been reported by), whereby an increase in tree age subsequently increased forest ET. The spatial distribution of forest ET presented in Figure 4.12. The mean annual ET as a relative percentage of average precipitation for the study area was 46% and 52% for the 1980s and 2000s periods respectively. Spatially, the northern part of the catchment, which is mostly vegetative, showed higher ET values of 720 mm – 730 mm in the 1980s while in the southern part the ET values were less than 720 mm.

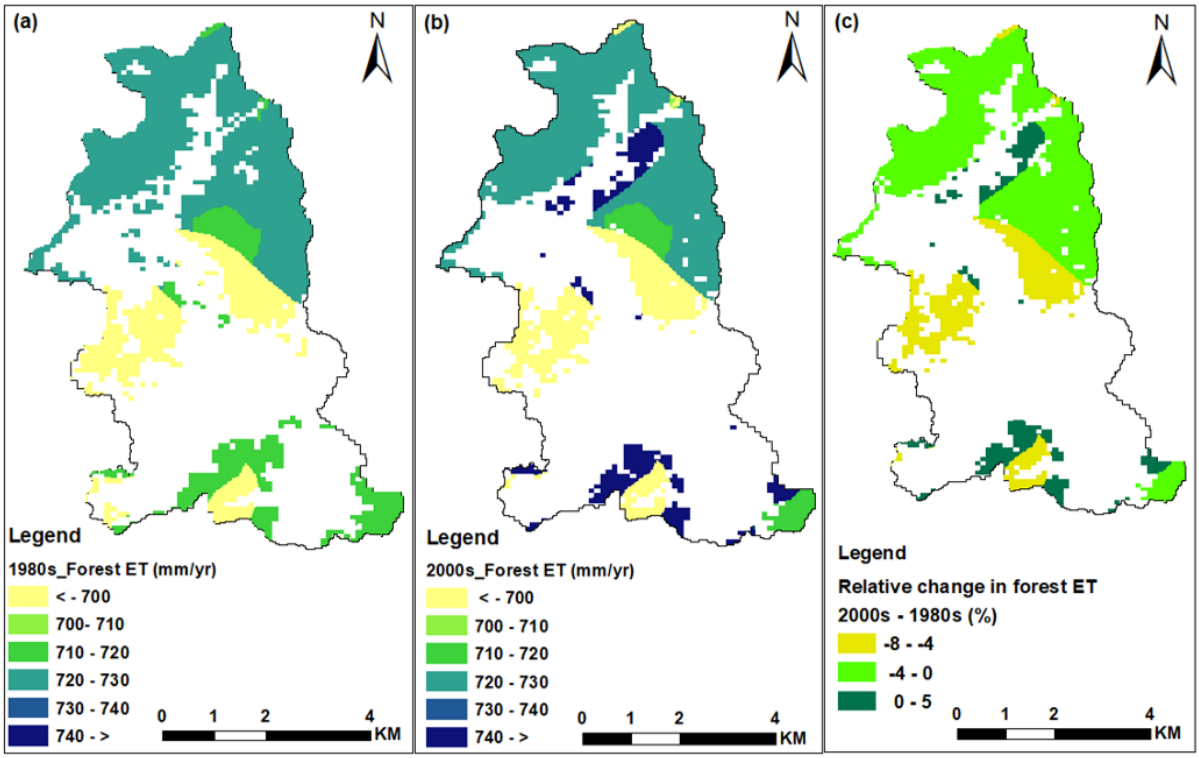

Figure 4.12: Change in forest Evapotranspiration in the (a) 1980s, (b) 2000s, and (c) relative change in forest ET from 1980s to 2000s in the Kurose River catchment.

However, by the 2000s, the ET values had increased and decreased in some parts of the southern and northern sections of the catchment area (Figure 3.12). This might suggest forest growth with elevated ET as older trees tend to have higher transpiration rates than younger trees. Also, the decline in ET can be explained by forest degradation in the observed sections, as residential areas encroach into forest land. In addition, more than 80% of the forest area showed a decreasing trend in ET values, thus, the decline in forest vegetation influenced the reduction in ET and increased surface runoff. Consequently, infiltration tends to decrease whereas surface runoff rates increased as soil water storage capacity is inhibited, subsequently reducing groundwater recharge (Brown et al., 2005). However, because evapotranspiration was not calibrated in this study and considering the use of only one weather station, ET values might have been underestimated. Coupled with this, variations in ET may be influenced by several factors, such as soil, precipitation, and atmospheric changes.

In addition, more than 80% of the forest area showed a decreasing trend in ET values, thus, the decline in forest vegetation influenced the reduction in ET and increased surface runoff. Consequently, infiltration tends to decrease whereas surface runoff rates increased as soil water storage capacity is inhibited, subsequently reducing groundwater recharge (Brown et al., 2005). Similarly, forest growth decreased groundwater recharge due to increases in transpiration due to increases in temperature. However, because evapotranspiration was not calibrated in this study and considering the use of only one weather station, ET values might have been underestimated. Coupled with this, variations in ET may be influenced by several factors, such as soil, precipitation, and atmospheric changes.

4.4.5 Land use change and climate change scenarios

The response of groundwater recharge, surface runoff and evapotranspiration to different scenarios based on the last 30yrs is depicted in Table 4.3. The response of

groundwater recharge and evapotranspiration to different scenarios based on the baseline scenario (2000s) is depicted in Table 4.3. In scenario 1, groundwater decreased only by 9 % meanwhile under scenario 2, groundwater recharge will be further reduced by 23% compared to the baseline scenario. In scenario 3, the combined effect of land use change and climate change will have a greater impact on the groundwater recharge with a total decline in the available groundwater by 29%. This will be primary due to encroachment of paddy areas which are the major recharge zones by industrial and infrastructural development in the catchment. The effect on groundwater environment will be more severe when combined with climatic variability in the catchment. In addition, evapotranspiration will equally reduce significantly under scenario 2 by 1%. Vegetation cover lowers surface and air temperatures through evapotranspiration which helps to improve and regulate the urban temperature as well as mitigate heat island effect (Kurn et al., 1994), but with the loss in vegetation cover in the study area, this will further increase the urban thermal environment and possible heat island conditions.

Table 4.3: Mean annual Evapotranspiration (ET), surface runoff (SurfQ), and groundwater recharge (RCHG) in land use and climate change scenario simulation.

Scenarios	Rainfall	ET	ET rate	SurfQ	SurfQ rate	RCHG	RCHG rate	Decreased recharge
	mm	mm	%	mm	%	mm	%	%
Baseline	1374.9	663.5	48	212.7	36	415.21	30.2	0
Scenario 1	1374.9	657.1	48	253.6	42	381.49	27.8	8.1
Scenario 2	1196.9	656.9	55	156.7	35	323.22	27.1	23
Scenario 3	1196.9	650.3	54	191.6	42	295.4	24.7	29

In addition, it is reported that the thermal environment may worsen due to increased heat discharge from industries, vehicles, and buildings, with urban temperatures being relatively higher than the surrounding countryside (Guo-yu et al., 2013), which is likely to

occur in the study area. Therefore, groundwater recharge will be reduced over time due to the increased urban population, which will increase the pressure on water supply and may impair the quality as well as quantity of the available water resources. Thus, the impact of both land use change and climate change deserves more attention for future urban planning and water resource management.

4.5 Summary

The SWAT model is a promising tool for assessing spatial variation in water balance components and for evaluating scenario analyses for urbanization and climate change. to identify approaches that would minimize the impact of these changes on the available groundwater environment. Based on the statistical index for the daily time steps of streamflow predictions, the model SWAT showed good criteria for hydrological simulations, demonstrating its ability to reasonably replicate daily streamflow. Due to the significant magnitude of change in vegetation cover, land use is a major factor affecting the components of the water balance in the Kurose River basin, as shown by the substantial increase in surface runoff and decrease in groundwater recharge. In addition, the predicted scenario showed that relative groundwater recharge will be reduced due to future increase in urbanization (i.e. 10% increase in residential areas and decrease in rice paddy areas) and the increase in global warming, characterized by a 1°C temperature increase by 2030 to 2050. Therefore, the combined impacts of land use change and climate change deserve more attention for future urban planning and water resource management in the study area.

4.6 References

Abbaspour, K.C., Vejdani, M., Haghighat, S., Yang, J. SWAT-CUP calibration and uncertainty programs for SWAT. MODSIM 2007 International Congress on Modelling

and Simulation, Modelling and Simulation Society of Australia and New Zealand. **2007**, 1596–1602.

Arnold J.G., Moriasi D.N., Gassman, P.W., Abbaspour, K.C., White,M.J., Srinivasan, R., Santhi, C., Harmel, R.D., Van Griensven A., Van Liew, M.W., Kannan, N., Jha, M.K. (2012). SWAT model use calibration, and validation. *Trans ASABE*. 2012, 55, 1491–1508.

Arnold, J.G., Srinivasan, R., Muttiah, R.S., William, J.R. Large area hydrologic modeling and assessment part i: model development. *J. Am. Water. Resour. Assoc.***1998**, 34, 73–89.

Baier, K., Schmitz, K.S., Azzam, R., Strohschon, R. Management Tools for Sustainable Ground Water Protection in Mega Urban Areas-Small Scale Land Use and Ground Water Vulnerability Analyses in Guangzhou, China. *Int. J. Environ. Res*. **2014**, 8, 249−262.

Baker, T.J., Miller, S.N. Using the Soil and Water Assessment Tool (SWAT) to assess land use impact on water resources in an East African watershed. *J. Hydrol.* **2013,** 486,100–111.

Brath, A., Montanari, A., Moretti, G. Assessing the effect on flood frequency of land use change via hydrological simulation (with uncertainty). *J. Hydrol*. **2006**, 324, 141–153.

Brown, A. E., Zhang, L., McMahon, T. A., Western, A. W. (2005). A review of paired catchment studies for determining changes in water yield resulting from alterations in vegetation. *J. Hydrol*. 2005, 310, 28-61.

Chekol, D. A., Tischbein, B., Eggers, H., Vlek, P. Application of SWAT for assessment of spatial distribution of water resources and analyzing impact of different land management practices on soil erosion in Upper Awash River Basin watershed. In proceedings, Catchment and Lake Research. **2007**, 110-117.

Chen, Y.R., Bofu, Y. Impacts of climate and land-use changes on floods in an urban catchment in Southeast Queensland, Australia. Climate and Land-surface Changes in Hydrology, Proceedings of H01, IAHS-IAPSO-IASPEI Assembly, Gothenburg, Sweden, July 2013, *IAHS Publ*. **2013**, 35.

Chung, I.-M., Kim, N.-W., Lee, J., Sophocleous, M. Assessing distributed groundwater recharge rate using integrated surface water-groundwater modelling: Application to Mihocheon watershed, South Korea. *Hydrogeol. J*. **2010**. 18, 1253–1264.

Climate Service Center. Climate Fact Sheet: Indonesia. **2018,** updated version 2018.

Coutu, G.W., Vega, C. Impacts of land use changes on runoff generation in the east branch of the Brandywine Creek watershed using a GIS-based hydrologic model. Middle States Geographer. **2007**, 40,142–149.

Daloglu, M., Nassauer, J.I., Riolo, R., Scavia, D. An integrated social and ecological modeling framework: Impacts of agricultural con-servation practices on water quality. *Ecol. Soc*. **2014**, 19.

Doveri, M., Menichini, M., Scozzari, A. Protection of groundwater resources: worldwide regulations and scientific approaches. **2015**.

Fadil, A.H.R., Abdelhadi, K., Youness, K., Bachir, O.A. Hydrologic modeling of the bouregreg watershed (morocco) using GIS and SWAT model. GIS and SWAT Model" *Int. J. Geogr. Inf. Syst*. **2011**, 3,279–289.

Fan, Junliang., Kasper, T.O., Adrien, G., David, A. Lockington. Estimating groundwater recharge and evapotranspiration from water table fluctuations under three vegetation covers in a coastal sandy aquifer of subtropical Australia. *J. Hydrol*. **2014**, 519, 1120–1129.

Faramarzi, M., Abbaspour, K.C., Vaghefi, S.A., Farzaneh, M.R., Zehnder, A.J.B., Yang, H. Modelling impacts of climate change on freshwater availability in Africa. *J. Hydrol*. **2013,** 480, 85-10.

Fiseha, B., Setegn, S., Melesse, A., Volpi, E., Fiori, A. (2014). Impact of climate change on the hydrology of upper Tiber River Basin using bias corrected regional climate model. *Water. Resour. Manag.* **2014**, 28, 1327–1343.

Flörke, M., Schneider, C., McDonald, R. I. Water competition between cities and agriculture driven by climate change and urban growth. *Nat. Sustain*. **2018**, 1, 51−58.

Francesconi, W., Srinivasan, R., Pérez-Miñana, E., Willcock, S.P., Quintero, M. Using the Soil and Water Assessment Tool (SWAT) to model ecosystem services: A systematic review. *J. Hydrol*. **2016**, 535,625–636.

Gassman, P.W., Reyes, M., Green, C.H., Arnold, J.G. The soil and water assessment tool: Historical development, applications, and future directions. *Trans. ASABE*. **2007**, 50,1211–1250.

Gatwaza, O.C., Cao, X., Beckline, M. Impact of Urbanization on the Hydrological Cycle of Migina Catchment, Rwanda. *Open Access Library J*. **2016**, 3, 1–12.

Gibson, C.A., Meyer, J.L., Poff, N.L., Hay, L.E., Georgakakos, A. Flow regime alterations under changing climate in two river basins: implications for freshwater ecosystems. *River. Res. Applic*. **2005**, 21,849– 864

Green, W.H., Ampt, G.A. (1911). Studies on soil physics, 1. The flow of air and water through soils. *J. Agric. Sci*. **1911,** 4, 11−24.

Guo-yu, Q., Hong-young, L., Qing-tao, Z., Wan, C., Xiao-jian, L., Xiang-ze, L. Effects of Evapotranspiration on Mitigation of Urban Temperature by Vegetation and Urban Agriculture. *J. Integr. Agric.* **2013**. 12, 1307−1315.

Gupta, H.V., Beven, K.J., Wagener, T. Model calibration and uncertainty estimation. In: *Encyclopedia of hydrological sciences*. **2006**, 11–131.

Haase, D., Nuissl, H. Does urban sprawl drive changes in the water balance and policy? The case of Leipzig (Germany) 1870–2003. Landsc. Urban Plann. **2007**, 80, 1–13.

Hamel, P., Daly, E., Fletcher, T.D. Source-control stormwater management for mitigating the impacts of urbanisation on baseflow: A review. *J. Hydrol*. **2013**, 485, 201–211.

Hardison, E.C., O'Driscoll, M.A., DeLoatch, J.P., Howard, R.J., Brinson, M.M. Urban land use, channel incision, and water table decline along coastal plain streams, North Carolina. *J. Am. Water. Resour. Assoc*. **2009**, 45, 1032–1046.

Hargreaves, G.L., Hargreaves, G.H., Riley, J.P. Agricultural benefits for Senegal River Basin. *J. Irrig. Drain. Engr*. **1985**, 111,113-124.

Higashihiroshima city report, **2021**. https://www.city.higashihiroshima.lg.jp. (accessed on 12, November **2021**).

Japan Meteorological Agency, **2020**. Available from: http://www.jma.go.jp/jp/amedas (accessed on 9 April 2020).

Jat, M.K., Khare, D., Garg, P.K. Urbanization and its impact on groundwater: A remote sensing and GIS-based assessment approach. *Environmentalist*. **2009**, 29, 17–32.

Kagami, H., Honma, H., Shirahase, T., Nureki, T. Rb-Sr whole rock isochron ages of granites from northern Shikoku and Okayama, Southwest Japan: Implications for the migration of the Late Cretaceous to Paleogene igneous activity in space and time. *Geochem. J.* **1988**, 22, 69–79.

Kundu, S., Khare, D., Mondal, A. Individual and combined impacts of future climate and land use changes on the water balance. *Ecol. Eng*. **2017**, 105, 42–57.

Kurn, D., Bretz, S., Huang, B., Akbari, H. The Potential for Reducing Urban Air Temperatures and Energy Consumption through Vegetative Cooling. Department of Energy's (DOE) OSTI.GOV. **1994**.

Li, F., Jackson, T. J., Kustas, W. P., Schmugge, T. J., French, A. N., Cosh, M. H., Bindlish, R. "Deriving land surface temperature from Landsat 5 and 7 during SMEX02/SMACEX," *Remote Sens. Environ*. **2004**, 92, 521−534.

Lipczynska-Kochany, E. Effect of climate change on humic substances and associated impacts on the quality of surface water and groundwater: A review. *Sci. Total Environ*. **2018**, 640, 1548–1565.

Lv, X., Zuo, Z., Sun, J., Ni, Y., Wang, Z. Climatic and human-related indicators and their implications for evapotranspiration management in a watershed of Loess Plateau, *China. Ecol. Indic*. **2019**, 101, 143–149.

Marhaento, H., Booij, M.J., Rientjes, T.H.M., Hoekstra, A.Y. Attribution of changes in the water balance of a tropical catchment to land use change using the SWAT model. *Hydrol. Process*. **2017**, 31, 2029–2040.

Miguez, M.G., Magalhaes, L.P.C. Urban Flood Control, Simulation and Management - An Integrated Approach, Methods and Techniques in Urban Engineering. Armando Carlos de Pina Filho and Aloisio Carlos de Pina (Ed.), **2010**, ISBN: 978-953-307-096-4.

Minnig, M. Christian, M., Dirk, R., Mario, S. Impact of urbanization on groundwater recharge rates in Dübendorf, Switzerland. *J. Hydrol*. **2018**, 564.

Monteith, J.L. Evaporation and environment. *Symp. Soc. Exp. Biol*. **1965**, 19, 205– 234.

Moriasi, D.N., Arnold, J.G., Van Liew, M.W., Bingner, R.L., Harmel, R.D., Veith, T.L. Model evaluation guidelines for systematic quantification of accuracy in watershed simulations. *Trans. ASABE*. **2007**. 50, 885–900.

Morris, B.L., Lawrence, A.R.L., Chilton, P.J.C., Adams, B., Calow, R.C., Klinck, B.A. Groundwater and its susceptibility to degradation: A global assessment of the problem and options for management (Eary warning and assessment report series). United Nations Environment Programme. **2003**, 126.

Naef, F., Scherrer, S., Weiler, M. A process-based assessment of the potential to reduce flood runoff by land use change. *J. Hydrol*. **2002**, 267, 74–79.

Nash, J.E., Sutcliffe, J.V. River flow forecasting through conceptual models: part I. A discussion of principles. *J. Hydrol*. 1970, 10, 282–290.

Nasiri, S., Ansari, H., Ziaei, A.N. Simulation of water balance equation components using SWAT model in Samalqan watershed Iran. *Arab. J. Geosci*. **2020**, 13, 421.

National Library of Medicine (NLM), "Urbanization". **2014**.

Neitsch, S. L., Arnold, J. G., Kiniry, J. R., Williams, J. R. Soil and Water Assessment Tool Theoretical Documentation Version 2009. *J. Agric. Sci*. **2011**, 4, 11-24.

Nguyen, H.Q and Kappas, M. Modelling surface runoff and evapotranspiration using SWAT and BEACH for a tropical watershed in North Vietnam, compared to MODIS products. *Int. J. Adv. Remote. Sens. GIS*. **2015**, 4, 1367–1384.

Onodera, S.I. Groundwater and Subsurface Environments. Springer Japan, Tokyo. **2011**, 159–184.

Ou, X, Gharabaghi, B., McBean, E., Doherty, C. Investigation of the tank model for urban storm water management. *J. Water. Manag. Model*. **2017**.

Oudin,L., Salvati, B., Furusho-Percot, C, Ribstein, P., Saadi, Mohamed. Hydrological impacts of urbanization at the catchment scale. *J. Hydrol*. **2018**, 559, 774-786.

Owuor, S.O., Butterbach-Bahl, K., Guzha, A.C., Rufino, M.C., Pelster, D.E., Díaz-Pinés, E., Breuer, L. Groundwater recharge rates and surface runoff response to land use and land cover changes in semi-arid environments. *Ecol. Process*. **2016**, 5, 116.

Penman, H.L. Evaporation: An introductory survey. Netherlands J. Agric. Sci. **1956**, 4,7−29.

Petersen-Perlman, J. D., Veilleux, J. C., Wolf, A. T. International Water Conflict and Cooperation: Challenges and Opportunities, *Water Int*. **2017**,

Phuong, T. T., Thong, C. V. T., Ngoc, N. B., Chuong, H. V. Modeling soil erosion within small mountainous watershed in central Vietnam using GIS and SWAT. *Resources and Environment*. **2014**, 4,139–147.

Priestley, C.H.B., Taylor, R.J. On the assessment of surface heat flux and evaporation using large-scale parameters. *Mon. Weather Rev*. **1972**, 100:81−92.

Ridwansyah, I., Yulianti, M., Apip, Onodera, S.I., Shimizu, Y., Wibowo, H., Fakhrudin, M. The impact of land use and climate change on surface runoff and groundwater in Cimanuk watershed, Indonesia. *Limnology*. **2020**, 21, 487–498.

Ritchie, H., Roser, M. Urbanization. Our world in data. **2018**.

Santhi, C., Arnold, J.G., Williams, J.R., Dugas, W.A., Srinivasan, R., Hauck, L.M. Validation of the SWAT model on a large river basin with point and non-point sources. *J. Am. Water. Resour. Assoc*. **2001**, 37,1169−188.

Sellami, H., Benabdallah, S., La Jeunesse, I., Vanclooster, M. Quantifying hydrological responses of small Mediterranean catchments under climate change projections. *Sci. Total. Environ.* **2016**, 543, 924–936.

Shivhare, V., Goel, M.K., Singh, C.K. Simulation of surface runoff for upper Tapi sub catchment Area (Burhanpur Watershed) using SWAT. *Int Arch Photogram Remote Sens Spatial Inf Sci*. **2014**, 40, 391.

Shrivastava, P. K., Tripathi, M. P., Das, S.N. Hydrological modelling of a small watershed using satellite data and GIS technique. *J. Indian Soc. Remote. Sens*. **2004**, 32, 145–157.

Shuttle Radar Topography Mission of the United States Geological Survey, **2020**. Retrieved on 10 April 2020. https://eart hexplorer.usgs.gov/.

Singh, A., Gosain, A.K. Climate-change impact assessment using GIS-based hydrological modelling. *Water Int*. **2011**, 36, 386–397.

Singh, J., Knapp, H.V., Demissie, M. (2004). Hydrologic modeling of the Iroquois river watershed using HSPF and SWAT. *J. Am. Water. Resour. Assoc.* **2004**, 41, 343–360.

Singh, V, Bankar, N, Salunkhe, S. S, Bera, A. K, Sharma, J. R. Hydrological stream flow modelling on Tungabhadra catchment: parameterization and uncertainty analysis using SWAT-CUP. *Current Science*. **2013**, 104, 1187−1199.

Soil Conservation Service Engineering Division. Urban hydrology for small watersheds. U.S, Department of Agriculture, Technical Release. **1986**, 55.

Suryavanshi, S., Pandey, A., Chaube, U., Joshi, N. Long term historic changes in climatic variables of Betwa basin, India. *Theoretical and Applied Climatology*. **2014**, 117, 403–418.

Tao, C., Chen, X.L., Lu, J. Z., Gassman, P. W., Sabine, S., José-Miguel, S.P. Assessing impacts of different land use scenarios on water budget of Fuhe River, China using SWAT model. *Int. J. Agric. Biol. Eng*. **2015**, 8, 95−109.

Tashie, A.M., Mirus, B.B., Pavelsky, T.M. Identifying long-term empirical relationships between storm characteristics and episodic groundwater recharge. *Water Resour. Res*. **2016**, 52, 21–35.

Terskii, P.K.A., Chalov, S., Terskaia, A., Pluntke, T., Karthe, D. Assessment of Water Balance for Russian Subcatchment of Western Dvina River Using SWAT Model *Frontiers in Earth Science.* **2019**, 7, 241).

Thakur, B., Parajuli, R., Kalra, A., Ahmad, S., Gupta, R. Coupling HEC-RAS and HEC-HMS in precipitation runoff modelling and evaluating flood plain inundation map. *World Environ Water Resour Congress*. **2017**, 240–251.

Tudose, N.C., Marin, M., Cheval, S., Ungurean, C., Davidescu, S.O., Tudose, O.N., Mihalache, A.L., Davidescu, A.A. SWAT Model Adaptability to a Small Mountainous Forested Watershed in Central Romania. *Forests*. **2021**, 12, 860.

Vazquez-Amabile, G and Engel, B.A. (2008). Fitting of time series models to forecast streamflow and groundwater using simulated data from SWAT. J Hydrol Eng. **2008**, 13, 554–562.

Wakode, H. B., Baier, K., Jha, R., Ahmed, S., Azzam, R. Assessment of impact of urbanization on groundwater resources using GIS techniques – Case study of Hyderabad, India. *Int J Environ Res*. **2014**, 8,1145–1158.

Wakode, H. B., Baier, K., Jha, R., Azzam, R. Impact of urbanization on recharge and urban water balance for the city of Hydera, India. *Int. Soil Water Conserv. Res*. **2018**, 6,51–62.

Wang. G., & Xia, J. Improvement of SWAT2000 modelling to assess the impact of dams and sluices on streamflow in the Huai River basin of China. *Hydrol. Process. In.t J.* **2010**, 24, 1455–1471.

Wang, K., Onodera, S.I., Saito, M., Shimizu, Y. Long-term variations inwater balance by increase in percent imperviousness of urban regions. *J. Hydrol*. **2021**, 602, 126767.

Wang, K., Onodera, S. I., Saito, M., Shimizu, Y., Iwata, T. Effects of forest growth in different végétation communities on Forest catchment water balance. *Sci. Total Environ*. **2022**, 809, 151159.

Yigzaw, W., Hossain, F. Land use and land cover impact on probable maximum flood and sedimentation for artificial reservoirs: case study in the Western United States. *J Hydrol Eng*. **2016**, 21, 05015022.

Zareian, M.J., Eslamian, S.S., Safavi, H.R. Investigating the effects of sustainability of climate change on the agriculture water consumption in the Zayandeh-Rud River basin. *JWSS-Isfahan Univ Technol.* **2016**, 20,113–128.

Zhang, L., Nan, Z., Yu, W., Zhao, Y., Xu, Y. Comparison of baseline period choices for separating climate and land use/land cover change impacts on watershed hydrology using distributed hydrological models. *Sci. Total Environ*. **2018**, 622–623, 1016–1028.

Zomlot, Z., Verbeiren, B., Huysmans, M.; Batelaan, O. Spatial distribution of groundwater recharge and base flow: Assessment of controlling factors. J. *Hydrol. Reg. Stud*. **2015**, 4, 349–368.

Chapter 5

Groundwater Contamination Status in Saijo Basin. Insights From Hydrochemistry and Dual Isotope

5.1 Introduction

Groundwater is an important resource for human development. It is a dependable source of water supply in many areas of the world (Zakaria et al., 2021). The rapid increase in the population, industrialization and human activities have led to the degradation in water quality, and globally, water resources overexploitation has been reported by many researchers globally (Maurya et al., 2019). The quality of groundwater is mostly determined by natural and hydrogeological factors as well as the anthropogenic activities prevailing in an area (Cao et al., 2019). It is important to understand the hydrochemistry and quality of groundwater for efficient management and resource conservation. Groundwater hydrochemistry has been used to identify and interpret groundwater quality, the impact of anthropogenic activities on groundwater quality and to determine the water chemistry (Kortatsi et al., 2008; Gibrilla et al., 2011; Zakaria et al., 2012). Generally, the quality of groundwater depends on physiochemical properties of aquifer and its composition. This state is controlled by the properties of soil and rocks of aquifer media (Foster et al., 2002). Chemical components of industrial, agricultural, urban sewage, mining extracts are the main causes of high pollutant contamination in groundwater (Amirabdollahian and Datta 2013). Many previous studies have been conducted on the assessment of groundwater pollution in different parts of the world and findings revealed significant deterioration in water quality for both drinking and irrigation purposes (Raymohan et al. 2008; Bhunia et al., 2018).

Saijo is an agricultural and industrial town in the heart of higashihiroshima which has experienced rapid urbanization since the 1970s. Due to increasing population, rapid socio-economic development, intensification of industrial and irrigation activities in the watershed, the pressure on groundwater demand has significantly increased in the last 50yrs. Deep borehole construction in the area for groundwater extraction commenced in the 1970s with over twelve sake brewery located within 1km span from east to west of the watershed. Considering the above-mentioned possible threats to groundwater quality, there a need to assess the groundwater quality for proper management of water resources. On this note, the physiochemical properties of water sources were explored with an insight into determining the source of contaminants using Isotopic indicators.

5.2 Materials and Methods

The study area is situated in the eastern part of the Kurose River catchment in Higashihiroshima with an estimated area of 17km^2 (Figure 5.1). The catchment is characterized by a warm humid climate with mean annual daily temperature varying from 12 °C to 15 °C. The mean annual precipitation is approximately 1469 mm and there exists a clear difference in rainfall pattern between the four seasons in the watershed. Sixteen groundwater and surface water (eight borehole (BH), two hand-dug wells (HDW), three rivers and three spring samples) were collected in the month of October 2021 from the study area for hydrochemical analyses and Isotope 15 of nitrogen. Groundwater and surface water samples were collected into sterilized 250ml and 100ml polyethylene bottles. Samples in 250ml bottles were filtered in the laboratory after conducting acid-base titration on the water samples. Also, ten groundwater samples were collected in 100ml bottles after filtering through a 0.2µm filter membrane for $\delta^{15}N\text{-}NO_3^-$ and $\delta^{18}O\text{-}NO_3^-$ analyses. The temperature, pH, electrical conductivity (EC), oxygen redox potential (ORP) and dissolved oxygen (DO) were measured on the field; pH and

temperature were tested with the HM-200 pH meter and the electrical conductivity and DO were measured with the WTW Multi 3320 multi-parameter instrument.

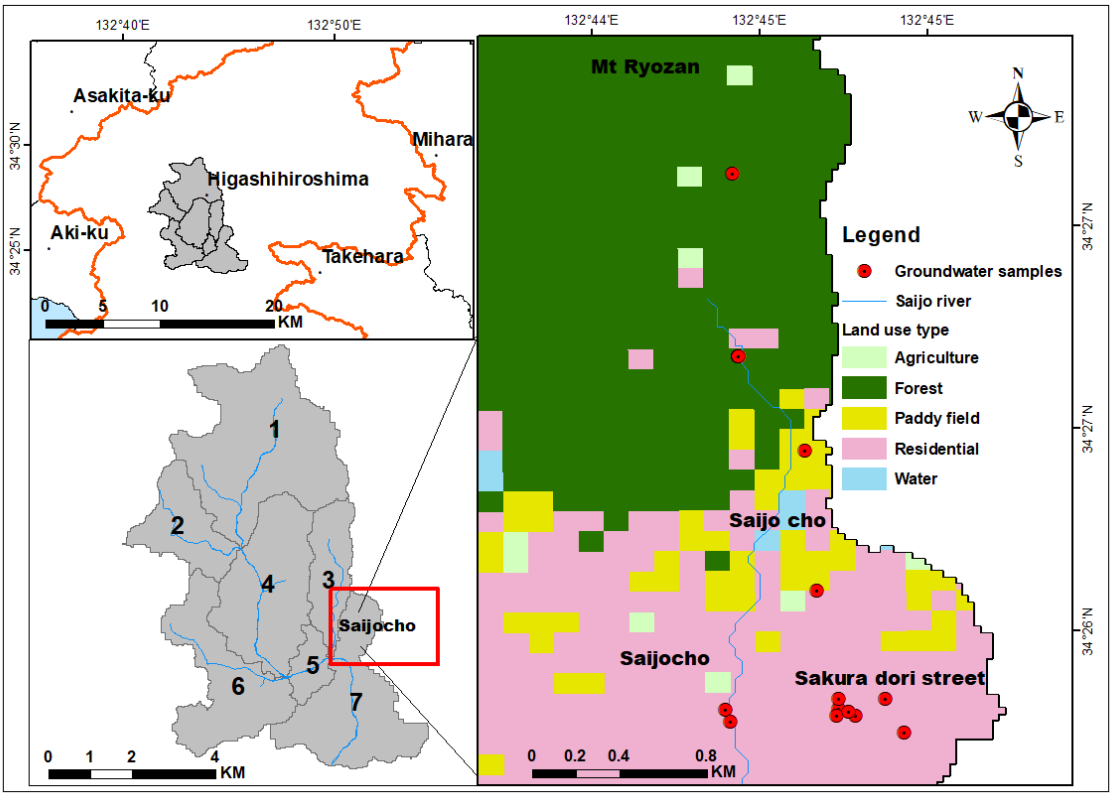

Figure 5.1: Location map of study area showing sample collection points.

Samples were then transported to the laboratory and stored at 4 °C until analysis. The cations and anions were analysed with the HPLC Shimadzu LC-20AD Ion Chromatograph. Alkalinity was determined by titration using 0.05 HCl. Sample duplicates and standards were routinely analysed to ensure quality control of analytical data. The electroneutrality of the data was assessed by calculating the charge-balance error (E) using equation (2.1).

5.3 Results and Discussion

5.3.1 Characterization of major ions in different water sources

The physico-chemical parameters of collected water samples in the study are presented in (Table 5.1) which are analysed individually and systematically for understanding the general water quality.

Table 5.1: Descriptive statistics of the different physicochemical properties of the collected groundwater samples.

Sample	pH	EC	DO	SO_4^{2-}	Cl^-	NO_3^-	HCO_3^-	Na^+	K^+	Mg^{2+}	Ca^{2+}
Ryou Spring	6.6	63.3	1.0	5.0	3.8	2.9	19.5	8.8	0.2	1.1	4.4
Dam left	6.5	139.0	7.1	0.5	2.9	BDL	73.9	6.2	1.1	2.2	14.2
Dam Middle	6.8	68.4	7.9	3.7	3.5	2.3	29.4	7.0	0.8	1.6	5.5
Dam River	6.9	63.3	8.6	4.1	3.5	2.6	22.1	6.9	0.7	1.4	4.5
Saijo River	7.0	115.9	7.9	5.5	8.5	4.7	33	9.8	2.0	2.0	9.6
Kamotsuru	6.2	222.0	4.0	18.1	17.2	8.2	65.1	20.7	3.9	4.7	19.4
Hakuboran	6.2	210.0	5.7	25.9	14.6	9.7	46.3	18.0	13.4	5.7	12.3
Hamotsuru	6.48	264	7.25	17.7	15.1	16.0	80.6	BDL	7.4	24.5	BDL
Fujiwara	6.7	187.0	7.0	7.3	2.1	8.4	86.9	5.1	6.0	2.6	26.9
Manoki	6.2	217.0	6.5	22.8	13.4	17.2	43.3	17.8	5.4	4.1	17.1
Fukubijin	6.2	222.0	5.3	24.1	14.5	13.0	93.8	18.3	4.7	6.5	31.1
Jiroma	6.4	345.0	4.6	38.1	18.8	16.9	95.2	27.0	6.0	8.6	31.2
Yamamoto	5.4	89.1	5.9	26.2	13.9	18.9	12.3	14.6	2.1	7.1	10.9
Tsumura	7.3	224.0	3.0	3.9	3.8	BDL	123.3	5.8	8.8	3.0	33.9
Upstream Well	6.1	89.1	5.9	1.0	8.3	11.8	17.3	10.3	1.4	1.1	5.3

BDL: Below detectable limit. Anions, cations and DO are given in mg/L, EC: µS/cm

The pH value ranged from ranged from 5.43 to 7.29 in boreholes and wells, 6.8 to 6.54-99 in rivers and springs which shows that the waters were alkaline in nature but for one well sample with relatively high redox potential (403mv). Electrical conductivity in µS/cm shows a range of 89.1 µS/cm to 345 µS/cm in boreholes and wells, 63.3 µS/cm to 139 µS/cm in rivers and springs. Major ion hydrogeochemistry is characterized by the prevalence of calcium and bicarbonates as the dominant cation and anion, respectively (Figure 5.2).

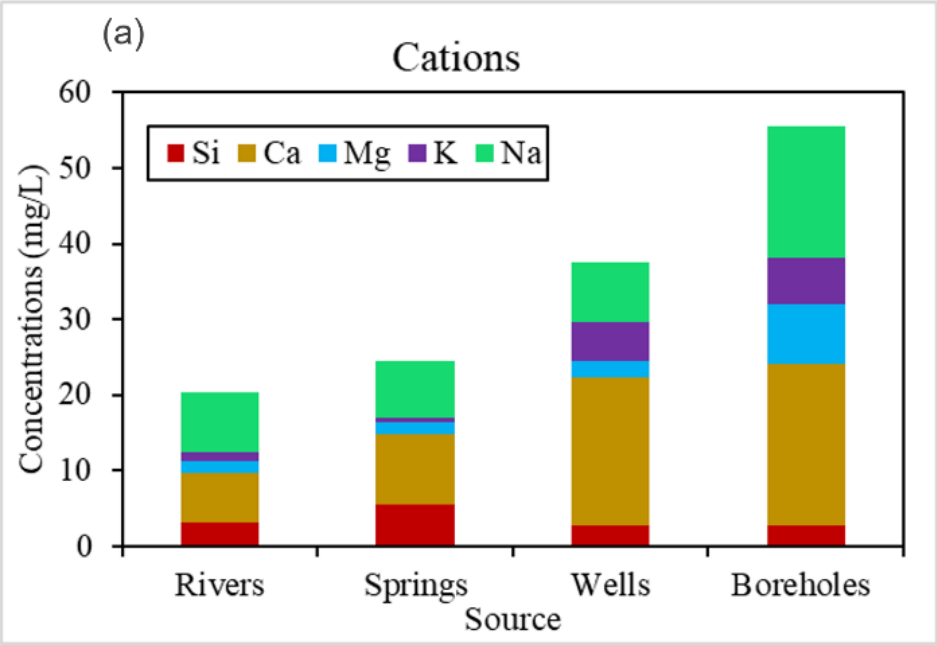

Figure 5.2a: Average relative concentrations (mg/l) of cations in the investigated water types.

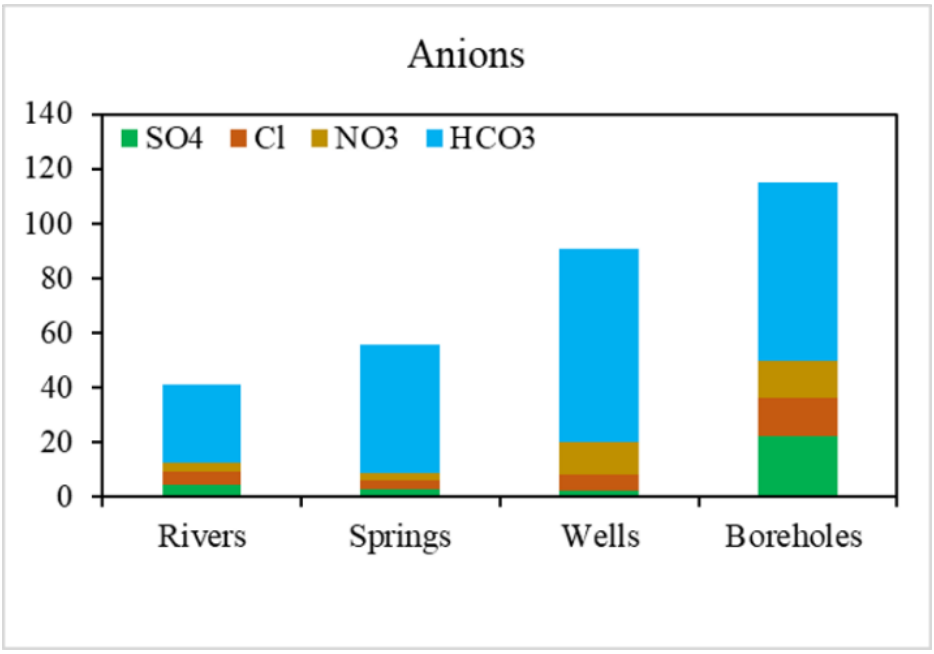

Figure 5.2b: Average relative concentrations (mg/l) of cations and silica in investigated water types.

The average concentration (mg/l) of dissolved species in the samples was in the order of $Ca^{2+} > Na^{+} > Mg^{2+} > K^{+}$ for the cations and $HCO_3^{-} > SO_4^{2-} > NO3^{-} > Cl^{-}$ for the anions. Figure 4.2b shows the average relative concentrations of major anions, cations, and silica in all

the water types in which dissolved ions increase progressively from a minimum in rivers, springs, and maximum in the groundwater. Such an evolution indicates that the groundwater is a chemically enriched equivalent of more diluted surface waters. The Piper trilinear diagram (Piper, 1944) has been used for the purpose of characterizing the water types present in the study area. Trilinear analysis suggested that all but one the samples belong to a mixed Ca-Mg-HCO3 water type as seen in Figure 5.3.

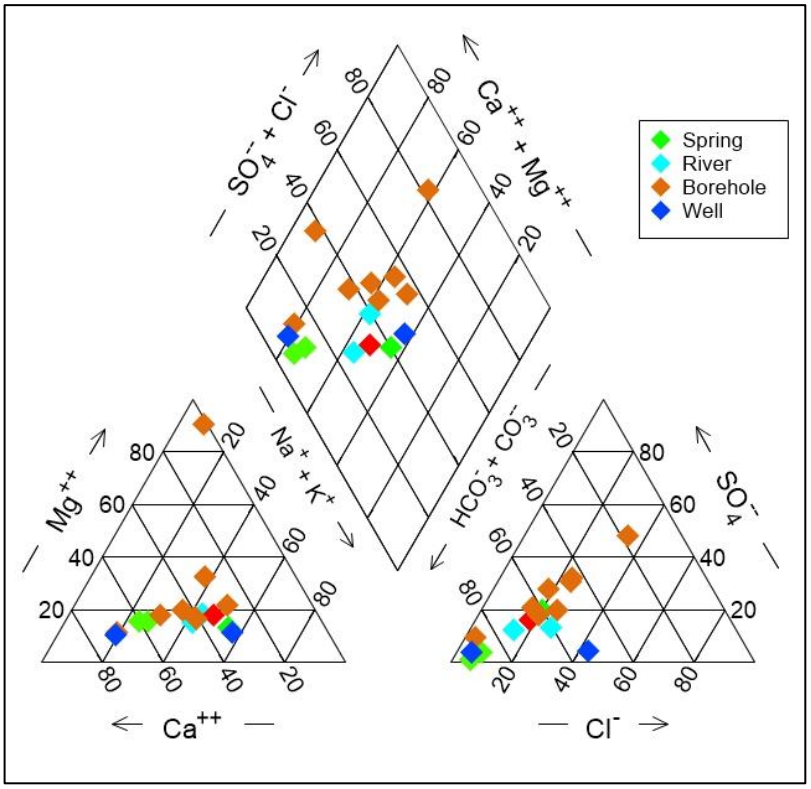

Figure 5.3: Piper trilinear diagram showing major groundwater types and geochemical evolution in the Saijo basin.

The high concentration of HCO_3^- have two possible sources. The main one is related with dissolution of rocks during chemical weathering processes taking place in this aquifer. whilst secondarily their concentration might be enriched by the decomposition of organic matter and root respiration in the soil zone which creates under the precipitation effect initially weak carbonic acid (H_2CO_3) and finally bicarbonates (HCO_3^-) through the sequence of following reactions:

$CO_2 + H_2O \rightarrow H_2CO_3$

$H_2CO_3 \rightarrow H + HCO_3$

5.3.2 Gibbs plot to determine the geochemical process prevailing

Gibbs diagram (Gibbs, 1970) helps in understanding the relationship possesses between the aquifer lithology and the water composition. It consists of three different distinct fields that are; evaporation dominance, rock-water or rock dominance and the precipitation dominance. For cations TDS and $(Na^+ + K^+)/(Na^+ + K^+ + Ca)$ are plotted whereas for anions TDS and $(Cl^-/Cl^- + HCO_3)$ are plotted to determine the prevailing mechanisms leading to the variable concentrations of the ion in the groundwater and its impact on the surrounding country rock (Figure 5.4).

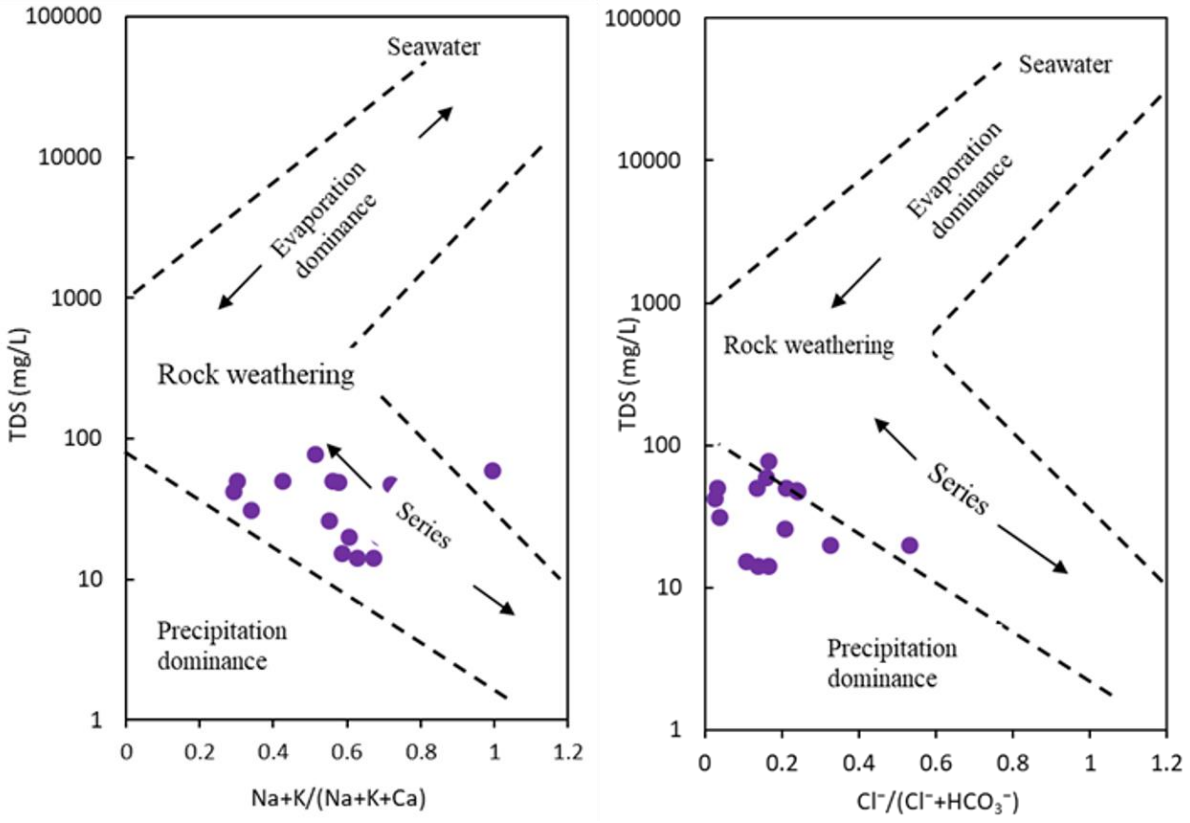

Figure 5.4: Gibbs diagram representing controlling factors of groundwater quality.

The results illustrate that all the samples point towards precipitation domain. Thus, suggesting that incongruent dissolution of minerals through rainwater controls the major ion chemistry of groundwater. Information about the weathering processes (carbonate vs silicate) can be explained by a plot of ratios of (Ca + Mg) against (HCO_3 + SO_4) in meq/L (Figure 5.5).

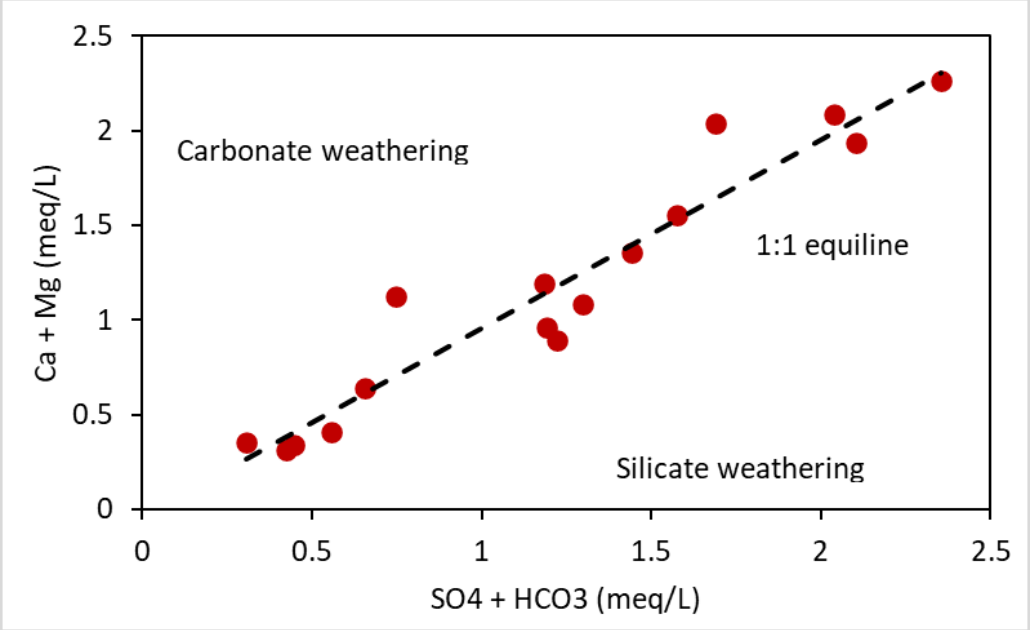

Figure 5.5: Identification of dominant mineral weathering in groundwater

According to Abdul-Wahab et al., (2016) if Ca, Mg, SO_4 and HCO_3 are derived from a simple dissolution of calcite, dolomite, and gypsum, a 1:1 stoichiometry of (Ca + Mg) to (SO_4 + HCO_3) should exist (McLean et al., 2000). Sample points that lie in the right of 1:1 equiline suggest, apart from potential ion-exchange, a significant contribution of silicate weathering in groundwater chemistry. Indeed, most of the samples fell around or slightly below the equiline which may suggest weathering of the aluminosilicate minerals of metamorphic rocks and quaternary deposits, as a major impact in groundwater chemistry. However, some samples plotted around or slightly above the equiline and suggest the contribution from carbonate weathering.

5.4 Potential Sources of Nitrate-Nitrogen in Groundwater Systems

According to Table 5.1, All groundwater samples had relatively low DO concentrations while elevated values were recorded in rivers samples; (Mean DO = 8.2 mg/l river, 5.8 mg/L borehole, 4.5 mg/L wells, and 4.1 spring). This suggest that the denitrification process was likely to occur in the groundwater samples. The mean concentrations of NO_3^-–N were in the order 3.5 mg/l wells, 2.9 mg/L in boreholes, 0.7 mg/L in rivers, and 0.5 to 5 mg/L in springs. Mean SO_4^{2-} and Cl^- showed similar trend decreasing from Boreholes (19.7 mg/L and 12.4 mg/L) to wells (13.6 mg/L and 11.1 mg/L) to rivers (4.4 and 5.2 mg/l) and finally the lowest concentrations in spring (2.8 mg/L and 3.4 mg/L) respectively. The compositional groups were identified by plotting NO_3^-–N against SO_4^{2-}, Cl^-, EC and DO (Figure 5.6) for all samples obtained from the Saijo groundwater source.

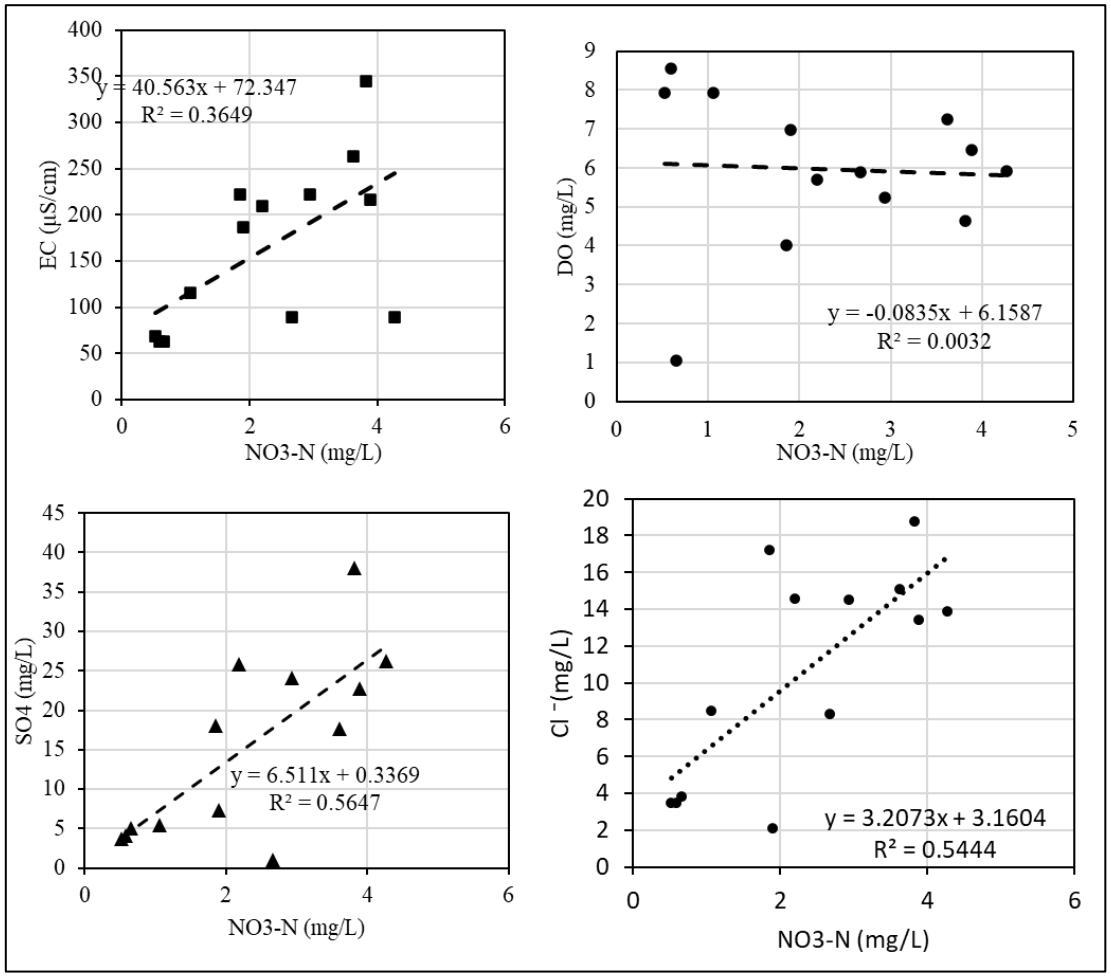

Figure 5.6: Relationship of NO_3^-–N vs SO_4^{2-}, Cl^-, EC, and DO in groundwater samples.

The bi-plot of NO_3^-–N against Cl^- concentrations and SO_4^{2-} concentrations highlight a positive moderate degree of correlation of 0.54 and 0.56 respectively. Nitrate and chloride are often used as indicators of contamination in groundwater. However, their behaviour tends to be different in groundwater depending on various factors: While chloride is a conservative tracer that does not typically undergo biological transformations or attach to soil, nitrate in groundwater can be reduced by denitrification processes in the presence of appropriate bacteria and redox conditions (Rivett et al., 2008; Kohn et al., 2016). Thus, the presence of this process in Saijo's groundwater could have reduced the degree of correlation between the parameters in the biplot of Figure 5.6. Also, the biplot NO_3^-–N against EC highlights low degree of correlation while no correlation was observed between NO_3^-–N and DO.

5.5 Nitrate isotopes for the identification of sources and fate

The $\delta^{15}N\text{-}NO_3^-$ of nitrate ranged from +6.7 ‰ to +11.9 ‰ in Boreholes and +9.5 ‰ to + 12.3 ‰ in wells while $\delta^{18}O\text{-}NO_3^-$ values of nitrate varied between -0.9 ‰ to 4.2 ‰ in boreholes and 0.0 ‰ to 2.2 ‰ in wells (Table 4.4). The spring sample had $\delta^{15}N\text{-}NO_3^-$ and $\delta^{18}O\text{-}NO_3^-$ values of 0.11 ‰ and 4.51‰. In order to define the main sources of nitrate in groundwater, isotope data of nitrate were plotted in Figure 5.7.

Table 5.2: $\delta^{15}N\text{-}NO_3^-$ and $\delta^{18}O\text{-}NO_3^-$ in groundwater water and surface water in Saijo.

Sample Name	Type	NO_3^-–N (mg/L)	$\delta^{15}N\text{-}NO_3^-$	$\delta^{18}O\text{-}NO_3^-$
Ryou Spring	Spring	0.6554	0.11864	4.515304
Saijo River	River	1.0622	7.265371	-2.417
Maneki	Borehole	3.8872	11.13735	4.134532
Jiroma	Borehole	3.8194	11.21773	1.085061
Hamotsuru	Borehole	3.616	8.988091	0.693675
Fukubijin	Borehole	2.938	11.97817	4.175538
Hakuboran	Borehole	2.1922	7.32371	3.16281
Fujiwara	Borehole	1.8984	6.670061	-0.93167

Yamamoto	Well	4.2714	12.24176	2.123642
Upstream	Well	2.6668	9.483232	0.002013

The application of the dual isotope method of measuring the $\delta^{15}N\text{-}NO_3^-$ and $\delta^{18}O\text{-}NO_3^-$ values of dissolved NO_3^-–N in this study identified two major contamination sources (Aravena et al., 1993): nitrate derived from soil organic nitrogen (0.1‰ to 7.3 ‰, Figure 5.7) and nitrate resulting from animal waste and human sewage, e.g via septic systems (+9.8‰ to +11.9‰). The $\delta^{15}N$ values of nitrate derived from manure are often in the range of +10 to +20‰ or higher (Karr et al., 2001).

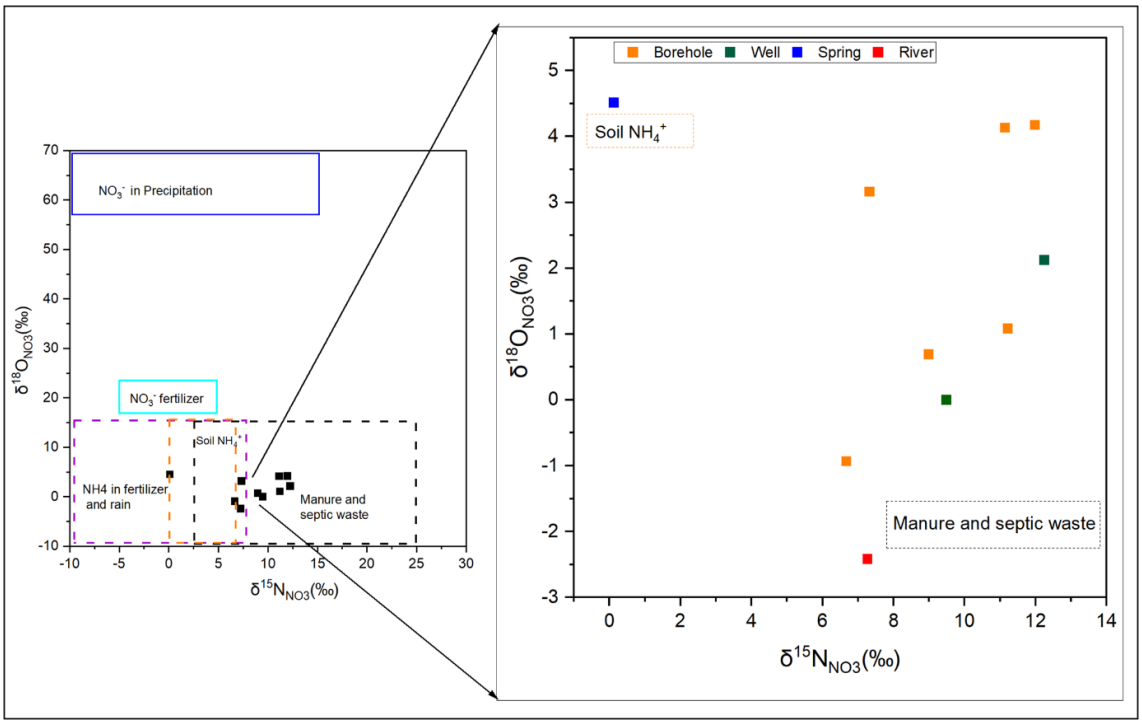

Figure 5.7: Schematic diagram of the isotopic composition of typical nitrate sources including data for groundwater, spring and wells in the vicinity of the groundwater source. Typical ranges of $\delta^{15}N\text{-}NO_3^-$ and $\delta^{18}O\text{-}NO_3^-$ values for different nitrate sources were taken from Kendall (2001).

The results of $\delta^{15}N\text{-}NO_3^-$ revealed an absence of nitrate originating from mineral fertilizers in the investigated groundwaters due to either little use of mineral fertilizers or the proper use of fertilizers according to crop needs. In addition to nitrate sources identification,

the correlation analysis $\delta^{15}N\text{-}NO_3^-$ and $\delta^{18}O\text{-}NO_3^-$ was also used to evaluate the denitrification and nitrification processes. According to Choi et al. (2003), nitrification produces a positive correlation between the nitrate concentrations and $\delta^{18}O\text{-}NO_3^-$ due to isotopic fractionation. Indeed, since ^{14}N reacts faster than ^{15}N during nitrification, incomplete nitrification results in ^{15}N-depleted nitrate (Mariotti et al. 1981).

Therefore, preferential inflows into groundwater of nitrate produced through incomplete nitrification results in low nitrate concentrations and $\delta^{15}N_{NO3}$. With the proceeding of nitrification to completion, the concentration of nitrate and $\delta^{15}N\text{-}NO_3^-$ increase gradually. The slope of regression line would be different depending on the initial $\delta^{15}N\text{-}NO_3^-$ of original source-N (Choi et al., 2003). A significant denitrification, highlighted by a progressive enrichment in $\delta^{15}N\text{-}NO_3^-$, which is distinguished in the groundwater samples (Figure 5.8).

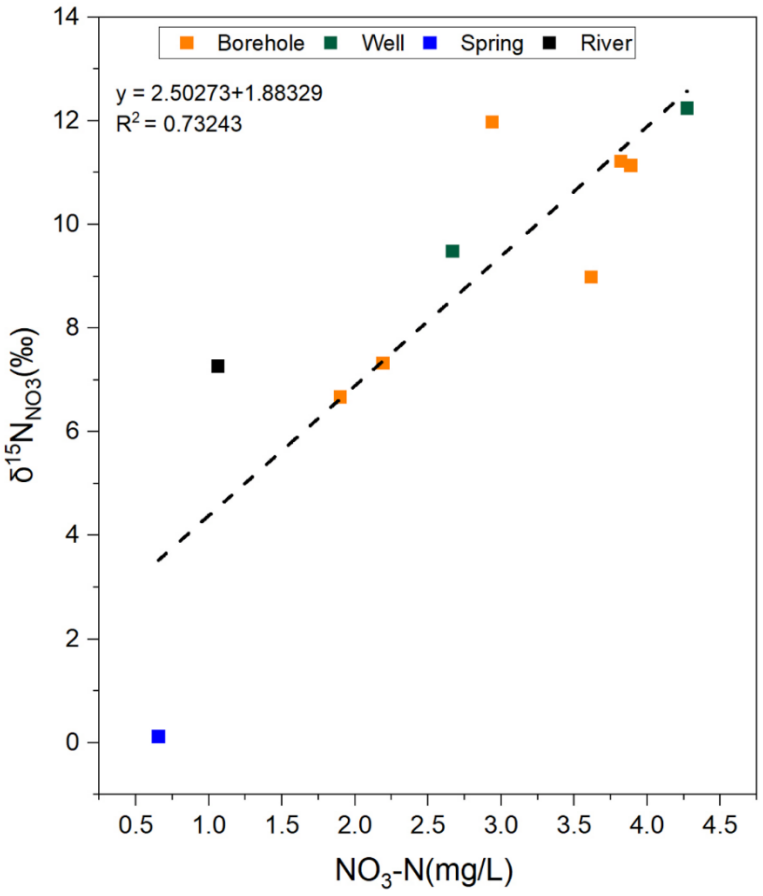

Figure 5.8: Relationship between NO_3^-–N and $\delta^{15}N\text{-}NO_3^-$.

This is consistent with the results of Figure 5.7, in which all but one sample shows isotopic composition corresponding to synthetic sources, partially nitrified Similar results have equally been highlighted in previous studies (Debernardi et al., 2008).

5.6 Summary

Groundwater and surface water samples were analysed for their physico-chemical properties. The groundwater samples are fresh with TDS values less 1000 mg/L. The Calcium (Ca^{2+}) and bicarbonate (HCO_3^-) were the most abundant cation and anion respectively. The major water types in the study area are of Ca–Mg–HCO3 and the mixed Ca–Mg–Cl type. Gibbs diagrams showed that the geochemical evolution of groundwater in the present study site which is controlled primary by precipitation The application of the dual isotope method of both δ^{15}N-NO_3^- and δ^{18}O-NO_3^- measurements of dissolved nitrates at the groundwater source identified two major contamination sources with values characteristic for nitrate derived from nitrification of soil organic nitrogen (+0.1 ‰ to +7.3 ‰ for δ^{15}N) and nitrate derived from animal wastes or human sewage, e.g., via septic systems (+8.9 ‰ to + 12.3 ‰ for δ^{15}N) in two distinct zones. In spite of agricultural activities in the study area, we found no evidence of nitrate originating from synthetic fertilizers in the groundwater. Elevated δ^{15}N values of dissolved nitrate were associated with higher nitrate-nitrogen concentrations.

5.7 References

Abdul-Wahab, D. Hydrogeochemical and isotopic studies of ground and surface waters in the Lower Anayari catchment area, Upper East region of Ghana (Doctoral dissertation, University of Ghana). **2016**.

Amirabdollahian, M., Datta, B. Identification of contaminant source characteristics and monitoring network design in groundwater aquifers: an overview. *J Environ Prot*, **2013**, 4, 26−41.

Aravena, R., Evans, M.L., Cherry, J.A. Stable isotopes of oxygen, and nitrogen source identification of nitrate from septic systems. *Ground Water*.**1993**, 31, 180–186.

Bhunia, G. S., Shit, P. K., Maiti, R. Comparison of GIS-based interpolation methods for spatial distribution of soil organic carbon (SOC). *J. Saudi Soc. Agric. Sci*. **2018**, 17, 114−126.

Cao X., Lu Y., Wang C., Zhang M., Yuan J., Zhang A., Song S., Baninla Y., Khan K., Wang Y. Hydrogeochemistry and quality of surface water and groundwater in the drinking water source area of an urbanizing region *Ecotoxicol. Environ. Saf*. **2019**, 186, 109628.

Choi, W.J., Lee, S.M., Ro, H.M. Evaluation of contamination sources of groundwater NO3 using nitrogen isotope data: a review. *Geosci J*. **2003**, 7, 81–87.

Debernardi, L., De Luca, D.A., Lasagna, M. Correlation between nitrate concentration in groundwater and parameter affecting aquifer intrinsic vulnerability. *Environ Geol*. **2008**, 55, 539–558.

Foster, S. S. D., Hirata, R., Gomes, D., D'Elia, M. and Paris, M. Groundwater quality protection: a guide for water utilities, municipal authorities and environment agencies. World Bank, Washington DC. **2002**.

Gibrilla, A., Bam, E.K.P., Adomako, D., Ganyaglo, S., Osae, S., Akiti, T.T. (2011). Application of water quality index (WQI) and multivariate analysis for groundwater quality assessment of the birimian and cape coast granitoid complex: Densu River Basin of Ghana. *Water Qual Expo Health*. **2011**, 3, 63.

Karr, J. D., Showers, W. J., Gilliam, J. W., Andres, A. S. Tracing nitrate transport and environmental impact from intensive swine farming using delta nitrogen-15. *J. Environ. Qual*. **2001**, 30,1163-1175.

Kendall, C., Coplen, T.B. Distribution of oxygen-18 and deuterium in river waters across the United States. *Hydrol. Process*. *2001*, 15, 1363–1393.

Kohn, J., Soto, D. X., Iwanyshyn, M., Olson, B., Kalischuk, A., Lorenz, K., Hendry, M.J. (2016). Groundwater nitrate and chloride trends in an agriculture-intensive area in southern Alberta, Canada. *Water Qual. Res. J*. **2016**; 51, 47–59.

Kortatsi, B.K., Tay, C.K., Anornu, G., Hayford, E., Dartey, G.A. Hydrogeochemical evaluation of groundwater in the lower Offin basin, Ghana. *Environ. Geol*. **2008**, 53, 1651–1662.

Kumar, M., Ramanathan, A.L., Rao, M.S., and Kumar, B. Identification and evaluation of hydrogeochemical processes in the groundwater environment of Delhi, India: *J. Environ. Geol*, **2006**, 50, 1025–1039.

Mariotti, A., Germon, J. C., Hubert, P., Kaiser, P., Letolle, R., Tardieux, A., & Tardieux, P. Experimental determination of nitrogen kinetic isotope fractionation: some principles;

illustration for the denitrification and nitrification processes. Plant and soil. **1981**, 62, 413-430.

Maurya, P., Kumari, R., Mukherjee, S. Hydrochemistry in integration with stable isotopes (δ18O and δD) to assess seawater intrusion in coastal aquifers of Kachchh district, Gujarat, India. *J. Geochem. Explor*. **2019**, 196, 42-56.

McLean, W., Jankowski, J., Lavitt, N. Groundwater quality and sustainability in an alluvial aquifer, Australia. In: Groundwater, past achievements and future challenges (Sililo et al.,Eds): Balkema, Rotterdam. 2000, 567–573.

Piper, A.M. A graphic procedure in the geochemical interpretation of water-ana- lyses. Eos, Trans. Am. Geophys. Union 25, **1944**, 914–928.

Rajmohan, N., Al-Futaisi, A., Jamrah, A. Evaluation of long-term groundwater level data in regular monitoring wells, Barka, Sultanate of Oman. Hydrological Processes: *An International Journal*. **2007**, 21, 3367−3379.

Rivett, M.O., Buss, S.R., Morgan, P., Smith, J.W.N, Bemment, C.D. Nitrate attenuation in groundwater: a review of biogeochemical controlling processes. *Water Res*. **2008**. 42, 4215–4232.

Zakaria, N., Akiti, T.T., Osae, S., Dickson, A., Ganyaglo, S.Y., Hanson, J.E.K., Ayanu, G. Hydrogeochemistry of groundwater in parts of the Ayensu Basin of Ghana. *Proc. Int. Acad. Ecol. Environ. Sci*. **2012**, 2, 128–135.

Zakaria, N., Anornu, G., Adomako, D., Owusu-Nimo, F., Gibrilla, A. Evolution of groundwater hydrogeochemistry and assessment of groundwater quality in the Anayari catchment. Groundwater for Sustainable Development. **2021**, 12, 100489.

Chapter 6

Discussion

6.1 Anthropogenic influence on groundwater resources

6.1.1 Groundwater recharge assessment from hydrological model

Land use is a key factor affecting water balance, which in turn affects the water resource availability. Increasing urbanization has altered water balances in river catchments and the effects of urbanization processes have been poorly understood at the catchment and sub catchment scale. The contribution from groundwater is vitally important for water supply especially for developing rural catchments whereby groundwater is largely used for food production and drinking water supply. The results of the modelling simulation have clearly shown the strong impact of land use change on the water balance in the Kurose River catchment from the 1980s to 2000s with a significant decline in groundwater recharge (Figure 6.1).

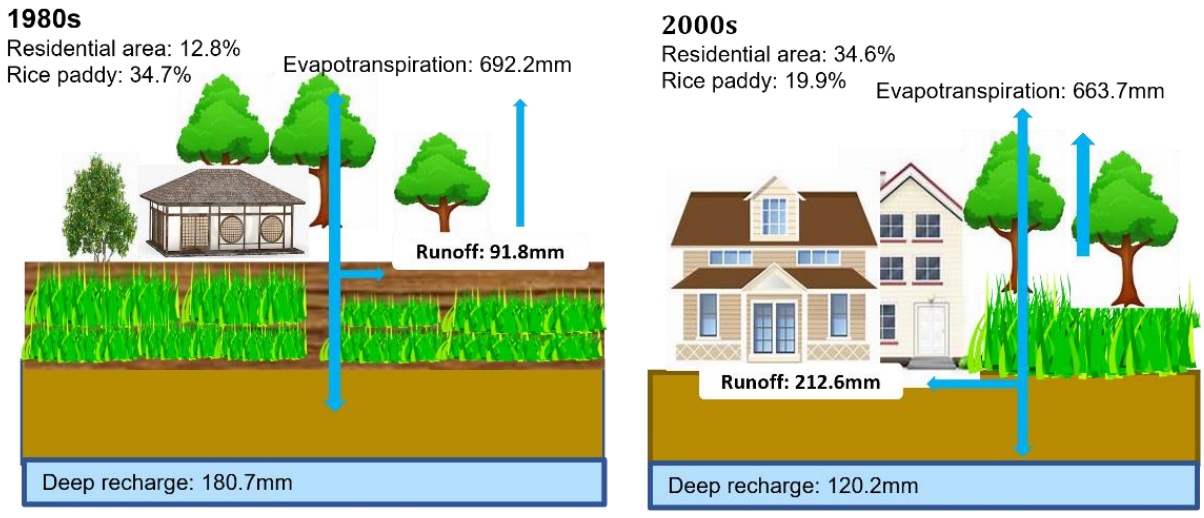

Figure 6.1: Actual evapotranspiration, runoff, leakages, and groundwater recharge for the two years of investigation (1980s and 2000s) for the Kurose River catchment.

Several studies have highlighted the fact that watersheds that are urbanized exhibit significantly lower groundwater recharge than watersheds that remain in their natural condition as surface sealing prevents infiltration and increases surface water runoff compared to natural landscapes (Grischek et al., 1996; Hardison et al., 2009). Other studies indicate an increase in groundwater recharge rates due to the reduction in evapotranspiration linked with surface sealing (Barron et al., 2013; Garcia-Fresca, 2007). Results from this study align with those mentioned above. During the period 1980s to 2000s, residential areas which occupied only 12% of the catchments total area increased to approximately 34.6% resulting to a substantial decrease in rice paddy fields which have been recognised as good recharge zones. This led to significant decrease in the catchment's groundwater rates (Figure 6.1). Furthermore, land use change and anthropogenic activities in the catchment such as surface sealing due to streets and buildings modified the infiltration and movement of water which led to a significant increase in the catchment's runoff. Inferring from (Figure 4.4), the recent historic years are proven to be more susceptible to flooding and in case of heavy rainfall events. The immediate repercussions of urbanization the hydrological cycle has been documented by various researchers which has been summarized below (Jha, Singh, and Vatsa, 2008; Strohschon et al., 2013).

- Flooding (e.g because of increased soil sealing)
- water shortage (e.g. due to rising consumption)
- changes in the river and groundwater regimes
- Groundwater pollution (Urban areas generate both nonpoint and point sources of contaminants are due to leakage from drainage and, industrial wastage and effluent

The impact of urbanization on groundwater sources is not only quantitative, but also qualitative. For qualitative assessment of urbanization processes on groundwater sources in the study area, a sub-basin in the Kurose River basin was studied

6.1.2 Influence of social aspects on groundwater nitrate nitrogen contamination: Case study; Saijo and Osakishimojima

Groundwater plays a significant role in the ecosystem, and it is a vital local water source for industrial, agricultural, and domestic purposes. When comparing to surface water, it is usually higher in quality with better protection from direct pollution as well as less subject to evapotranspiration. As much as urbanization processes lead to groundwater decline, it equally leads to groundwater contamination. Groundwater contamination sources are usually varied and difficult to detect thus using tracer-methods can help distinguish potential contamination source. Both Saijo and Osakishimojima are agricultural catchments with different cropping types, while rice paddy dominates in Saijo, citrus orchard is the main agricultural crop in Osakishimojima. However, the level of urbanization is significantly different in the two study areas, Saijo is a rapid developing rural catchment and is still undergoing development while Osakishimojima is a rural island with an aging population. However, from our studies, results show higher NO_3^-−N contamination levels in Osakishimojima as compared to Saijo. In Saijo NO_3-N concentration ranged from 0.4 mg/L to 4.3 mg/L with a mean value of 2.1 mg/l in all investigated water types. Mean NO_3^-−N values increased from 0.5mg/L in springs to 0.7 mg/L in rivers to 2.9 mg/L in boreholes and 3.5 mg/L in wells. This concentrations are relatively low when compare with those from the investigated study sites in Osakishimojima. For instance, in Kubi, NO_3^-−N concentration ranged from 0.5 mg/L to 13m/L with a mean value of 6.54 mg/L while in Ocho NO_3^-−N values ranged from 0.7 mg/L to 15.1 mg/L with a mean value of 4.75 mg/L. Mean groundwater (wells ad boreholes) NO_3^-−N concentration were higher in Kubi (7.2 mg/L) than Ocho (4.94 mg/L), and Saijo (1.9 mg/L). Almost twice the concentration in Ocho

and more than thrice in Saijo. This results are quite interesting especially seeing as all study sites are agriculture oriented, however several factors may affect the variation in NO_3^-–N levels in this areas. For instance,

1. Proportion of land use under cultivation which will affect fertilizer ratios during application: In Kubi approximately 40.19% is orchard cultivation and 24.62% Ocho while in Saijo, (20.91%) is cultivated by rice paddy. The proportional difference between Ocho and Kubi may be the reason for the elevated concentrations in groundwater, whereas for Saijo, this may not be the case; reasons being that most of the groundwater samples were collected in the residential area with little or no agricultural activity in its vicinity.

2. Type of fertilizer used and method of application: From field investigation. The difference in fertilizer usage in both villages maybe due to the difference in farmer age group (76> in Kubi and 73 > in Ocho). Fertilizers provide plants with the nutrients they need to grow immediately, thus aged farmers will prefer to use chemical fertilizers which are more cost effective, less time consuming and more convenient for maximum crop yield. However further investigations need to be carried to confirm this assumption. This factor is ruled out in Saijo due to the above-mentioned reason.

3. Housing density: The residential area in Kubi and Ocho varies significantly as seen from (Figure. 3.2). Ocho has a higher ratio of residential area (75.4 %) as compared to Kubi (59.8%). When compared with Saijo, Saijo has a much lower percentage (34.4%). However, the low NO_3^-–N concentrations in Saijo may be due to the more advanced development status in Saijo especially when taking into consideration sewage system which maybe a contributing factor to the higher NO_3^-–N in Ocho and Kubi.

Generally, the variation of NO_3^-−N concentration in groundwater from the three study sites may be related to several contributing factors however this results may be limited by the sample number and frequency of collection. Also, geology plays an important role in contamination status through mineral dissolution.

6.2 References

Barron, O. V., Barr, A. D., Donn, M. J. Effect of urbanization on the water balance of a catchment with shallow groundwater, *J. Hydrol*. **2013**, 485, 162–176,

Garcia-Fresca, B. Urban-enhanced groundwater recharge: review and case study of Austin, Texas, USA, Urban Groundwater, Meeting the Challenge: IAH Selected Papers on Hydrogeology 8. **2007**.

Grischek, T., Nestler, W., Piechniczek, D., Fischer, T. Urban groundwater in Dresden, Germany. *Hydrogeol. J*. **1996**, 4, 48–63.

Hardison, E.C., O'Driscoll, M.A., DeLoatch, J.P., Howard, R.J., Brinson, M.M. (2009). Urban land use, channel incision, and water table decline along coastal plain streams, North Carolina. *Am. Water Resour. Assoc*. **2009**, 45, 1032–1046.

Jha, R., Singh, V. P. and Vatsa, V. (2008). Analysis of urban development of Haridwar, India, using entropy approach. KSCE Journal of Civil Engineering, 12, 281−288.

Strohschön, R., Wiethoff, K., Baier, K., Lu, L., Bercht, A., Wehrhahn, R. and Azzam, R. Land use and Water Quality in Guangzhou, China: A survey of ecological and Social Vulnerability in Four Urban Units of the Rapidly Developing Megacity. *Int J Environ Res*. **2013**, 7, 343−358.

Chapter 7

Conclusion and Recommendation

7.1 Conclusion

In order to confirm the social effect (aging and depopulation) and environmental effect (land use change, urbanization, and climate change) on the groundwater resources, we made use of hydrochemical and isotopic tracer methods as well as a watershed hydrology model in three mountainous rural catchments. As many cities in Japan and third-world countries are either experiencing or are rapidly approaching similar demographic challenges, this study will also provide the public with an insight into the environmental and social challenges associated with aging and depopulating societies on groundwater resources. The general conclusions are as follows:

Employing hydrochemical and stable nitrogen 15 isotopes, the villages of Ocho and Kubi, where found to have different NO_3^--N contamination status (Ocho: 4.8 mg/Land Kubi: 6.7 mg/L) partly due to the slight difference in their social aspects (population size and farmer age) which tends to influence their choice of fertilizer. The proportional source contributions of NO_3^- in each village was determined using an end–member method which showed that Kubi had a greater contribution from chemical fertilizer while Ocho village was from Organic fertilizer. However, both villages had minor contributions from sewage. It was believed that the older farmers in Kubi employed a significant quantity of chemical fertilizers due to their smaller population size (reduced work force) and older farmer group (reduced work efficiency), which caused inefficient nitrogen uptake by plants, leading to increased leaching, and more groundwater contamination than in Ocho.

Similarly, the same approach was conducted in a developing rural catchment; Saijo and contrary to Kubi and Ocho, 99% of the groundwater samples plotted in the manure and sewage zone. Despite the agricultural activities in the area, we found no evidence of nitrate originating from synthetic fertilizers in the groundwater. This could either be as a result of proper agricultural practices or limited dataset, however future investigations will employ long term-time series data for proper investigation.

Furthermore, based on the result of study about SWAT and GIS application to address impact of urbanization and climate change on groundwater resources in the Kurose River catchment area, the general conclusions have been formulated. The population growth and economic development in the Kurose River catchment area in the last three decades had an impact on land use change and also on groundwater availability.

During the 1980s – 2000s most of the land use change was caused by the conversion of rice paddy fields to residential areas resulting in increased impervious surfaces with negative implication on the catchment hydrology. From SWAT simulation, results suggest that the water balance in the 1980s and the 2000s was greatly influenced by land use change, urbanization, and potential contributions from climate change on the catchments hydrology characteristics. The most significant change was observed in the decrease in the mean annual groundwater recharge by approximately 25% over the past three decades. Additionally, the predicted land use and climate scenario highlighted that groundwater recharge will be significantly affected by the combined effect of future land use and climate change which is projected to decrease groundwater recharge by 29% by 2040**.**

7.2 Recommendation

In order to achieve better results, input data and process need to be improved, especially by using better resolution data set (spatial and temporal) and including irrigation function to fully estimate recharge in paddy fields. Additionally, to obtain better results on the temporal

changes in groundwater recharge with changing land use and climate, SWAT can also be integrated with fully distributed MODFLOW groundwater models (SWAT-MODFLOW).

Appendix

Appendix 1: Hydrochemical compositions of the groundwater and surface water sources in Kubi and Ocho village for the 2021 sampling campaign.

Note: BDL = below detection limit; NM = not measured, ionic concentrations, TDS and DO = mg/L; EC = µS/cm; Temp = °C

	Typology	Well depth	pH	Temp	EC	TDS	DO	DOC	Cl^-	$SO42^-$	$NO3^-$	NO3-N	$HCO3^-$	Na^+	K^+	$Mg2^+$	$Ca2^+$
OKBH	Borehole	30	7.5	19	472	302.1	6.1	4.1	10.1	67.6	56.7	12.9	39.1	28.6	0.6	14.4	35.5
OKR1	River		7.9	24	274	175.4	9	3.8	7.4	36.8	20.9	4.8	61.2	14.4	2.4	7.8	23.2
OKR2	River		8.59	24.7	206	131.9	8.3	5.3	6.4	16.8	5.5	1.3	50.6	10.1	1.6	4.5	9.8
OKU1	Well	5.11	6.46	20.7	333	213.2	3.9	11.6	7	37.7	32.1	7.3	30.2	13.1	3.3	8.2	22.1
OKU2	Well	3.12	6.45	20.6	326	208.7	8.2	13.3	8.1	50.8	49.2	11.2	14.2	15.5	4.1	11.4	25.4
OKU3	Well	3.78	6.51	18.3	321	205.5	7.5	6	7.6	74.6	40.8	9.3	28.4	14.8	1.4	13.9	29.3
OKU4	Well	7.59	6.44	21.2	265	169.6	6.5	3.3	9.9	36.2	27.9	6.4	43.5	15.5	4.5	8.2	22
OKU5	Well	12.5	6.94	20.9	238	152.4	5.5	NM	11.7	26.3	22	5	43.5	17.5	1.7	5.4	18.5
OKU6	Well	70	6.89	18.3	465	297.6	4.7	4.8	10.7	64.1	57.2	13	62.1	27.9	0.8	14.4	38.1
OKU7	Well	4.68	6.49	24.3	407	260.5	3.8	4.1	6.5	34.3	13.7	3.1	121.6	9.8	6.6	9.7	30.1
OKU8	Well	4.46	6.41	21.7	255	163.2	4.9	3	9.5	37.6	28.6	6.5	47.1	13.4	4.1	8.9	23.7
OKU9	Well	5.71	6.74	24.9	106.3	68.1	8.6	2.5	9	5.1	2.1	0.5	55.9	9.6	1	1.6	7.8
OKU10	Well	5.65	6.5	20.6	226	144.7	3	3.6	4.2	13.6	10.4	2.4	57.7	6	4.9	4.2	13.6
OKU11	Well	1.2	6.68	26.7	354	226.6	3.9	3.7	14.3	51.5	54.9	12.5	0	14.4	5.4	15.3	BDL
OKD1	Well	NM	7.32	20.4	283	181.2	1.1	4.9	9.4	36.3	26.1	5.9	37.3	16.3	4.9	9.5	24
OKD2	Well	NM	7.09	20.6	418	267.6	2.8	4.9	10	41.2	42.8	9.7	70.1	19.3	0.8	11.2	27.3
OKD3	Well	3.72	7.16	22	378	242	3.8	2.8	11.1	38.2	33.5	7.6	47.1	16.4	7.1	10.8	27.9
OKD4	Well	4.35	6.4	20.4	261	167.1	4.6	4.6	8.7	32.6	28.5	6.5	24.9	11.7	4.7	8.5	21
OKD5	Well	6.76	NM	20.7	248	158.8	6	3.5	10.8	41.6	32	7.3	37.3	15.9	5.2	9.4	24.8

OKD6	Well		6.64	6.89	18.3	465	297.6	4.7	4.1	10.5	31.1	11.2	2.6	55.9	17.4	2.7	8.4	17.1
O-KUS	Spring			7.21	19.1	185.7	118.9	9.2	3.6	14.7	22.9	7.1	1.7	7.2	21	2.2	9.8	24.6
OOG1	Well		2	6.72	23.6	266	170.3	0.8	6.7	8.4	11.3	3.5	0.8	89.8	12.2	2	5	13.9
OOG2	Well			6.72	28.3	346	221.5	4.5	3.5	15.4	49	21.3	4.9	141.2	27.1	1.9	19.1	43.3
OOG3	Well		3	6.64	22.6	239	153	3.1	3.4	13.6	22.8	11.6	2.7	98.7	20.6	8	8.9	29.7
OOG4	Well		9	6.4	22.5	191.7	122.7	5.3	2.2	8	18.1	19.7	4.5	55.6	12.9	5.4	5.7	20.2
OOG5	Well		5	6.53	20.4	229	146.6	2.3	2.2	11.8	39.5	13.5	3.1	55.2	20.1	3.6	9.1	21.3
OOG6	Well			6.74	24.6	479	306.6	2.9	1.7	37.5	34.1	26.5	6	150.2	28.1	1.9	15.3	39.4
OOG7	Well		5	6.52	19.2	373	238.8	4.9	3.2	13	47	48.8	11.1	75.7	18.6	0.7	13.9	29.1
OOG8	Tap	NM		7.16	22.8	164.9	105.6	9.1	3.2	5.3	19.8	13.3	3.1	34	9.4	1	4.9	13.5
OOG9	Well		4	6.34	22.4	237	151.7	3.4	7	9.7	14.2	22.1	5	51.3	9.5	4.8	5.1	14.2
OOG10	Well		4	6.27	21	301	192.7	1.1	2.9	8.4	19.2	12.3	2.8	107	21.2	8.8	8	BDL
OOG11	Well		5	6.19	19.6	453	290	2.8	4.4	17.9	145.1	66.4	15.1	54.1	57.6	2.2	22.2	42.8
OOG12	Well		7	6.22	20.9	354	226.6	2.3	3	18.3	58.4	31.9	7.3	70.4	22.6	2.7	14.3	32.4
OOG13	Well		6	6.44	23.1	378	242	1.7	4.8	14.6	84.3	19.2	4.4	82.3	15.8	7.2	11	48.1
OOG14	Well		4	6.44	21.4	285	182.4	3.2	5	13.8	22.2	33.4	7.6	69	16.8	10.5	7.4	29.6
OOG15	Well		4	6.57	22.6	269	172.2	3.2	4	7.9	14.6	16.1	3.7	105.1	11.1	5.5	5.4	24.5
OOG16	Well		5	6.94	21.3	317	202.9	1.6	3.1	12	10.1	7.4	1.7	143.6	22.2	3.2	7.3	BDL
OOG17	Well		2	7.08	20.6	340	217.6	8.2	4.1	5.1	46.4	28.5	6.5	78.9	15.3	0.7	11.4	27
OOG18	Well		6	6.34	21.3	236	151.1	3.3	5.9	9.2	21.5	23.5	5.4	70.7	14.7	10.2	7.5	26.4
OOG19	Well	NM		6.27	21.6	323	206.8	1.1	3.3	21.3	BDL	19.6	4.5	89.7	21.5	0.3	13.6	8.8
OOG20	Well		5	6.89	23.5	318	203.6	1.7	4.9	10.9	26.4	11.2	2.6	133.2	19.3	6.1	7.8	BDL
OOG21	Well		5	6.5	22.7	410	262.4	1.7	2.5	12	27	28	6.4	83.4	12.4	1.4	6.5	BDL
OOG22	Spring			7.45	23.6	217	138.9	7.7	0	10.9	22.9	13.7	3.1	9.3	0	8.4	25.8	BDL
OOG23	Spring			7.45	17.6	133	85.2	9.5	3.5	4.6	4.5	2.7	0.7	4	5.5	3.2	1.4	4.6
OOG24	Well		5	6.83	22.2	331	211.9	3.6	2.8	13.7	71.4	41.9	9.5	8.9	21.5	4.7	16.8	45
OOG25	Well		10	6.95	22.7	333	213.2	2.4	2.8	4.1	45	18.9	4.3	9.1	10.2	0.8	6.5	28.9
OOG26	Well		4	6.74	21.6	210	134.4	7.5	-3.7	5.9	35.2	24.3	5.5	4.5	12	1.9	8.5	23.6
OOG27	Well		5	6.58	23.3	324	207.4	3.4	2.5	11	74.2	12.5	2.9	12.8	22	4.8	22.1	50.8
OOG28	Well		6	8.44	22.8	291	186.3	4.1	3.6	11.3	24.3	24.3	5.5	11.4	16.6	4.3	7.6	35.1

OOG29	Well	NM		6.41	22.9	266	170.3	1.8	2.4	9.7	28.8	14.2	3.3	7	14.6	6.3	7.3	BDL
OOG30	Well		4	6.76	21.8	347	222.1	2.1	3.6	6.6	21.7	10.1	2.3	10.5	12.4	2.7	5.7	18.7
OOG31	Well		3	6.81	22.1	368	235.6	1.6	1.8	12.8	36.7	3.7	0.9	14	27.1	5.1	9.9	BDL
OOG32	Well		3	7.1	21.9	275	176	8.1	2.2	6.4	22.9	21	4.8	8.5	11	4.3	5.9	23.3

Appendix 2: Groundwater level data collected in various observation wells in the 1974 and 2000 for the Kurose River catchment. Note: All measurements are in meters (m)

1974								20000				
Well	**Long**	**Lat**	**Well height**	**Water depth**	**Bottom depth**	**Surface elev.**	**Groundwater elev.**	**Well height**	**Water depth**	**Bottom depth**	**Surface elev.**	**Groundwater elev.**
107	132.7525	34.42417	0.35	1.44	3.11	212.5	211.41	0.26	2.66	3.29	212.5	210.1
112	132.7506	34.41194	0.38	0.92	3.14	208.7	208.16	0.5	2.52	3.57	208.7	206.68
113	132.7581	34.40167	0	1	2.58	210.1	209.1	0.62	2.61	3.45	210.1	208.11
116	132.7436	34.41278	0.49	3.04	5.09	225.4	222.85	0.19	3.17	5.39	225.4	222.42
117	132.7453	34.41028	0.35	2.63	4.39	217.5	215.22	0.33	3.71	4.36	217.5	214.12
123	132.7519	34.40194	0.46	0.4	8.35	225	225.06	0.29	6.27	8.55	225	219.02
127	132.7572	34.40722	0.33	1.69	4.45	216	214.64	0.09	1.99	4.18	215.2	213.3
128	132.7501	34.40944	0.52	1.02	4.08	215.2	214.7	0.28	2.55	3.65	210	207.73
129	132.7581	34.41028	0.36	1.31	3.28	210	209.05	0.46	2.69	3.95	219	216.77
132	132.7503	34.40361	0.47	0.62	4.54	219	218.85	0.47	1.11	2.1	210.5	209.86
137	132.735	34.40972	0.61	0.66	2.02	210.5	210.45	0.44	1.89	2.37	208	206.55
138	132.7461	34.4	0.53	1	2.36	208	207.53	0.59	2.86	3.1	214.5	212.23
139	132.7453	34.40722	0.72	2.14	3.19	214.5	213.08	0.14	5.22	5.75	214.5	209.42
140	132.7458	34.40028	0.34	3.64	5.38	214.5	211.2	0.34	4.44	5.69	208	203.9
141	132.7594	34.4275	0.3	1.67	5.67	208	206.63	0.55	1.9	3.45	212.5	211.15
143	132.7756	34.42167	0.47	1.07	2.71	212.5	211.9	0.51	5.25	6.61	234	229.26
145	132.7619	34.43139	0.65	4.14	6.75	234	230.51	0.58	1.62	3.61	250	248.96
146	132.7506	34.4425	-9999	-9999	-9999	250	-9999	0.41	1.12	2.8	212	211.29
203	132.7356	34.43694	0.51	0.69	2.84	212	211.82	0.155	1.9	6.53	223	221.255
206	132.7481	34.43667	0.46	1.71	3.5	223	221.75	0.56	2.14	3.62	235	233.42
207	132.7486	34.41917	0.45	1.31	9.28	237.5	236.64	0.36	5.6	6.19	236	230.76
208	132.77	34.44139	0.37	2.57	5.04	235	232.8	0.49	1.15	4.3	225	224.34
211	132.7622	34.44	0.4	5.6	6.23	236	230.8	0.24	1.32	2.46	215	213.92
212	132.7519	34.41833	0.4	0.71	4.03	225	224.69	0.54	1.94	2.93	214	212.6

228	132.7514	34.41889	0.27	0.88	2.5	215	214.39	0.23	3.72	6.3	221	217.51
229	132.7439	34.43556	0.7	1.31	3.15	214	213.39	0.39	2.74	4.68	221	218.65
231	132.7608	34.43556	0.45	4.08	6.36	221	217.37	0.265	9.51	10.95	229	219.755
238	132.7394	34.43861	0.35	10.29	11.55	229	219.06	0.355	1.76	6.02	225	223.595
243	132.7297	34.44333	0.4	1.45	6.03	225	223.95	0.61	5.33	5.85	240	235.28
305	132.7214	34.42972	0.23	4.85	6.86	240	235.38	0.424	2.7	3.27	235	232.724
309	132.7189	34.42167	0.48	2.59	5.54	222.9	220.79	0.37	2.65	5.23	222.9	220.62
312	132.7364	34.43361	0.46	0.5	3.89	214.2	214.16	0.1	0.88	4.17	214.2	213.42
319	132.7381	34.43333	0.48	0.52	2.44	240	239.96	0.45	1.2	2.51	240	239.25
320	132.7347	34.43528	0.67	1.34	4.04	229	228.33	0.58	2.01	3.09	229	227.57
329	132.7428	34.43917	0.59	1.32	4	226	225.27	0.59	1.86	4.1	226	224.73
330	132.735	34.43278	0.03	1.4	5.55	221.5	220.13	0.03	1.15	5.16	221.5	220.38
331	132.7086	34.41056	0.08	1.67	3.94	217	215.41	0	1.1	3.65	217	215.9
402	132.7156	34.42639	0.72	1.66	4.48	218	217.06	0.635	2.08	4.54	218	216.555
404	132.7136	34.4275	0.21	0.47	2.78	220	219.74	0.185	0.89	2.85	220	219.295
414	132.7297	34.42167	0.59	1.67	4.09	228	226.92	0.445	2.64	4.09	228	225.805
425	132.7017	34.42583	0.57	0.99	3.69	217	216.58	0.56	1.5	3.72	217	216.06
430	132.7006	34.40972	0.36	5	5.95	225	220.36	0.445	4.03	6.05	225	221.415
431	132.7197	34.40083	0.18	2.77	4.1	225	222.41	0.425	2.91	6.16	225	222.515
432	132.7208	34.41	0.44	1.37	5.2	220	219.07	0.54	2.21	5.58	220	218.33
434	132.7047	34.46028	0.63	0.67	8.43	221.5	221.46	0.44	1.3	7.75	221.5	220.64
435	132.7253	34.45472	0.6	0.57	5.49	221.5	221.53	0.48	1.59	3.1	221.5	220.39
438	132.7039	34.45639	0.78	1.61	3.65	227.5	226.67	0.735	1.92	3.69	227.5	226.315
509	132.6858	34.45222	0.49	3.08	7.6	252.5	249.91	0.135	1.08	1.64	252.5	251.555
516	132.6858	34.45222	0.3	0.81	2.3	245	244.49	0.055	4.89	6.15	245	240.165
524	132.7114	34.435	0.35	0.61	2.1	246	245.74	0.74	2.18	6.2	246	244.56